PEOPLE'S DEMOCRATIC REPUBLIC OF ALGERIA

وزارة التعليم العالي و البحث العلمي

MINISTRY OF HIGHER EDUCATION AND SCIENTIFIC RESEARCH

جامعة غليزان

RELIZANE UNIVERSITY

FACULTY OF SCIENCE AND TECHNOLOGY

PHYSICS DEPARTMENT

LMD 3rd cycle DOCTORATE THESIS

Sector: Energetic Physics

Specialty : physics

Thesis title:

Ab initio study of the optoelectronic and thermal properties of double perovskites

Presented by:

Hadji Chikh Ali

publicly defended on May 02, 2026, in front of a jury made up of:

President	OUFELLA Sarah	MCA	Relizane University
Thesis Director	ARRAR Amina	MCA	Relizane University
Thesis Co-Director	TOUAA Zaza	MCB	Relizane University
Examiners	BENSTAALI Wafa	MCA	Mostaganem University
	SEFIR Yamina	MCA	Mostaganem University
	SLAMANI Amel	MCA	Relizane University
Guest	BENDJILALI Hadjer	MCB	USTHB University

2025/2026

ACKNOWLEDGMENTS

would like to thank ALLAH the Almighty first and foremost for giving me the courage, willpower, and patience to complete this work.

This work was carried out within the Laboratory of Physics Thin Layer and Advanced Technologies, University of Relizane, BP 48000, Bourmadia, W. Relizane, Algeria.

I'd like to express my gratitude to everyone who helped make this study feasible. My supervisor, **Dr. Arrar Amina**, in the Physics Department at the University of Relizane, Algeria, has provided me with invaluable assistance and advice, for which I am truly grateful. She has been incredibly understanding and patient as my thesis has developed. Her encouraging words and recommendations encouraged me to carry out more investigation. Her outstanding guidance and support throughout my PhD studies allowed me to acquire a wealth of information and experience that will be useful to me going forward. Without her help, I never would have been able to accomplish the aim.

I would like to express my sincere gratitude to • **Dr. Oufella Sarah**, President of the Thesis Defense Committee, for kindly accepting to chair the jury and for her careful reading and evaluation of this work. I would also like to warmly thank: • **Dr. Touaa Zaza**, Thesis Co-Director, as well as the honorable members of the examination committee: • Dr. Benstaali Wafa, Examiner, • **Dr. Sefir Yamina**, Examiner, • **Dr. Slamani Amel**, Examiner. I also extend my special thanks to: • Dr. Bendjilali Hadjer, Guest Member, for her valuable time, careful reading, and constructive comments that greatly contributed to the improvement of this thesis.

DEDICATIONS

With heartfelt gratitude, I extend my appreciation to my beloved parents. Their

unwavering encouragement and steadfast support echo in my ears.

Their energy and unwritten joy fueled me throughout this remarkable journey.

To my my sisters Soumia & Meriem—who stood by my side, unwavering and ever-present, this dissertation is dedicated.

I also extend this dedication to my first friend, my brother Mohammed, whose unwavering support sustained me through this process. To my friends and my entire family, your encouragement has been invaluable.

Special thanks go to my professors, Dr. Arrar Amina ,my greatest cheerleaders during my doctoral program.

Thank you all

Table of contents

List of figures

List of tables

List of Publications

- Hadji, C. A., Arrar, A., Ghaleb, M., Bendjilali, H., & Zerrouki, O. (2024). Ab initio study of the optoelectronic and thermoelectric properties of the new double perovskite Cs_2ZnPbX_6 (X= Br, Cl). Materials Science and Engineering: B, 310, 117707. https://doi.org/10.1016/j.mseb.2024.117707
- Ghaleb, M., Arrar, A., Chikh, A. H., Bendjilali, H., & Zerrouki, O. (2024). I-$MASnBr_3$/CZTGS Heterojunction Solar Cell Layer Optimization Investigated Using Scaps-1D Software Exhibited Excellent Performance at 50%. Annals of the West University of Timisoara. Physics Series, 66, 191-214.10.2478/awutp-2024-0012

- Hadji, C. A., Arrar, A., Ghaleb, M., Zerrouki, O., & Bendjilali, H. (2025). Structural, elastic, optoelectronic, thermodynamic and thermoelectric properties of the new halide double perovskite Cs_2CaGeI_6: first-principles study. The European Physical Journal B, 98(5), 1-20. https://doi.org/10.1140/epjb/s10051-025-00949-8
- Ghaleb, M., Arrar, A., Hadji, C. A., Bendjilali, H., & Zerrouki, O. (2025). The structural, electronic, elastic, and optical properties of new double perovskite Cs_2CdPbI_6 were investigated using a DFT and SCAPS-1D simulation. Journal of Inorganic and Organometallic Polymers and Materials, 1-15. https://doi.org/10.1007/s10904-024-03545-y

Abstract

This thesis work aims to study double perovskites by numerical simulation calculation which allowed improved comprehension of the thermal and optical characteristics of these materials, perovskites are promising materials for optical and thermal applications, simulations showed that the band gap of perovskites is sensitive to the chemical composition and crystal structure and that the addition of ions can reduce the width of the band gap and increase the optical response, the simulations also revealed that the conductivity thermal properties of the atoms in the material and that this conductivity, Ab-inition studies thus provide valuable information for the creation of novel materials for thermal and optical uses, additionally, Wien2k software is used to simulate and optimize heterojunction PSCs with the suggested structure, this study's objective is to examine how well PSC with active layers of $Cs_2ZnPbCl_6$ and $Cs_2ZnPbBr_6$ perovskite as permeable layer.

The work uses the WIEN$_2$k code and DFT to investigate the double perovskite compounds $Cs_2ZnPbCl_6$ and $Cs_2ZnPbBr_6$, The compounds exhibit strong electrical conductivity, high thermoelectric performance, and a stable cubic structure. The thermal conductivity patterns indicate an increase with temperature, and the Seebeck coefficients are excellent. Applications for the compounds in thermoelectric generators, in particular, hold promise for sustainable energy, additionally, the study validates the compounds' mechanical stability, which is essential for real-world device applications, these discoveries advance our knowledge and use of double perovskite materials, additionally, the double perovskite materials under investigation have a favorable At room temperature, their thermodynamic and thermoelectric qualities show promise for use in thermoelectric technology, as evidenced by their figure of merit.

Resumé

Ce travail de thèse vise à étudier les pérovskites doubles par calcul de simulation numérique, ce qui a permis une meilleure compréhension des propriétés optoélectroniques et thermiques de ces matériaux, les pérovskites sont des matériaux prometteurs pour les applications optoélectroniques et thermiques , les simulations ont montré que la bande interdite des pérovskites est sensible à la composition chimique et à la structure cristalline et que l'ajout d'ions peut réduire la largeur de la bande interdite et augmenter la réponse optique , les simulations ont également montré que les propriétés thermiques, en particulier la conductivité thermique, sont fortement influencées par les interactions atomiques au sein du matériau les études ab initio fournissent ainsi des informations précieuses pour le développement de nouveaux matériaux pour des applications optoélectroniques et thermiques, En plus de la simulation et de l'optimisation des cellules solaires à pérovskite à hétérojonction (PSC) avec la structure proposée en utilisant le logiciel wien2k , l'objectif de cette étude examine la performance des cellules solaires à pérovskite (PSC) avec des couches actives de pérovskite $Cs_2ZnPbCl_6$ et $Cs_2ZnPbBr_6$ comme couche perméable.

Le travail utilise le code WIEN2k et la DFT pour étudier les composés de pérovskite double $Cs_2ZnPbCl_6$ et $Cs_2ZnPbBr_6$, Les composés présentent une forte conductivité électrique, une haute performance thermoelectrique et une structure cubique stable, Les motifs de conductivité thermique indiquent une augmentation avec la température, et les coefficients de Seebeck sont excellents, Les applications des composés dans les générateurs thermoélectriques, en particulier, promettent une énergie durable, de plus, l'étude valide la stabilité mécanique des composés, ce qui est essentiel pour les applications réelles des dispositifs , ces découvertes font progresser notre connaissance et notre utilisation des matériaux de double pérovskite , de plus, les matériaux de double pérovskite étudiés présentent un facteur de mérite favorable à température ambiante, ce qui indique que leurs propriétés thermodynamiques et thermoelectriques offrent un potentiel pour une application dans la technologie thermoelectrique.

الملخص

يهدف هذا العمل البحثي إلى دراسة البيروفسكيت المزدوج من خلال حسابات المحاكاة العددية التي سمحت بفهم أفضل للخصائص البصرية والإلكترونية والحرارية لهذه المواد البيروفسكيتات هي مواد واعدة للتطبيقات البصرية والإلكترونية والحرارية أظهرت المحاكاة أن فجوة الطاقة في البيروفسكيت حساسة للتكوين الكيميائي والبنية البلورية وأن إضافة الأيونات يمكن أن تقلل من عرض فجوة الطاقة وتزيد من الاستجابة البصرية كشفت المحاكاة أيضًا أن الموصلية والخصائص الحرارية للذرات في المادة وأن هذه الموصلية , تقدم دراسات Ab-initio بذلك معلومات قيمة لتطوير مواد جديدة للتطبيقات البصرية والإلكترونية والحرارية, بالإضافة إلى محاكاة وتحسين خلايا الشمسية البيروفسكيتية ذات الوصلة غير المتجانسة (PSC) بالهيكل المقترح باستخدام برنامج wien2k. الهدف من هذه الدراسة هو التحقيق في أداء خلايا الشمسية البيروفسكيتية (PSC) مع الطبقات النشطة من $Cs_2ZnPbCl_6$ و$Cs_2ZnPbBr_6$ كطبقة نفاذة.

يستخدم العمل كود WIEN2k ونظرية الكثافة الوظيفية للتحقيق في مركبات البيروفسكايت المزدوجة $Cs_2ZnPbCl_6$ و$Cs_2ZnPbBr_6$ تظهر المركبات موصلية كهربائية قوية, وأداء حراري كهربائي عالي, وهيكل مكعب مستقر تشير أنماط الموصلية الحرارية إلى زيادة مع درجة الحرارة, ومعاملات سيبيك ممتازة, تطبيقات المركبات في المولدات الحرارية الكهربائية, على وجه الخصوص تحمل وعدًا للطاقة المستدامة بالإضافة إلى ذلك تؤكد الدراسة على الاستقرار الميكانيكي للمركبات وهو أمر ضروري لتطبيقات الأجهزة في العالم الحقيقي تُعزز هذه الاكتشافات معرفتنا واستخدامنا لمواد البيروفسكايت المزدوج بالإضافة إلى ذلك فإن المواد البيروفسكيتية المزدوجة التي يتم التحقيق فيها تتمتع بمعامل جيد عند درجة حرارة الغرفة مما يشير إلى أن خصائصها الديناميكية الحرارية والكهربائية الحرارية تقدم إمكانيات للتطبيق في تكنولوجيا الكهرباء الحرارية.

GENERAL INTRODUCTION

GENERAL INTRODUCTION

The development of efficient and sustainable materials that can facilitate the shift to low-carbon technologies has become increasingly important in the global energy environment in recent years. Halide perovskites are one of these materials that has attracted a lot of interest because of its exceptional performance in optical and thermoelectric applications. [1,2] . Although perovskite compounds were first discovered in the 19th century [3], their emergence as a cornerstone of modern materials science is a relatively recent phenomenon, largely sparked by breakthroughs in photovoltaic efficiency and crystal engineering over the past decade [4].

The group of substances referred to as metal halide perovskites, with general formulas such as ABX_3 and the more complex $A_2BB'X_6$ (in the case of double perovskites), is particularly notable for its tunable crystal structures and exceptional semiconducting behavior. These compounds exhibit a suite of desirable traits: direct and adjustable bandgaps, large carrier diffusion lengths, low exciton binding energies, high absorption coefficients, and intrinsic defect toleranc[5,6]. Such properties not only making them the best options for solar cells of the future, but also for other optical applications including light-emitting diodes (LEDs), photodetectors, and lasers[7, 8].

The performance of perovskite solar cells (PSCs), in particular, has undergone a revolutionary transformation. Since the initial demonstration of a power conversion efficiency (PCE) of around 3.8% in 2009, the efficiency of PSCs has skyrocketed to exceed 25% in laboratory settings [9,10]. This remarkable progress has made perovskite-based technologies a serious competitor to well-established silicon photovoltaics. Moreover, the relatively low cost and facile fabrication of these materials via solution-processed techniques further enhances their commercial appeal [11].

However, despite their excellent performance metrics, conventional lead-based perovskites are hindered by toxicity concerns and environmental instability, prompting a shift toward lead-free alternatives and double perovskite structures[12,13]. The introduction of compounds like Cs_2ZnPbX_6 (X = Cl, Br) represents a promising development in this direction. These materials seek to combine the favorable optical characteristics of lead-halide perovskites with enhanced thermal and structural stability, and reduced ecological impact [14].

The current work examines the structural, electrical, elastic, optical, thermodynamic, and transport characteristics of $Cs_2ZnPbCl_6$ and $Cs_2ZnPbBr_6$ in their cubic phase from the ground up (ab initio). Density Functional Theory (DFT) with the WIEN2k computational framework is the foundation of the methodology used, which enables a very accurate description of the physical behavior of these materials under varying conditions [15]. The FP-LAPW method, implemented within WIEN2k, is particularly suitable for calculating total energy, band structure, and elastic constants for systems with complex unit cells [16].

This thesis is organized into three main chapters:

Chapter 1 introduces the theoretical background of halide perovskite materials, with emphasis on their structural classification, synthesis, and emerging applications in energy conversion.

Chapter 2 outlines the computational approach and theoretical models used in this study, including simulation parameters and software tools.

Chapter 3 presents and discusses the results obtained, covering structural, electronic, mechanical, optical, and thermoelectric analyses, and assessing the viability of the compounds for practical applications.

By providing a comprehensive theoretical analysis of Cs_2ZnPbX_6 compounds, this study aims to contribute to the growing body of knowledge on lead-reduced or lead-free perovskites, and to support the development of innovative materials for renewable energy technologies. The insights gained from this work could aid in the design of new, environmentally friendly semiconductors that offer both performance and durability, essential traits for future optical and thermoelectric systems.

CHAPTER 1 :

Theoretical Insights into Double Perovskite Materials for Energy Applications

1- Introduction to perovskite structures

Perovskite materials have attracted tremendous attention due to their outstanding optoelectronic, electrical, and thermal properties, which make them suitable for a wide range of energy applications, including photovoltaics, photodetectors, light-emitting devices, and thermoelectric systems. However, conventional perovskites also suffer from critical limitations such as structural instability and environmental concerns. These challenges have motivated the development of various perovskite-derived structures, ultimately leading to the emergence of double perovskites as a highly promising class of materials.

2- Conventional perovskites (ABX_3)

The ideal perovskite structure is described by the general formula ABX_3, where A is a monovalent cation, B is a divalent metal cation, and X is an anion. This structure exhibits excellent light absorption, tunable band gaps, and favorable charge transport properties. Nevertheless, issues related to toxicity, ion migration, and thermal instability limit their long-term applicability in energy devices [17]. The perovskite-type crystalline structure is one of the structures whose properties are the most exploited in modern technology. Several of them lead to applications relevant to all fields of research.

In 1830, geologist Gustav Rose made the discovery of the mineral perovskite using samples he had taken from the Ural Mountains. The Russian mineralogist Count Lev Aleksevich von Perovski is credited with giving it its name [14,15]. Originally, the mineral $CaTiO_3$ was referred to as perovskite.

Since Goldschmidt (1926) of the University of Oslo (Norway) created the first synthetic perovskites, the name "perovskite" has been used to refer to a class of chemicals that have the same general formula as $CaTiO_3$.

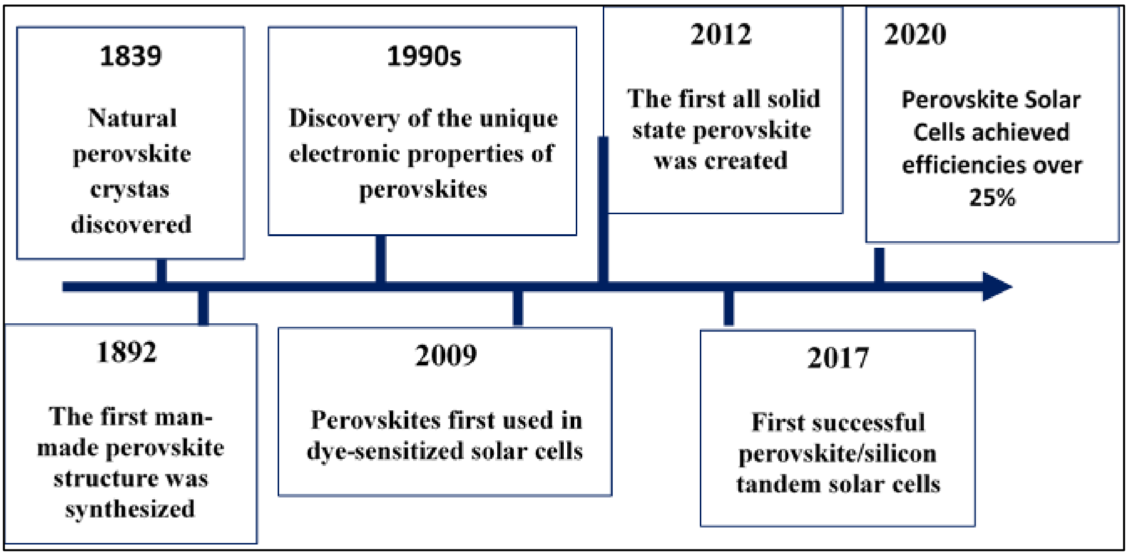

Figure 1.1. Major milestones in the development of perovskite materials [17].

Overview

3- Brief historical background of perovskite discovery and evolution

The history of perovskite materials is as enigmatic as it is influential. The initial crystals of perovskite found in the Ural Mountains during the 19th century marked the beginning of a long and evolving narrative [18]. Originally identified as a naturally occurring mineral a form of calcium titanate the crystal's origins are shrouded in mystery. While the exact identity of the discoverer remains uncertain, the mineral was eventually entrusted to prominent figures in mineralogy.

4- History of perovskites and perovskite solar cells

In 1839, Chief Mines Inspector Gustav Rose of the University of Berlin received the item from August Alexander Kämmerer for a thorough examination [19]. Rose, a distinguished mineralogist and crystallographer, had participated in significant scientific expeditions alongside renowned figures such as Alexander von Humboldt and Christian Gottfried Ehrenberg. His subsequent work, published in a renowned scientific journal, laid the groundwork for naming the mineral in honor of Count Lev Aleksevich Perov [20].

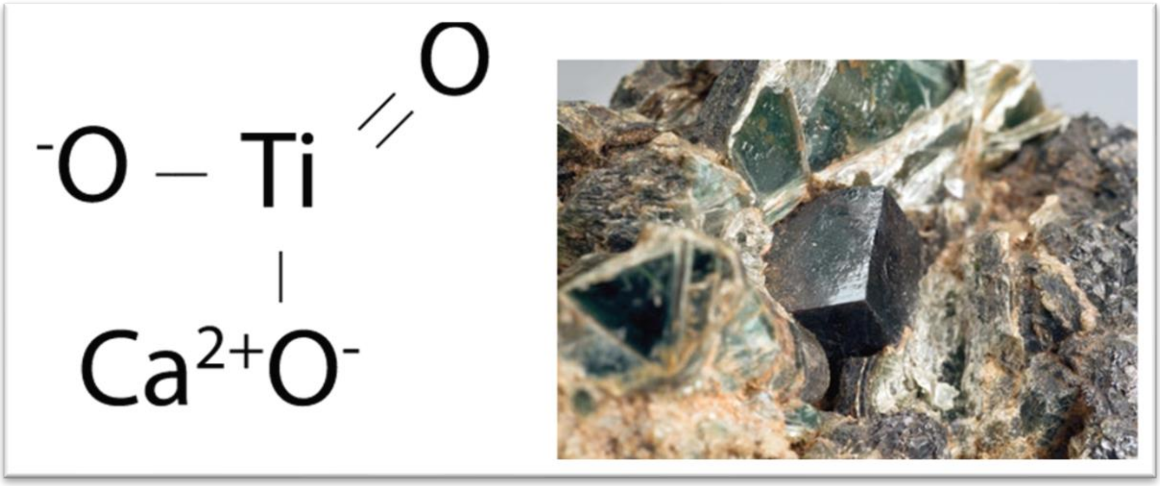

Figure I.2 Russia perovskite crystal with 7mm edge length from achmatovsk mine, slatoust, ural Mountains, chemical formula and a sample are shown [21].

5- Structural characteristics of perovskite materials

The term perovskite originally referred to a specific mineral, calcium titanate ($CaTiO_3$), named in honor of the Russian mineralogist Lev Aleksevich von Perovski (1792–1856). The compound was first identified in 1839 by Gustav Rose, who analyzed mineral samples collected from the Ural Mountains. Today, the term "perovskite" is commonly used to describe a large class of compounds that share the same or similar crystal structure as $CaTiO_3$.

The ideal perovskite structure adopts the general chemical formula ABO_3, where "A" and "B" are metal cations of different sizes and valences, and "O" represents the oxygen anion. Typically, the A-site is occupied by a large, low-valence cation such as Ba^{2+}, Ca^{2+}, Na^{+}, Pb^{2+}, or K^{+}, with a coordination number of 12. The B-site hosts smaller, high-valence cations like Ti^{4+}, Zr^{4+}, or Nb^{5+}, usually coordinated by six oxygen atoms, forming BO_6 octahedral [22].

Structurally, the perovskite framework is cubic and belongs to the space group $Pm\bar{3}m$, with a lattice parameter close to 4 Å. The BO_6 octahedra share corners and are arranged along the <100> crystallographic directions, forming a three-dimensional network. The larger A cations occupy the 12-fold coordinated cubo-octahedral cavities created by the surrounding octahedra.

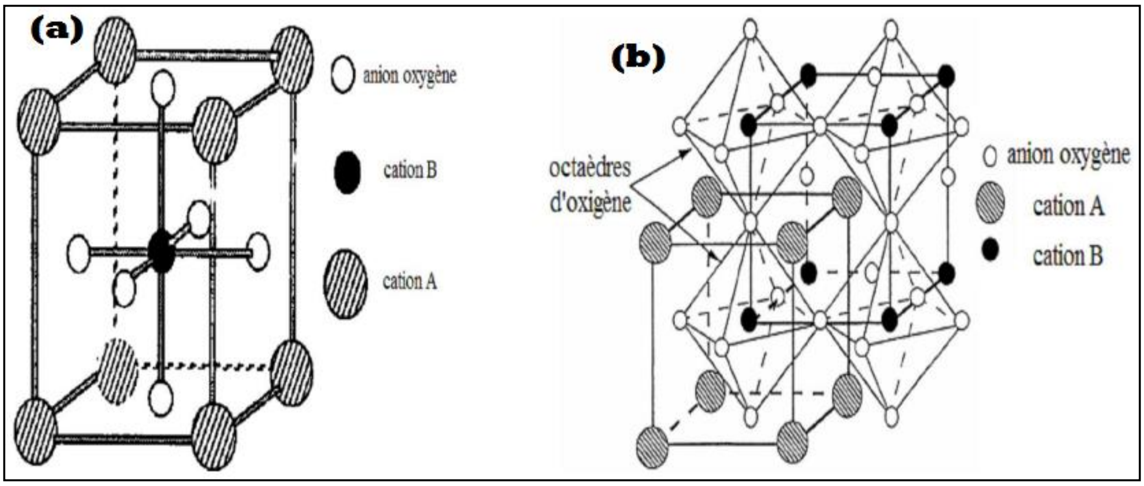

Figure I.3. (a) Ideal unit cell.(b) unit cell of a simple cubic ABO_3 perovskite, highlighting the oxygen octahedron [17].

There are two conventional ways to describe the atomic positions within the unit cell, depending on the choice of the origin:

- In the first configuration, the A cation is positioned at the origin (0, 0, 0), the B cation is located at the center of the cube (½, ½, ½), and the oxygen anions are found at the face centers: (0, ½, ½), (½, 0, ½), and (½, ½, 0).
- Alternatively, if the origin is shifted by a vector (½, ½, ½), the B cation then lies at (0, 0, 0), the A cation at (½, ½, ½), and the oxygen atoms at positions such as (0, 0, ½).

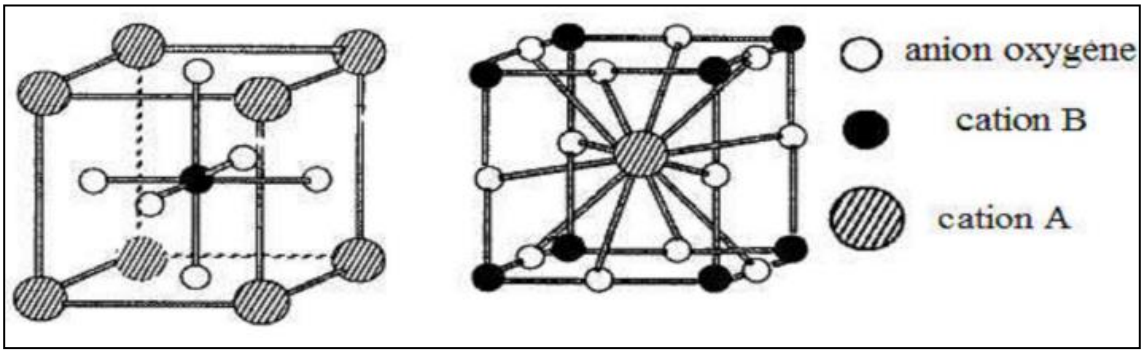

Figure I.4 Atomic arrangements within the unit cell of ABO_3 perovskites(a): origin at A-site;(b) origin at B-site [17].

Depending on the atomic arrangement, perovskites are generally categorized into:

- **Simple perovskites**, in which the A and B sites are occupied by a single type of cation (e.g., $BaTiO_3$, $KNbO_3$, $NaTaO_3$, $PbTiO_3$, $CaTiO_3$).
- **Complex perovskites**, in which one or both of the A and B sites are occupied by a mixture of different cations (e.g., $PbMg_{1/3}Nb_{2/3}O_3$, $PbSc_{1/2}Ta_{1/2}O_3$, $Na_{1/2}Bi_{1/2}TiO_3$).

It is important to note that not all compounds with the perovskite structure exhibit ferroelectricity. For example, materials like $SrTiO_3$ and $BaZrO_3$ maintain the perovskite lattice but are not ferroelectric under standard condition [23].

6- Crystal stability tolerance factor and octahedral factor

Two empirical descriptors Goldschmidt's tolerance factor (t) and the octahedral factor (μ) provide essential geometric criteria for predicting whether a given set of ionic radii will adopt the perovskite topology. The tolerance factor quantifies the fit of the A-site cation within the cubo-octahedral cavity formed by corner-sharing BX_6 units, while the octahedral factor assesses the relative size compatibility of the B-site cation and the anion. For halide perovskites (X = F, Cl, Br, I), stable 3D frameworks are typically realized when $0.81 < t < 1.11$ and $0.44 < \mu < 0.90$, defining a compositional 'Goldschmidt window' for material design [24,…,26].

6-1- Goldschmidt tolerance factor

Goldschmidt's tolerance factor

$$t = \frac{(rA + rX)}{\sqrt{2}(r_B + r_X)}$$

expresses the geometrical compatibility between the A-site cation radius (rA), the B-site cation radius r_B and the anion radius r_X [27]. Ideal cubic perovskites satisfy $t \approx 1$, whereas deviations lead to lattice distortions: $0.9 \leq t \leq 1.0$ generally yields nearly cubic or slightly distorted structures; $0.8 \leq t < 0.9$ often produces orthorhombic or rhombohedral variants; $t < 0.8$ typically destabilizes the 3D perovskite network in favor of layered or alternative motifs[28,29] . Goldschmidt's original concept (1926) remains widely used, though recent work has introduced modified tolerance factors to improve predictive accuracy for complex compositions[30].

6-2- Octahedral factor

The octahedral factor

$$t = \frac{r_A + r_X}{\sqrt{2}(r_A + r_X)}$$

measures the fit of the B-site cation within the BX_6 octahedron [25]. A minimum threshold of $\mu \approx 0.41$ is required to sustain corner-sharing octahedra; below this value, the framework collapses or transforms into edge- or face-sharing networks [26]. Conversely, $\mu > 0.90$ can induce excessive strain, leading to symmetry lowering or phase segregation.

6-3- Stability map and structure property correlations

Plotting t versus μ yields a perovskite stability map (Figure 1.3), in which known halide perovskites cluster within a bounded region ($0.81 < t < 1.11$, $0.44 < \mu < 0.90$) [26,31]. Compounds near the edges of this window often exhibit pronounced octahedral tilting or polar distortions, enhancing ferroelectric or piezoelectric responses but possibly reducing thermal and chemical stability [32]. Designing new perovskites thus requires balancing ionic radii to remain within this 'Goldschmidt window' while tuning electronic and optical functionality.

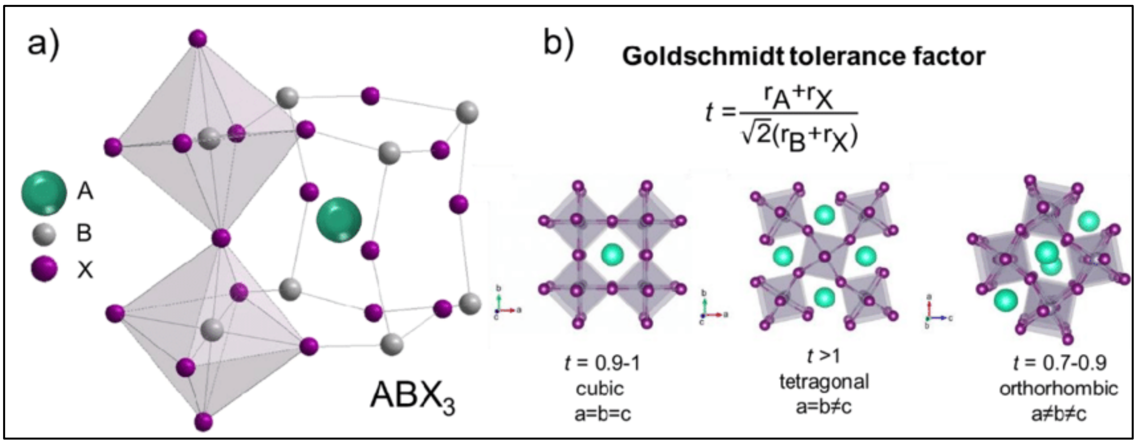

Figure I.5. Stability map of perovskite formation in Goldschmidt parameter space [33].

Table I.1. Typical tolerance and octahedral factors for selected halide perovskites [26].

Compound	A-Site (rA / Å)	B-Site (rB / Å)	X-Site (rX / Å)	T	μ
$CsPbCl_3$	1.88	1.19	1.81	0.86	0.66
$CsPbBr_3$	1.88	1.19	1.96	0.83	0.61
$CH_3NH_3SnI_3$	2.17	1.18	2.20	0.93	0.54
$FA_{0.8}Cs_{0.2}PbI_3$	2.53 (FA_avg)	1.19	2.20	1.03	0.54
$RbPbI_3$	1.72	1.19	2.20	0.75	0.54

6-4- Perovskite properties and phase behavior

6-4-1- Temperature

Temperature significantly influences the phase transitions and structural stability of perovskites. As temperature varies, so do the symmetry and unit cell dimensions of the perovskite lattice.

High temperature

At elevated temperatures, perovskites often adopt a cubic phase due to increased thermal energy, allowing ions to occupy higher symmetry positions[33] .

Low Temperature

As temperature decreases, thermal energy diminishes, leading to phase transitions toward lower symmetry structures such as tetragonal or orthorhombic phases. These transitions occur to minimize the system's free energy[33] .

In two-dimensional perovskites, temperature-dependent photoluminescence studies have shown that bandgap variations are influenced by thermal expansion and electron phonon interactions. For instance, in certain perovskite series, the photoluminescence peak shifts from red to blue with increasing temperature, attributed to the competition between these interactions [33].

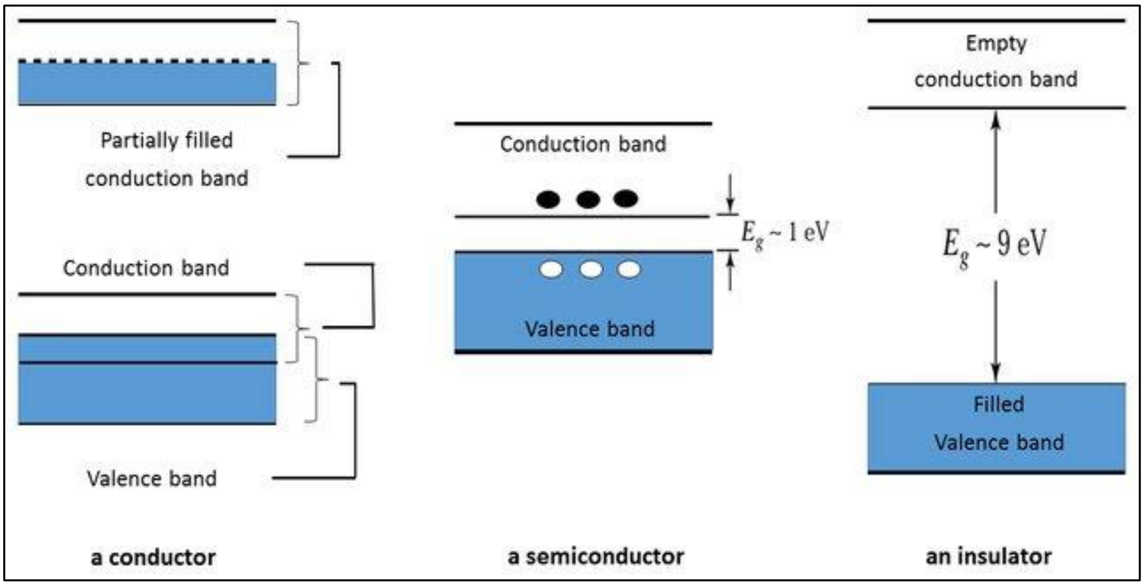

Figure I.6. Energy band diagrams illustrating the differences between conductors, semiconductors, and insulators [34].

6-4-2- Pressure

Pressure profoundly affects the crystalline behavior of perovskites, influencing their structural, elastic, and electronic properties. Studies have indicated that under high pressure, perovskites can undergo phase transitions leading to changes in mechanical stability [35].

For example, in the case of $CsSnBr_3$ perovskite, applying hydrostatic pressure results in a semiconductor-to-metal phase transition. At ambient pressure, $CsSnBr_3$ exhibits a bandgap of approximately 0.63 eV. However, as pressure increases, the valence and conduction bands converge, leading to metallic behavior at pressures around 14 GPa [35].

This transition is attributed to the shifting of the valence band maximum and conduction band minimum toward the Fermi level under pressure, effectively closing the bandgap. Such pressure-induced transitions are critical in determining the mechanical and electronic stability of perovskite materials [35].

6-4-3- Properties of perovskites

Due to their unique properties, perovskites find applications in optical and energy sectors. Key properties include:

A. Electronic roperties

The electronic properties of perovskites can be effectively described using band theory, which provides insights into electron behavior within these materials.

Band theory

Band theory explains how atomic orbitals combine to form energy bands in solids. In perovskites, this theory applies to the arrangement of atoms and the resulting electronic states.

- Valence Band Formed by bonding orbitals, this band is fully occupied by electrons and represents the highest energy levels of electrons in the material.
- Conduction Band Formed by anti-bonding orbitals, this band is typically unoccupied in insulators and semiconductors. The energy difference between the valence and conduction bands is known as the bandgap (Eg).

The energy band diagram visually represents the valence and conduction bands and the bandgap between them. The width of this gap is crucial in determining the electrical behavior of the material:

- Insulators Possess a wide bandgap (usually > 4 eV), preventing electron movement from the valence to the conduction band.
- Semiconductors Have a moderate bandgap (approximately 0.1 eV to 4 eV), allowing some electron movement under certain conditions, such as increased temperature or doping.
- Metals The conduction band overlaps with the valence band, permitting free electron movement and high conductivity.

In perovskites, the bandgap can be tuned by altering their composition and structure. For instance, methylammonium lead iodide perovskites exhibit a direct bandgap, which is beneficial for optical applications. However, due to spin-orbit coupling, a weakly indirect bandgap may also be present [36] .

B. Optical properties

Perovskites exhibit outstanding optical properties, making them ideal for applications in solar cells and optical detectors.

- High absorption coefficient perovskites display a high absorption coefficient within the visible spectrum, enabling efficient light capture. This characteristic is crucial for enhancing the performance of solar cells and photodetectors [37].

- Tunable band gap the band gap of perovskites can be tuned by altering their composition. this flexibility allows optimization for specific applications, enhancing their versatility across various optical devices [38].

- Long carrier lifetimes charge carriers (electrons and holes) in perovskites exhibit extended lifetimes, reducing recombination and boosting the efficiency of solar cells and photodetectors [38].

- High Photoluminescence quantum yield perovskites efficiently convert absorbed light into emitted light, which is essential for applications such as light-emitting diodes (LEDs) [38].

- Low recombination rates the low recombination rate of carriers in perovskites further contributes to the enhanced performance of photovoltaic and optical devices [38].

Property	**Benefit**
High Absorption Coefficient	Enhanced light capture
Tunable Band Gap	Customization for specific applications
Long Carrier Lifetimes	Improved device efficiency
High Photoluminescence Quantum Yield	Efficient light emission
Low Recombination Rates	Reduced carrier loss

C. Electrical properties

Perovskites show excellent electrical properties critical for electronic and optical applications.

- High charge carrier mobility the mobility of electrons and holes in perovskites is significantly high, allowing for rapid and efficient charge transport [39] .

- Long diffusion lengths photo-generated carriers can travel long distances before recombination, which is vital for the efficiency of optical devices .

D. Thermal and mechanical properties

Thermal and mechanical behaviors of perovskites are key for their integration into technologies like photovoltaics and flexible electronics.

- Thermal stability maintaining structural integrity at high temperatures is essential, especially in environments with significant thermal stress like solar panel surfaces [40].

- Mechanical flexibility some perovskite materials can be fabricated as thin, flexible films, making them suitable for wearable electronics and flexible displays[41].

E. Ferroelectric and piezoelectric properties

Certain perovskite structures exhibit ferroelectric and piezoelectric characteristics.

- Ferroelectricity some perovskites possess spontaneous electric polarization that can be reversed by an external electric field[42].

- Piezoelectricity these materials can generate an electric charge in response to mechanical stress, making them useful for sensors and actuators [42].

F. Chemical properties

The ABX_3 structure of perovskites provides versatility for chemical modifications.

- A-Site cation substitution organic (e.g., methylammonium, formamidinium) and inorganic (e.g., cesium, rubidium) cations can be incorporated to tailor band gaps, stability, and charge transport [43].

- B^-Site cation substitution the metal cation (commonly Pb^{2+} or Sn^{2+}) can be replaced with elements like Ge^{2+} or Mn^{2+}, allowing fine-tuning of the material's properties [11].

- Halide anion substitution modifying the halide (Cl^-, Br^-, I^-) composition enables control over the optical and electronic behavior [43].

6-5- Derivatives of perovskite structures the exceptional structural

flexibility of the ABX_3 lattice enables the formation of a wide range of derivative perovskite structures. These derivatives are obtained through cation substitution, vacancy engineering, dimensional reduction, or cation ordering, and are designed to overcome the limitations of conventional perovskites while preserving their advantageous properties [44].

6-6- Vacancy ordered perovskites (A_2BX_6)

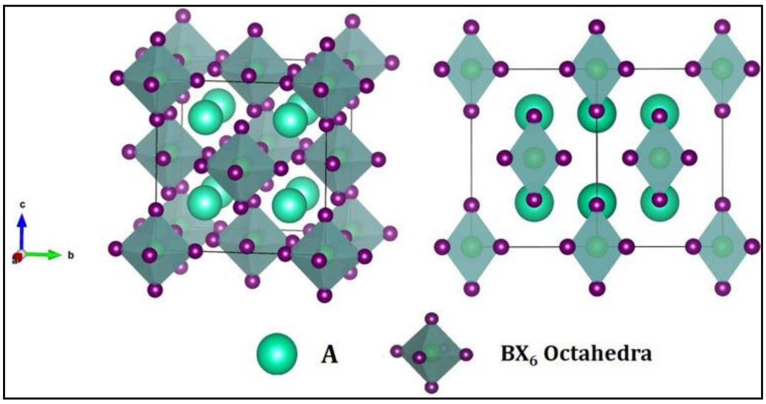

Figure I.7. Schematic crystal structures of A_2BX_6 compounds in cubic $Fm\overline{3}m$ (Left) and reorientation of the unit cell (right). The BX_6 octahedra are shaded, with the X atom on the corners. The A cations are in the hole between BX_6 octahedra [45].

Vacancy-ordered perovskites are derived from the parent ABX_3 structure by systematically removing half of the B-site cations, leading to compounds with the formula A_2BX_6 [45]. This modification introduces ordered vacancies that enhance chemical and environmental stability. However, the presence of vacancies often results in indirect band gaps and reduced charge carrier mobility

6-7- Layered and low dimensional perovskites

Perovskites Layered perovskites, such as Ruddlesden Popper and Dion Jacobson phases, are formed by inserting spacer layers between perovskite slabs [46]. This dimensional reduction improves moisture resistance and structural stability while introducing quantum confinement effects that modify the optical response [47].

Layered perovskite structures, such as the Ruddlesden Popper (RP) and Dion Jacobson (DJ) phases, are derived from the 3D perovskite network by inserting organic spacer cations between inorganic octahedral sheets. The differences in spacer type and interlayer interactions result in distinct stacking motifs and physical properties

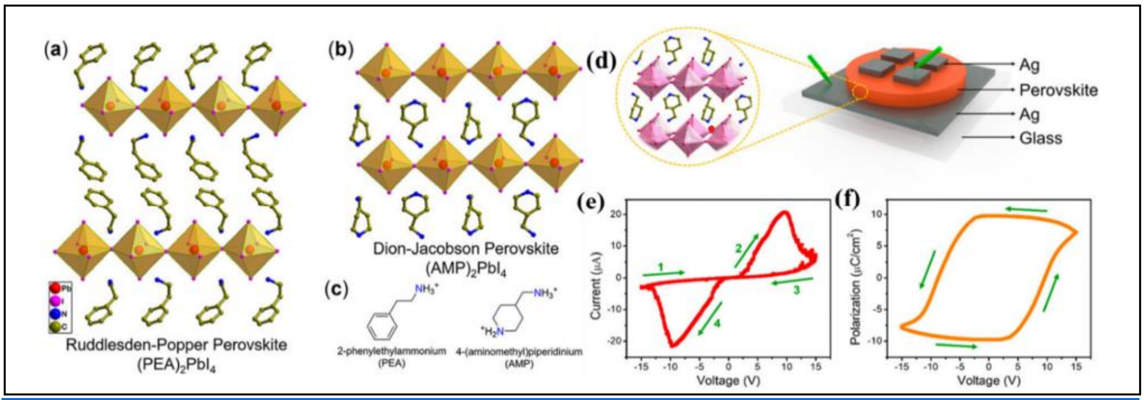

Figure I.8. Crystal structures of layered 2D perovskites: (a) ruddlesden popper (RP) iayered perovskite, and (b) dion Jacobson (DJ) iayered perovskite. these structures consist of inorganic octahedral sheets separated by organic spacer cations, with differences in interlayer bonding and stacking [47].

6-8- Mixed cation and mixed halide perovskites

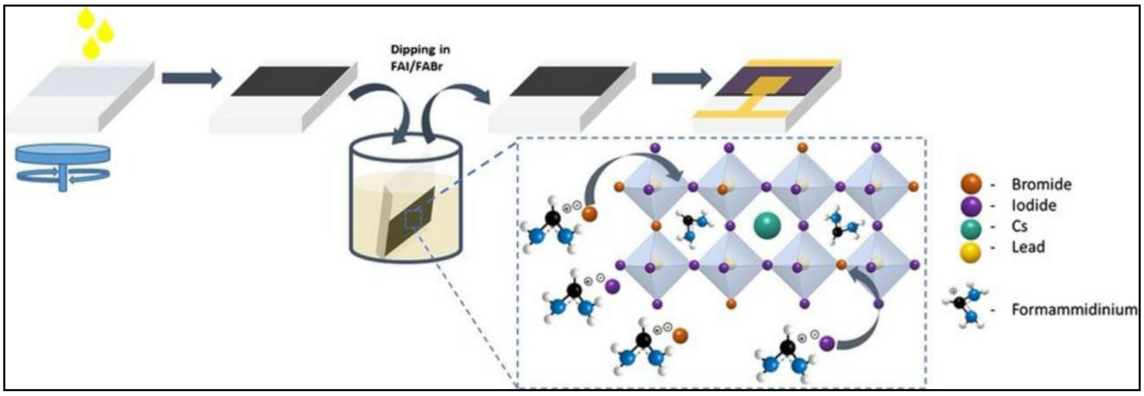

Figure I.9. Schematic illustration of mixed cation mixed halide perovskite structure showing partial substitution at both A site cations and halide (X) anions, enabling tunable band gaps and stability [48].

Another important derivative approach involves partial substitution at the A, B, or X sites. Mixed-cation and mixed-halide perovskites enable fine-tuning of band gaps, lattice constants, and carrier dynamics, although compositional disorder may affect long-term stability [48].

6-9- Transition toward double perovskites

While the aforementioned derivatives improve certain aspects of conventional perovskites, they do not fully resolve issues related to lead toxicity and thermal robustness. This limitation motivated the development of double perovskites, which represent a structurally ordered and chemically versatile evolution of the perovskite family.

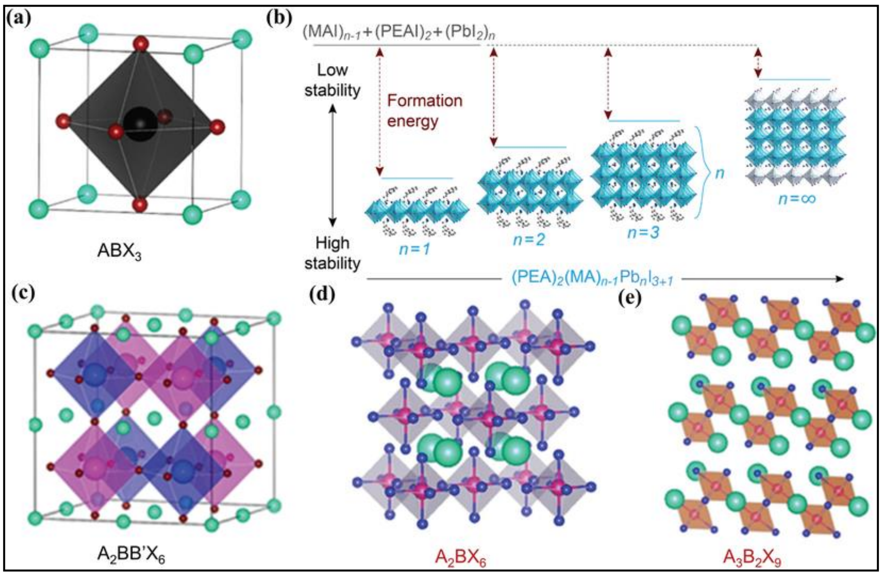

Figure I.10. Structural transition from 3D perovskite (ABX_3) to double perovskite ($A_2BB'X_6$) showing ordered B/B′ cations and enhanced stability [49].

The transition from the simple cubic perovskite (ABX_3) to the double perovskite ($A_2BB'X_6$) occurs through heterovalent substitution at the B-site, where two divalent cations are replaced by a monovalent (B^+) and a trivalent cation (B^{3+}), arranged in an ordered rock-salt pattern. This transformation expands the compositional space and enhances structural stability, which is crucial for tailoring optoelectronic and thermal properties in energy applications [50].

6-10- Double perovskites structure, physics, and energy applications Structural origin and chemical formula

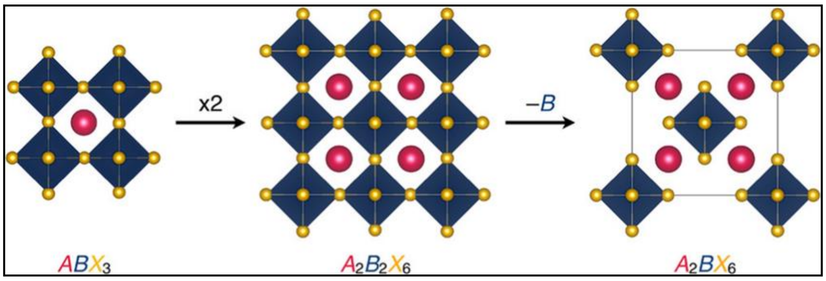

Figure I.11. A visual demonstration of the vacancy ordered double perovskite structure [51].

Double perovskites are characterized by the general formula $A_2BB'X_6$, where two different metal cations alternately occupy the B-site of the perovskite lattice. This ordered substitution preserves charge neutrality and significantly enhances structural stability compared to conventional ABX_3 perovskites [51].

7- Crystallography and cation ordering

Most halide double perovskites crystallize in the cubic Fm-3m space group [52]. The rock-salt ordering of B and B′ cations minimizes electrostatic repulsion and suppresses defect formation, leading to improved thermal and chemical stability [53].

1. General crystal structure and chemical framework

Double perovskites crystallize in the general chemical formula $A_2BB'X_6$ where A is a monovalent cation (e.g., Cs^+, Rb^+), B and B′ are heterovalent cations (commonly divalent and tetravalent), and X is an anion, typically a halogen (Cl^-, Br^-, or I^-). Structurally, double perovskites are derived from the parent ABX_3 perovskite by replacing two identical B-site cations with two chemically distinct cations, which induces long-range ordering and significantly modifies the crystal chemistry and lattice dynamics of the system [54].

The crystal structure consists of a three-dimensional framework of corner-sharing BX_6 and $B'X_6$ octahedra, forming a rigid inorganic network, while the A-site cations occupy 12-fold coordinated cuboctahedral cavities. The chemical bonding exhibits mixed ionic–covalent character due to strong hybridization between B/B′ orbitals and X p orbitals, which plays a crucial role in determining the electronic band structure and optical properties

2. Cation ordering mechanism and thermodynamic stability

A defining feature of double perovskites is the long-range ordering of B and B′ cations, which typically follows a rock-salt type ordering within the octahedral sublattice [4,11]. In this configuration, B and B′ cations occupy alternating crystallographic positions, maximizing B–X–B′ connectivity and minimizing electrostatic repulsion. The thermodynamic stability of this ordering is governed by the charge difference (ΔZ), ionic radius mismatch (Δr), electrostatic energy minimization, and the competition between ordering energy and configurational entropy at finite temperatures [55]. This ordered arrangement leads to a doubling of the primitive unit cell compared to conventional ABX_3 perovskites and suppresses antisite disorder, thereby lowering the total energy of the system

3. Cubic phase high symmetry reference structure ($\boldsymbol{Fm\bar{3}m}$)

In the ideal high-symmetry phase, double perovskites crystallize in the $Fm\bar{3}m$ (No. 225) space group, characterized by a face-centered cubic Bravais lattice, inversion symmetry, and high electronic band degeneracy [56].

Typical wyckoff positions are • A: 8c (¼, ¼, ¼) • B: 4a (0, 0, 0) • B′: 4b (½, ½, ½) • X: 24e (x, 0, 0) In this phase, all BX_6 and $B'X_6$ octahedra are undistorted, and B–X–B′ bond angles are exactly 180°, resulting in isotropic mechanical, electronic, and optical properties . The internal anion coordinate x controls the B–X bond lengths and provides a sensitive indicator of incipient structural distortions.

4. Structural distortions and lower symmetry phases

Upon temperature reduction, epitaxial strain, or pressure application, the cubic symmetry may be lowered, leading to a sequence of structural phase transitions .

5. Tetragonal phase

The tetragonal phase (I4/m or P4/mmm) is characterized by octahedral rotations mainly along the c-axis, slight deviations of B–X–B′ bond angles from 180°, and splitting of Wyckoff positions due to symmetry reduction .

These distortions introduce partial electronic and optical anisotropy and are commonly described using Glazer tilt notation $a^0a^0c^-$.

6. Orthorhombic phase

Further symmetry lowering leads to the orthorhombic phase (Pnma or Pbnm), associated with cooperative octahedral tilting along multiple crystallographic directions, unequal lattice parameters ($a \neq b \neq c$), and multiple inequivalent anion sites . This phase is often accompanied by enhanced electron–phonon coupling and stronger lattice anharmonicity .

7. Monoclinic phase

The lowest-symmetry structure frequently observed in double perovskites is the monoclinic phase ($P2_1/n$), which still preserves long-range B/B′ ordering .

It exhibits strong octahedral distortions, non-orthogonal lattice angles ($\beta \neq 90°$), and significant band-symmetry reduction, which strongly affects charge transport, dielectric response, and thermoelectric performance .

8. Octahedral tilting and glazer notation

Octahedral tilting in double perovskites is systematically classified using Glazer notation [57]. Cubic: $a^0a^0a^0$, Tetragonal: $a^0a^0c^-$, Orthorhombic: $a^-a^-c^+$, Monoclinic: $a^-b^-c^+$ These tilts reduce crystallographic symmetry, split electronic bands, activate Raman- and infrared-active phonon modes, and enhance electron phonon interactions[58].

9. Historical development

The first studies on double perovskites were conducted on oxide materials in the mid-20th century. However, modern interest in halide double perovskites began in 2016 with the work of Slavney et al., who introduced $Cs_2AgBiBr_6$ as a lead-free perovskite for optoelectronic applications [59].

10. Electronic and optical properties

The electronic structure of double perovskites enables band gap engineering through selective cation substitution. These materials exhibit tunable optical absorption and long carrier lifetimes, making them promising for photovoltaics and photodetectors.

11. Thermal properties and phonon transport

Double perovskites exhibit reduced lattice thermal conductivity due to mass disorder and phonon scattering. Phonon calculations confirm their dynamic stability, which is critical for thermoelectric and high-temperature energy applications .

12. Applications and relevance to this thesis

Double perovskites have emerged as a highly versatile class of functional materials, attracting considerable attention for a broad range of energy-related applications. In the field of photovoltaics, lead-free halide double perovskites offer a sustainable alternative to conventional lead-based perovskites, combining suitable band gaps, strong optical absorption, and enhanced environmental stability .

Their reduced sensitivity to moisture and thermal stress makes them promising candidates for long-term solar energy conversion devices . In light-emitting diodes (LEDs) and photodetectors, double perovskites exhibit efficient light matter interaction, long charge carrier lifetimes, and low non-radiative recombination rates, which are essential for achieving high luminescence efficiency and fast photoresponse . Furthermore, the presence of heavy elements in many double perovskite compositions enhances spin–orbit coupling, enabling tunable optical transitions and improved radiative recombination characteristics . From a thermoelectric perspective, double perovskites are particularly attractive due to their intrinsically low lattice thermal conductivity, which arises from mass contrast and phonon scattering associated with the ordered B-site cation sublattice.

When combined with favorable electronic transport properties, this feature makes double perovskites promising candidates for thermal energy harvesting and waste-heat recovery applications . In this thesis, ab initio density functional theory (DFT) calculations are employed to systematically investigate the structural, electronic, optical, and thermal properties of selected double perovskite compounds [60] . This computational approach enables a predictive understanding of structure–property relationships, allowing for the rational design and optimization of double perovskites for next-generation optoelectronic

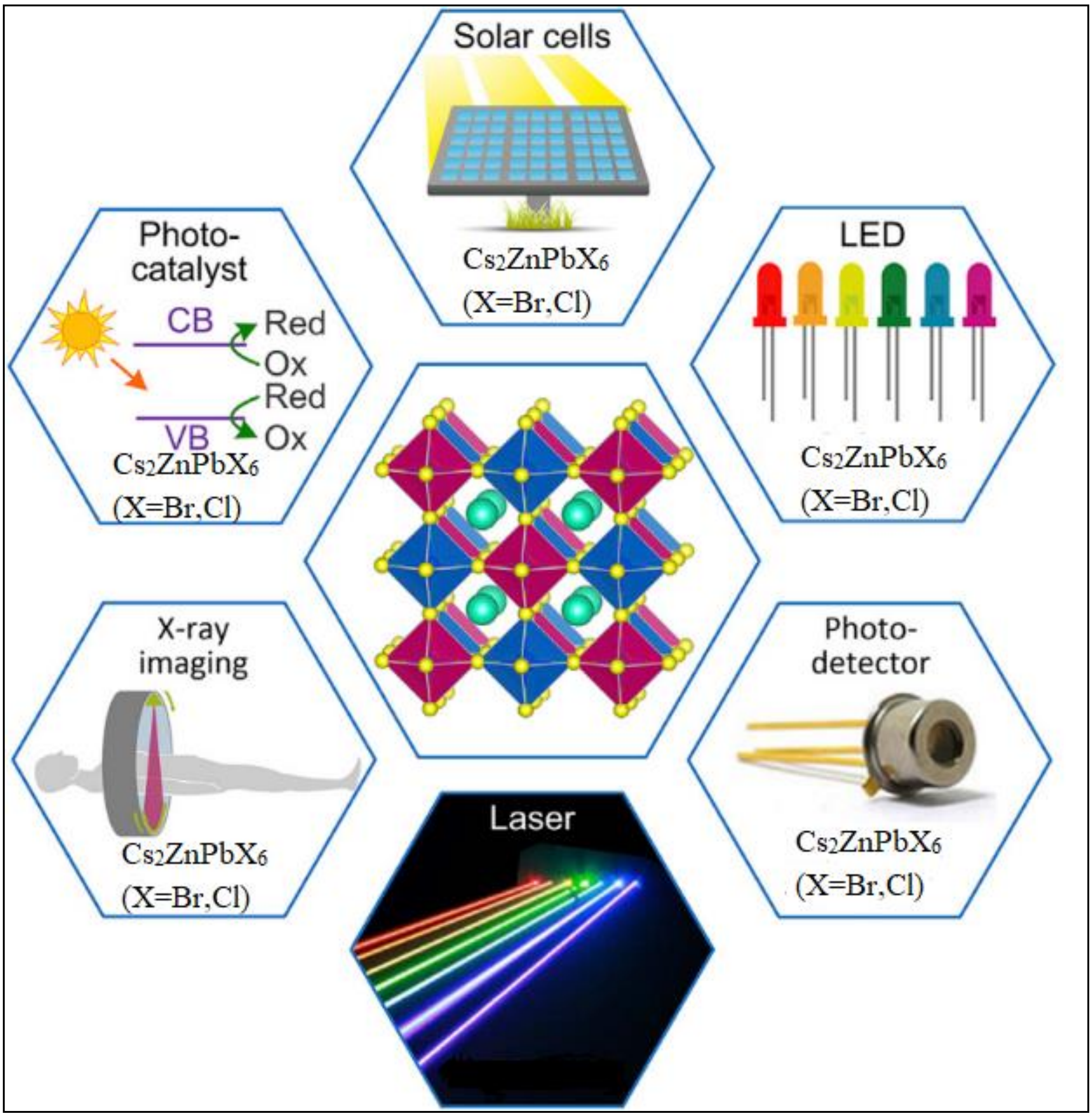

Figure I.12. Applications of double perovskite materials [49].

CHAPTER 2 :

Calculation techniques and Density Functional Theory (DFT)

1- Introduction

Numerical simulations have gained significant importance in recent years. in the physical sciences. The rapid development of computing has contributed significantly to the prediction of new materials or alloys whose properties are important. In materials science, this type of approximation has developed to understand and explore the behavior of matter at the atomic scale. The first-principles methods known as "ab-initio" are among the methods of modeling and simulation most accredited for studying materials at the atomic scale atomic, which allows for obtaining a wide range of information about the origin microscopic origin of the properties of materials. Quantum simulations allow

To study today systems comprising up to several hundred atoms.

Density Functional Theory (DFT) stands out as a widely embraced and highly effective quantum mechanical strategy for exploring matter. Rooted in the realm of quantum mechanical modeling, this approach delves into material behavior by determining the basic state of the system by the solution of the Schrödinger equation (SE). The core concept of Density Functional Theory (DFT) revolves around characterizing a complex interacting system of particles based on their density, rather than relying on the wave function. This approach holds great importance as it condenses the immense An N-body system has 3N degrees of freedom that are intrinsic to only three spatial coordinates., all achieved by utilizing the particle density. The theory finds its roots in the innovative contributions made by Thomas[61]. and Fermi [62]. during the early 1930s of the twentieth century. This foundation was subsequently built upon and enhanced by the efforts of Hartree[63]. Dirac [64]. Fock[65]. and Slater. However, it wasn't until nearly four decades after the seminal work of Thomas and Fermi that Hohenberg, Kohn, and Sham established a solid and comprehensive framework for the hypothesis.

Equilibrium geometries, electronic, optical, activation, and reaction energies are among the features that may be computed using DFT. This section will provide an exploration of the fundamental principles and historical context of DFT. Additionally; we will introduce essential concepts within the realm of DFT.

To better understand the techniques used in ab-initio methods, we we will now discuss the Schrödinger equation, the different methods, approximations and the basic concepts deemed necessary for understanding the work completed in this manuscript.

2- Many-body system

The behavior of a quantum system is dictated by the Hamiltonian operator$\widehat{H}$. If $|\Psi\rangle$ is a quantum state of the system in an abstract Hilbert space representation, its time-evolution is given by

$$i\hbar = \hat{H}\Psi \qquad \text{(II.1)}$$

The eigenvalue equation is solved to yield stationary states with specified energies, especially the system's ground state

$$\hat{H}|\Psi\rangle = E|\Psi\rangle , \langle\Psi|\Psi\rangle = 1 \qquad \text{(II.2)}$$

Alternatively, they are obtained as stationary solutions of the variational problem.

$$\frac{\langle\Psi|\hat{H}|\Psi\rangle}{\langle\Psi|\Psi\rangle} \rightrightarrows stationary \qquad \text{(II.3)}$$

Our focus lies on system encompassing N electrons and M nuclei, dynamically navigating through a specified external field while engaging in pairwise interactions. In this context, the total wave function of the system can be expressed as

$$\psi = \psi(\vec{r_1}, \vec{r_2}, \dots \vec{r_N}; \vec{R_1}, \vec{R_2}, \dots, \vec{R_M}) \qquad \text{(II.4)}$$

And the Hamiltonian consists of

$$\hat{H} = \hat{T}_N + \hat{T}_e + \hat{V}_{N-N} + \hat{V}_{N-e} + \hat{V}_{e-e} \qquad \text{(II.5)}$$

Where

$T_N = -\sum_{I=1}^{M} \frac{\hbar^2}{2M_I} \nabla_I^2$: Kinetic energy of nuclei

$T_e = -\sum_{I=1}^{N} \frac{\hbar^2}{2m_e} \nabla_i^2$: Kinetic energy of electrons

$$V_{N-N} = \frac{1}{2}\sum_{I\neq J} \frac{e^2}{4\pi\varepsilon_0} \frac{Z_I Z_J}{|\vec{R_I} - \vec{R_J}|} \qquad \text{(II.6)}$$

$V_{N-e} = \frac{1}{2}\sum_{i,J} \frac{e^2}{4\pi\varepsilon_0} \frac{Z_I}{|\vec{r_i} - \vec{R_J}|}$:Potential energy of nucleus-electron coulomb interaction

$V_{e-e} = \frac{1}{2}\sum_{i\neq J} \frac{e^2}{4\pi\varepsilon_0} \frac{1}{|\vec{r_i} - \vec{r_j}|}$: Electron-electron coulomb interaction potential energy

The wave function essentially holds all the details about a specific system [61]. When dealing with a system like the hydrogen atom, precise solutions to the Schrödinger equation can be obtained. When confronted with systems comprising multiple particles (referred to as Nbody systems), achieving exact solutions presents a formidable challenge. The complexity inherent in these systems necessitates the adoption of streamlined approaches and approximation techniques to effectively grapple with the intricacies of the problem at hand

3- Fundamentals of quantum chemistry

The fundamental concepts employed in modeling theories are briefly summarized here to provide a coherent framework for understanding the evolution of computational approaches.

3-1- Schrödinger equation

The foundational equation for describing the electronic structure of a system comprising multiple nuclei (of mass *M*) and electrons (of mass *m*) was formulated by Erwin Schrödinger in 1925. Known as the Schrödinger equation, it governs stationary states and is expressed as follows [66].

$$\mathrm{H}\Psi = \left[-\sum_{\mathrm{i}}^{\mathrm{N}}\frac{\hbar^2}{2\mathrm{m}}\nabla_{\mathrm{i}}^2 - \sum_{\mathrm{I}}^{\mathrm{A}}\frac{\hbar^2}{2\mathrm{M}}\nabla_{\mathrm{I}}^2 - \sum_{\mathrm{i,I}}^{\mathrm{N}}\frac{\mathrm{Z_I\ e^2}}{|\vec{\mathrm{r_i}}-\vec{\mathrm{R_I}}|} + \sum_{\mathrm{i}<I}^{\mathrm{N}}\frac{\mathrm{e^2}}{|\vec{\mathrm{r_i}}-\vec{\mathrm{r_I}}|} + \sum_{\mathrm{I}<J}^{\mathrm{N}}\frac{\mathrm{Z_I\ Z_J e^2}}{|\vec{\mathrm{R_I}}-\vec{\mathrm{R_J}}|}\right] = \mathrm{E}\Psi \qquad \text{(II.7)}$$

where

- *H* represents the molecular Hamiltonian, the operator associated with the system's total energy *E*.
- *Ψ* denotes the wave function depending on the coordinates of both nuclei and electrons, encompassing all information about the molecular system under study.

In this formulation, the first two terms of the Hamiltonian correspond to the kinetic energy operators for the N electrons (indexed by i) and the A nuclei (indexed by I), respectively. The subsequent three terms account for correlation potentials: the electron-nucleus Coulombic attraction, electron-electron repulsion, and nucleus-nucleus repulsion.

Through solving the Schrödinger equation, one can determine a range of molecular properties such as molecular geometries, relative stabilities between different systems, vibrational spectra, and dipole and multipole moments.

Generally, for complex molecular systems, obtaining exact solutions for electronic spectra and reactivity descriptors such as atomic charges is unfeasible. Thus, various approximations must be employed to overcome these inherent computational challenges.

3-2- Born-Oppenheimer approximation

To simplify the Schrödinger equation, the Born-Oppenheimer approximation [67]. assumes that atomic nuclei are significantly more massive than electrons. As a result, their motion is considered extremely slow relative to the rapid dynamics of electrons. Therefore, the electronic behavior within a molecule can be studied by assuming the nuclei are fixed at specific spatial positions (which are not necessarily equilibrium positions). This assumption leads to the neglect of the nuclei's kinetic energy and treats the nucleus-nucleus interaction term as a constant.

Numerous methods have been developed to solve the multi-electron Schrödinger equation by describing the wave function, for example, as a Slater determinant, as is the case in the Hartree-Fock (HF) method.

Alternatively, Density Functional Theory (DFT) offers a different approach by using the electron density as the fundamental entity for system description.

Under the Born-Oppenheimer approximation, the Schrödinger equation governing the electrons can be rewritten as

$$\mathrm{H_{el}\Psi_{el} = E_{el}\Psi_{el}} \qquad \text{(II.8)}$$

where

- $\boldsymbol{H_{el}}$ is the electronic Hamiltonian (excluding spin), which corresponds to the total Hamiltonian without the kinetic energy of the nuclei and the nuclear repulsion terms.

The total Hamiltonian of the system can be expressed as

$$\mathrm{H} = \mathrm{H_{el}} + \mathrm{V_{NN}} \tag{II.9}$$

where $\boldsymbol{V_{NN}}$ denotes the repulsion between nuclei.

This assumption implies that the nuclear repulsion term $\hat{V}_{NN}$ can be treated as constant. Consequently, for fixed nuclear positions, the total energy of the system is given by

$$\mathrm{E} = \mathrm{E_{el}} + \mathrm{V_{NN}} \tag{II.10}$$

3-3- Linear combination of atomic orbitals (LCAO) approximation

The **Linear Combination of Atomic Orbitals (LCAO)** approximation expresses the mono-electronic function $\boldsymbol{\psi_i(i)}$ as a linear combination of atomic orbitals centered on the atoms of the molecular structure

$$\Psi = \psi_1(1)\psi_2(2)\psi_3(3)\ldots\ldots\psi_n(n) \tag{II.11}$$

However, to fully describe the electron distribution, spin coordinates must be introduced. The product of a spatial wave function (OM) and a spin function $\boldsymbol{\eta(i)}$ is referred to as a spin-orbital

$$\chi(i) = \psi(i)\eta(i) \tag{II.12}$$

where

η(i) = *α(i)* or *β(i)*, representing one of the two possible spin functions for an electron.

- Consequently, for a system containing *n* electrons, the simplest form of the wave function is the product of the spin-orbitals

Consequently, for a system containing *n* electrons, the simplest form of the wave function is the product of the spin-orbitals

$$\Psi = \chi_1(1)\chi_2(2)\chi_3(3)\ldots\ldots\chi_n(n) \tag{II.13}$$

This wave function does not take into account the indistinguishability of electrons. It must satisfy the Pauli exclusion principle [68]. which dictates that exchanging the coordinates of two electrons *i* and *j* must result in a sign change of the wave function.

To address indistinguishability and ensure antisymmetry, the wave function is expressed as a **Slater determinant** [69].

$$\Psi = \frac{1}{\sqrt{n!}}\begin{vmatrix} \chi_1(1) & \chi_2(1) & \cdots & \chi_n(1) \\ \chi_1(2) & \chi_2(2) & \cdots & \chi_n(2) \\ \vdots & \vdots & \ddots & \vdots \\ \chi_1(n) & \chi_2(n) & \cdots & \chi_n(n) \end{vmatrix} \quad \text{(II.14)}$$

where $\frac{1}{\sqrt{n!}}$ is the normalization factor.

3-4- Linear combination of atomic orbitals (LCAO) approximation

The LCAO approximation involves expressing the mono-electronic function ψ_μ as a linear combination of atomic orbitals centered on the atoms within the molecular structure

$$\psi_i = \sum_\mu c_{\mu i}\phi_\mu \quad \text{(II.15)}$$

where

- ψ_i : denotes the molecular orbitals (OM),
- $\psi\mu$: denotes the atomic orbitals (OA).

Using the LCAO formalism, the determination of coefficients $c_{\mu i}$that minimize the electronic energy *E* requires recasting the previous equation into the **Roothaan-Hall equations** [70].

$$\sum_v F_{\mu v} c_{vi} = \varepsilon_i \sum_v S_{\mu v} c_{vi} \quad \text{(II.16)}$$

$$F_{\mu v} = H^c_{\mu v} + \sum_{\lambda\sigma} P_{\lambda\sigma}\left[(\mu v|\lambda\sigma) - \frac{1}{2}(\mu\sigma|\lambda v)\right] \quad \text{(II.17)}$$

where

- $S_{\mu v}$: elements of the overlap matrix,
- $F_{\mu v}$: elements of the Fock matrix,
- $H_{\mu v}^{c}$: elements of the core Hamiltonian matrix,

$P_{\lambda\sigma}$: Elements of the density matrix, defined as: $P_{\lambda\sigma} = 2\sum_{i}^{occ} c_{\lambda i}^{*} c_{\sigma i}$

- $(\mu v|\lambda\sigma)$and $(\mu\sigma|\lambda v)$: two-electron integrals corresponding to Coulomb and exchange terms respectively, defined as

$$(\mu v|\lambda\sigma) = \int_{(1)}\int_{(2)} \phi_{\mu}(1)\phi_{v}(1)\frac{1}{r_{12}}\phi_{\lambda}(2)\phi_{\sigma}(2)d\tau_{1}d\tau_{2} \qquad \text{(II.18)}$$

However, the energy obtained from the Roothaan-Hall equations is equivalent to the Hartree-Fock energy only if an infinite basis set is used.

4- Calculation methods

4-1- Empirical methods

Among empirical (i.e., non-quantum) methods, molecular mechanics and classical molecular dynamics are the most widely employed. Molecular mechanics is a conformational analysis technique based on the use of empirical force fields and energy minimization. It describes the energy as a function of atomic coordinates and seeks to identify energy minima corresponding to stable conformers[71,72].

However, this method does not account for energy variations over time or temperature effects (entropy, free energy), nor does it allow the crossing of energy barriers. Classical molecular dynamics aims to calculate the movements of molecules, often using energies derived from molecular mechanics, by applying the laws of classical mechanics. This approach enables the simulation of system evolution over time [73,74]

4-2- Semi-empirical methods

The Latin term ab initio means "from the beginning" and refers to calculations derived solely from theoretical principles (i.e., approximate quantum mechanical calculations) without incorporating experimental data. Ab initio calculations at the Hartree-Fock level—and especially post-Hartree-Fock methods—are highly demanding in terms of computational time. This computational cost increases rapidly with the number of atoms, or more precisely, with the number of basis functions. In response to this challenge, semi-empirical methods were developed [75]. These methods significantly reduce the number of integrals that need to be computed by introducing experimental data and rely on the following key approximations

1. Only valence shell orbitals, represented by Slater-type orbitals, are considered;
2. Overlap integrals are neglected when solving the SCF equations;
3. All three- and four-center two-electron integrals are assumed to be zero. Additionally, depending on the specific method, some one- and two-center two-electron integrals may also be neglected;
4. The off-diagonal elements of the core Hamiltonian matrix, assumed proportional to the overlap integrals between the corresponding atomic orbitals, are determined through empirical relations;
5. Most one- and two-electron integrals involving a single center are often estimated from experimental electronic spectra data.

Among the existing semi-empirical approaches are methods of the NDDO type (Neglect of Diatomic Differential Overlap), such as AM1 [76]. and PM3. At this level of approximation, all integrals involving the differential overlap between orbitals centered on different atoms are neglected. In parallel, in the CNDO (Complete Neglect of Differential Overlap) method, differential overlaps are completely disregarded.

5- Hartree-Fock (HF) method

A fundamental characteristic of the electronic Hamiltonian is the presence of a bi-electronic term (representing the interaction of each electron with other electrons). The HF theory employs the variational principle, which states that: The energy calculated for a given electronic state of a system (described by any arbitrary wave function Ψ) is always greater than the energy obtained for the same state using a wave function that is the solution to the Schrödinger equation.

5-1- Hartree-Fock equations

Given a wave function Ψ in the form of a Slater determinant, the equation to solve in order to calculate the corresponding electronic energy E is as follows

$$E = \langle \Psi | \hat{H} | \Psi \rangle = \sum_{i=1}^{n} \langle \chi_i(1) | H^c(1) | \chi_i(1) \rangle \quad + \sum_{i=1}^{n} \sum_{j=1}^{i-1} [\langle \chi_i(1)\chi_j(2) | \frac{1}{r_{12}} | \chi_i(1)\chi_j(2) \rangle - \langle \chi_i(1)\chi_j(2) | \frac{1}{r_{12}} | \chi_i(2)\chi_j(1) \rangle] \quad \text{(II.19)}$$

The solution of this equation relies on the variational principle, which aims to find the best spin-orbitals and, consequently, the best molecular orbitals that minimize the electronic energy E as much as possible [77,78]. It is important to note that these orbitals, corresponding to the minimum energy E, must satisfy the condition that any modification made to a given orbital (without altering its norm or orthogonality to other orbitals) does not result in a variation of the energy E. This condition requires the orbitals to be eigenfunctions of an operator F, called the Fock operator. The corresponding Hartree-Fock equations [77,79]. determine these orbitals as follows

$$F(1)\psi_i(1) = \varepsilon_i \psi_i(1) \qquad \text{(II.20)}$$

Where $\boldsymbol{\varepsilon_i}$ is the energy of the orbital $\psi._i$

with

$$\mathrm{F}(1) = H^c(1) + \sum_i J_i(1) - K_i\,(1) \qquad \text{(II.21)}$$

J_i: Coulomb operator

$\boldsymbol{K_i}$: Exchange operator

5-2- Hartree approximation

The complexity of solving equation (II.6) is due to electron-electron interactions, which prevents the separation of this equation into n electronic equations. In the Hartree approximation [80]. We consider the electrons as independent, in which each electron moves in a middle field created by nuclei and other electrons.

The Hamiltonian can be written

$$\hat{\mathrm{H}}_e = \sum_i \mathrm{h}_i \qquad \text{(II.22)}$$

Whereh$_i$is : the mono electronic hamiltonian.

$$\mathrm{h}_i = -\frac{\hbar^2}{2m_e}\nabla_i{}^2\ \hat{\mathrm{T}}_{\mathrm{e}} + \hat{\mathrm{V}}_{\mathrm{ext}}(\vec{r}) + \hat{\mathrm{V}}_{\mathrm{i}}(\vec{r}) \qquad \text{(II.23)}$$

With $\hat{\mathrm{V}}_{\mathrm{i}}(\vec{r}) = \int \frac{\rho\vec{r}\,'}{(\vec{r}-\vec{r}\,')} d^3\,\vec{r}\,'$ Hartree potential

$\hat{V}_{ext}(\vec{r})$:Coulomb interaction of the electron with all the nuclei of the system

The electronic wave function of this Hamiltonian is a product of mono-electronic functions (Hartree Product (HP)

$$\psi_e(\vec{r_1},\vec{r_2},\ldots \vec{r_N}) = \varphi_1(\vec{r_1})\ldots\ldots\varphi_N(\vec{r_N}) \qquad (II.24)$$

In this case, each of these mono-electronic wave function is then a solution of the Schrödinger equation to a particle which is written in the form

$$h_i(\vec{r})\phi_i(\vec{r}) = \varepsilon_i\phi_i(\vec{r}) \qquad (II.25)$$

The wave function described by equation (II.11) isn't quite finished. It doesn't follow Pauli's exclusion rule. his rule says that because electrons are a type of particle called "fermions," the wave function needs to switch its behavior if we swap the details of two electrons. This rule basically means that two electrons can't be in the exact same state [81]. The wave function that follows this rule has to be 'antisymmetric.'

$(r^{\rightarrow}1, r^{\rightarrow}2 \ldots r^{\rightarrow}i, r^{\rightarrow}j \ldots r^{\rightarrow}N)$ = -$(r^{\rightarrow}1, r^{\rightarrow}2 \ldots r^{\rightarrow}j, r^{\rightarrow}i \ldots r^{\rightarrow}N)$

$$\psi_e(\vec{r_1},\vec{r_2},\vec{r_i},\vec{r_j}\ldots \vec{r_N}) = -\psi_e(\vec{r_1},\vec{r_2},\vec{r_j},\vec{r_i},\ldots \vec{r_N}) \qquad (II.26)$$

5-3- Self consistent field (SCF) procedure

The previous Hartree-Fock equations are coupled because the definition of the operators J_i and $K_i$requires knowledge of the spin-orbitals that are solutions to the equation

$$F(1)\psi_i(1) = \varepsilon_i\psi_i \qquad (II.27)$$

To overcome this problem, these equations are solved iteratively. Such a procedure is known as the Self-Consistent Field (SCF) method. This method is based on an initial choice of spin-orbitals, and thus a density matrix P. Then, solving the Hartree-Fock equations yields a set of spin-orbitals, which in turn are used to define new operators. This procedure is repeated until the new density matrix ***P*** is the same as the previous one (internal consistency is reached), while considering a predefined convergence threshold [82].

5-4- Post-Hartree-Fock methods

The Hartree-Fock theory neglects the electron correlation energy. According to Lowdin [83]. the correlation energy of a system corresponds to the difference between the Hartree-Fock energy with an infinite basis (HF limit) and the exact non-relativistic energy of the system

$$\boldsymbol{E_{corr} = E_{HF}^{\infty} - E} \qquad \text{(II.28)}$$

Currently, two main categories of methods exist that allow for at least partial consideration of electronic correlation effects

- Single-reference methods
- Multi-reference methods

6- Perturbative approach møller plesset theory

Møller-Plesset perturbation theory (MP) represents one of the earliest strategies introduced to account for electronic correlation effects. Prior to the development of Density Functional Theory (DFT) methods, the MP2 approach was widely utilized to enhance Hartree-Fock (HF) calculations [84].

Within the Møller-Plesset formalism [84]. the correlation energy is treated as a perturbation to the electronic Hamiltonian, constructed from the sum of individual Fock operators

$$\mathrm{H_T = H_0 + V} \qquad \text{(II.29)}$$

where

- $\boldsymbol{H_0}$ is the zero-order term, composed of the sum of Fock operators, whose eigenfunctions correspond to the Hartree-Fock solutions,
- $\boldsymbol{V}$ represents the perturbation induced by electron correlation.

It is essential to highlight that the zero-order energy is equal to the sum of the orbital energies, whereas the first-order correction yields the Hartree-Fock energy.

In practical applications, second-order (MP2) and fourth-order (MP4) Møller-Plesset methods are the most frequently employed. Nevertheless, this approach remains valid only if the zero-order wavefunction provides a sufficiently accurate approximation of the true wavefunction. Although MP2 often delivers reliable geometries and energy predictions for many molecular systems, it may fail for systems exhibiting atypical electronic structures, such as hybrid compounds, where more sophisticated levels of theory are required.

6-1- Configuration interaction (CI) methods

Configuration Interaction (CI) methods construct a wavefunction by augmenting the Hartree-Fock (HF) wavefunction with additional determinants generated by exciting electrons from occupied to virtual orbitals. CI calculations are categorized based on the number of excitations involved in constructing each Slater determinant. Single excitation CI (CIS) considers the promotion of one electron per determinant, providing an approximation of excited states without altering the ground-state energy. In contrast, Configuration Interaction with Single and Double excitations (CISD) corrects the ground-state energy by incorporating electron correlation effects [85].

Starting from an initial Hartree-Fock wavefunction $\Psi_{\mathbf{0}}$ of defined spin multiplicity, the CI method represents the total wavefunction as a linear combination of determinants $\Psi_{\boldsymbol{a}}^{\boldsymbol{r}}$, $\Psi_{\boldsymbol{ab}}^{\boldsymbol{rs}}$., etc., which are orthogonal to each other, to $\Psi_{\mathbf{0}}$, and share the same spin multiplicity as $\Psi_{\mathbf{0}}$.

$$\Psi_{\mathrm{IC}} = \mathrm{c}_0\Psi_0 + \sum_{\mathrm{a,r}} \mathrm{c}_{\mathrm{a}}^{\mathrm{r}}\Psi_{\mathrm{a}}^{\mathrm{r}} + \sum_{\mathrm{a}<b,r<s} \mathrm{c}_{\mathrm{ab}}^{\mathrm{rs}}\Psi_{\mathrm{ab}}^{\mathrm{rs}} + \sum_{\mathrm{a}<b<c,r<s<t} \mathrm{c}_{\mathrm{abc}}^{\mathrm{rst}}\Psi_{\mathrm{abc}}^{\mathrm{rst}} \quad \text{(II.30)}$$

6-2- Configuration interaction (CI) approach

These determinants are generated by replacing one or more occupied spin-orbitals $\boldsymbol{\chi_a}$, $\boldsymbol{\chi_b}$., etc., in $\Psi_{\mathbf{0}}$ with one or more virtual spin-orbitals $\boldsymbol{\chi_r}$, et $\boldsymbol{\chi_s}$ .... , etc., resulting in configurations classified as singly, doubly, triply, and higher excited states.

The coefficients and the corresponding energies are determined based on the variational principle, which involves constructing the configuration interaction matrix $\langle\Psi_{IC}|H|\Psi_{IC}\rangle$ and solving for its eigenvalues. The lowest eigenvalue provides an upper bound for the ground-state energy, while the higher eigenvalues correspond to upper bounds of the excited-state energies.

When the wavefunction $\Psi_{\boldsymbol{IC}}$ includes all possible determinants formed from multiple excitations of $\Psi_{\mathbf{0}}$, the method is referred to as Full Configuration Interaction

(Full CI). In this case, using a complete basis set yields the exact properties of the system under study.

Certain theorems simplify the computation by eliminating some matrix elements. In particular, Brillouin's theorem [86]. states that there is no direct coupling between the Hartree-Fock wavefunction Ψ_0 and determinants corresponding to single excitations. Furthermore, all matrix elements $\langle \Psi_a | \boldsymbol{H} | \Psi_b \rangle$ where Ψ_a and Ψ_b differ by more than two spin-orbitals are zero [87].

7- Kohn-Sham equations (KS)

A practical application of density functional theory was developed by Kohn and Sham by formulating a method similar to the Hartree-Fock method. Kohn and Sham [88]. proposed that in a molecular system, the equations used to obtain the total electronic density are derived from the energy functional E[ρ(r)] which is expressed as

$$E[\rho(r)] = U[\rho(r)] + T[\rho(r)] + E_{xc}[\rho(r)] \qquad \text{(II.31)}$$

The classical electrostatic energy U[ρ(r)] represents the sum of electron-nucleus attractions and electron-electron repulsions

$$U[\rho(r)] = -\sum_A \int \frac{Z_A \rho(r)}{|r - R_A|} + \frac{1}{2} \int \int \frac{\rho(r)\rho(r')}{|r-r'|} \, dr dr' \qquad \text{(II.32)}$$

The second term T[ρ(r)] represents the kinetic energy of a system with the same density ρ(r), but in which the electrons do not interact with each other. The final term E_{xc}[ρ(r)] includes both the exchange and correlation contributions to the energy, as well as the difference between the term T[ρ(r)] and the true electronic kinetic energy of the system.

Following Kohn and Sham, the electronic density of a system with $\boldsymbol{N}$ electrons, containing $\boldsymbol{N^\alpha}$ high-spin electrons and $\boldsymbol{N^\beta}$ low-spin electrons, can be expressed as the sum of the squares of the magnitudes of orthonormal molecular orbitals, each occupied by a single electron. These molecular orbitals are called Kohn-Sham molecular orbitals.

$$\rho(r) = \rho^\alpha(r) + \rho^\beta(r) = \sum^{N_i^\alpha} |\psi_i^\alpha(r)|^2 + \sum^{N_i^\alpha} \left|\psi_i^\beta(r)\right|^2 \qquad \text{(II.33)}$$

Thus, the kinetic energy T[ρ(r)] is expressed as

$$T[\rho(r)] = \sum_{\sigma=\alpha,\beta}\sum_{i}^{N^{\sigma}} \int \psi_i^{\sigma} \frac{-\Delta}{2} \psi_i^{\sigma}(r)dr \qquad \text{(II.34)}$$

Since the energy functional is minimized with respect to the density of the ground state ρ(r), the energy functional E[ρ(r)] must be stationary with respect to any variation in the spin densities, i.e.

$$\frac{\delta E[\rho(r)]}{\delta \rho^{\alpha}(r)} = \frac{\delta E[\rho(r)]}{\delta \rho^{\beta}(r)} = \mathbf{0} \qquad \text{(II.35)}$$

This condition leads to the Kohn-Sham equations for a single electron

$$\left\{-\frac{\Delta}{2} - \left(\sum_{A} \frac{Z_A}{|r-R_A|}\right) + \int \frac{\rho'}{|r-r'|}dr' + \frac{\delta E_{xc}[\rho(r)]}{\delta \rho^{\alpha}(r)}\right\} \psi_i^{\alpha}(r) = \epsilon_i \psi_i^{\alpha}(r) \qquad \text{(II.36)}$$

With $\sigma = \alpha \; or \; \beta$, these equations are solved self-consistently, as in the case of Hartree-Fock equations.

Starting from an initial electronic density, the Kohn-Sham equations are constructed, and their solution results in a set of Kohn-Sham spin-orbitals $\boldsymbol{\psi_i^{\alpha}(r)}$, which are used to generate a new set of total spin densities $\boldsymbol{\rho^{\alpha}(r)}$ and $\boldsymbol{\rho^{\beta}(r)}$. This procedure is repeated until the system achieves self-consistency.

8- Born-oppenheimer approximation

Back in 1927, Born and Oppenheimer came up with what's called the BornOppenheimer approximation [89]. They noticed that because nuclei are way heavier than electrons (a proton weighs about 1836 times more than an electron), the nuclei move much more slowly (like a hundred times slower) compared to electrons. So, we can kind of treat their movements separately, and this is why it's called "adiabatic." When we focus on how electrons move, it makes sense to think of the nuclei as staying in one place. This simplifiesthings a bit. This way of thinking helps us write down the Hamiltonian, which is like a mathematical description of the system

$$\hat{H}_e = \hat{T}_e + \hat{V}_{N-e} + \hat{V}_{e-e} \qquad \text{(II.37)}$$

The total wave function can be written as

$$\psi\left(\overrightarrow{R_I}, \overrightarrow{r_i}\right) = \varphi N\left(\overrightarrow{R_I}\right) \psi_e\left(\overrightarrow{R_i}\right) \qquad \text{(II.38)}$$

Where $\varphi N(\overrightarrow{R_I})$ describes the nuclei and$\psi_e(\overrightarrow{R_\imath})$ describe the electrons (depending parametrically on the positions of the nuclei).With the BO approximation, The Schrödinger equation for electrons is written

$$\hat{H}_e\Psi_e = E_e\Psi_e \tag{II.39}$$

This approximation has made the problem less complicated, but it's not fully solved yet. When dealing with a system that has N electrons, we still have to keep track of 3N positions in space and N spin coordination.

9- Density functional theory

Density functional theory's main idea is to make electron density the key factor, unlike Hartree-Fock theory, which focuses on electron wave functions. The use of electron density greatly accelerates the calculations. Whereas the electronic wave function is a function of 3N variables (the coordinates of all N atoms in the system).while, the electron density is a function of only three variables (x, y, z). Therefore we need to be sure that we can derive something significant from it. Hohenburg and Kohn were the ones who introduced a theorem highlighting the usefulness of electron density. Since then, density functional theory has become extremely popular, leading to a surge of computational research in the fields of molecular and solid state physics.

For DFT, the energy is a functional of the electronic density of the system. DFT determines the properties of the ground state of a system composed of a fixed number of electrons, in Coulombic interaction with point nuclei, using only the knowledge of the electronic density. It was developed in two stages, in 1964 by Hohenberg and Kohn [90]. then in 1965 by Kohn and Sham [91]. DFT is defined as an exact theory that allows for the determination of the ground state of a system with N electrons. It consists of reducing the many-body problem to a one-body problem in an effective field that takes into account all the interactions and provides a main theoretical basis for the calculation of the band structure. Historically, the principle of this theory first appeared in the works of Thomas and Fermi [92,93]. starting from 1927. They independently demonstrated that one could use the electron density ($\rho(\vec{r})$) as a central variable to solve the Schrödinger equation. They considered the system as a homogeneous gas with kinetic energy as a functional of the electron density.

9-1- Electron density

The electron cannot be located as an individual particle, however, its probability of presence in a volume element can be estimated and corresponds to the electron density Electrons must therefore be considered in their collective (electron cloud). The electron density allows us to know the regions of the space where electrons reside most often. The electrons are essentially localized in the vicinity of the nuclei. The electron density is a positive function depending solely on the 3 coordinates (x,y,z) of space. This quantity cancels out { infinity and equals N when integrated over the entire space. It is sufficient for the determination complete determination of the properties of an atomic system.

It's not possible to localize an electron as a single particle in a specific location, but its probability of presence in an element of volume $d3r^{\rightarrow}$ can be estimated and corresponds to the electronic density $\rho(\vec{r})$

$$\psi\,(\vec{r}) = \psi_2(\vec{r}) = \rho(\vec{r}) \tag{II.40}$$

This ensures that $(\vec{r})$ will consistently possess a positive value (positive function), and this value expresses the relative probability of finding an electron at a particular position. This function has lots of properties

- $\int \rho(\vec{r})d\vec{r} = N$ (Integration over the entire space), while N is total number of electrons
- $\rho(r = \infty) = 0$
- $\rho(\vec{r})$is an observable that can be measured experimentally (by X-ray diffraction)

  All these points suggest that the electronic density alone is enough to fully understand the characteristics of an atomic system.

9-2- Hohenberg-kohn (hk) theorems

DFT really began in 1964 with the two fundamental theorems of Hohenberg and Kohn [90].This approach applies to any system { several interacting particles evolving in an external potential. The electronic wave function

electronic is a solution to the Schrödinger equation

DFT is achievable due to the presence of two cleverly uncomplicated theorems proposed and validated by Hohenberg and Kohn.in 1964

a. Theorem I

For any system of interacting particles in an external potential $V_{ext}(\vec{r}_i\,)$, the density is distinctly established. (in other words, the external potential is a unique functional of the density).

Proof

Let's assume there exist two separate external potentials $V_{ext}(\vec{r}_i)$and $V'_{ext}(\vec{r}_i)$ which differ by more than a constant and lead to the same ground state density $\rho_0(r)$. Obviously $V_{ext}(\vec{r}_i)$and $V'_{ext}(\vec{r}_i)$ belong to distinct Hamiltonians Ĥ and $\widehat{H'}$ which give rise to distinct wave functions $\Psi$and Ψ'with $\widehat{H}\,\Psi = E_0\,\Psi$and $\widehat{H'}'\,\Psi' = E'_0\,\Psi'$'. Since Ψ' is not the ground state of $\widehat{H}$,

$$E_0 < \langle \Psi' | \widehat{H} | \Psi' \rangle \tag{II.41}$$

$$E_0 < \langle \Psi' | \widehat{H'} | \Psi' \rangle + \langle \Psi' | \widehat{H} - \widehat{H'} | \Psi' \rangle \tag{II.42}$$

$$E_0 < E'_0 + \int \rho_0(r)[V_{ext}(\vec{r}_i) - V'_{ext}(\vec{r}_i)]d\vec{r} \tag{II.43}$$

Similarly

$$E_0 < \langle \Psi' | \widehat{H'} | \Psi' \rangle \tag{II.44}$$

$$E_0 < \langle \Psi' | \widehat{H'} | \Psi' \rangle + \langle \Psi' | \widehat{H'} - \widehat{H} | \Psi' \rangle \tag{II.45}$$

$$E_0 < E'_0 + \int \rho_0(r)[V'_{ext}(\vec{r}_i) - V_{ext}(\vec{r}_i)]d\vec{r} \tag{II.46}$$

Adding Eq. (II.20) and (II.23) lead to the contradiction

$$E_0 + E'_0 < E'_0 + E_0 \tag{II.47}$$

Therefore, it the ground state density $\rho_0(\vec{r})$, which defines the external potential, cannot be produced by two different external potentials $V_{ext}(\vec{r}_i)$. Except for a constant, $V_{ext}(\vec{r})$In other words, the fundamental element is no longer exclusively the wave function; instead, the essential element is now the electronic density, which completely describes the ground state and all its properties, this leads to the establishment of Hohenberg-Kohn's second theorem.

a. Theorem II

The density can be used to define a universal functional for the energy E[ρ]. The lowest global value of this functional corresponds to the exact ground state.

Evidence

All other observables of the system, such as kinetic energy, are uniquely determined since the density determines the external potential, which in turn uniquely determines the ground state wavefunction (unless in degenerate conditions). As a result, the energy can be expressed as a density function.

The functional$E\ [\rho(\vec{r})]$can be written as

$$E\ [\rho(\vec{r})] = [\hat{T}] + [\hat{V}_{\imath}] + \int V_{ext}(\rho(\vec{r}))d\vec{r} \qquad \text{(II.48)}$$

$$F\ [\rho(\vec{r})] = F[\rho(\vec{r})] + \int V_{ext}(\rho(\vec{r}))d\vec{r} \qquad \text{(II.49)}$$

Where $F\ [\rho(\vec{r})]$is a universal functional

In the ground state the energy is defined by the unique ground state density $\rho_0(\vec{r})$

$$E_0 = E\ [\rho(\vec{r})] =< \langle \Psi|\hat{H}|\Psi\rangle \qquad \text{(II.50)}$$

A variable density $\rho'(\vec{r})$ will inevitably yield a higher energy according to the variational principle.

$$E_0 =< \langle \Psi|\hat{H}|\Psi\rangle < \langle \Psi'|\hat{H}|\Psi'\rangle = E' \qquad \text{(II.51)}$$

The total energy of the system expressed as a functional of $\rho(\vec{r})$ is thus minimized with regard to $\rho(\vec{r})$ When one determines the ground state's total energy, the ground state density is the one that minimizes that energy.

The equations provided by Khon and Sham stand as the sole resolution to this predicament.

9-3- Kohn-sham equation

Hohenberg-Kohn theorems were put into practice by the Kohn-Sham (KS) equation, which also made DFT computations possible. to be conducted using just a single personal computer[14]. It achieved such remarkable success that Kohn was awarded the Nobel Prize in Chemistry in 1998. The KS equation transforms the initial A dynamic system with genuine potential Vextinto a fake, non-interactive system that has an efficient potential V_{eff} and assume that the two systems share an identical ground state density.As mentioned above in eq(II.25), The expressions of T and Vi were not known, Kohn and Sham proposed the next separateons

$$T[\rho(\vec{r})] = T_0[\rho(\vec{r})] + (T[\rho(\vec{r})] - T_0[\rho(\vec{r})]) = T_0[\rho(\vec{r})] + E_c[\rho(\vec{r})] \tag{II.52}$$

Where

$T_0[\rho(\vec{r})]$: Kinetic energy of non-interacting electron gas.

$E_c[\rho(\vec{r})]$: Correlation energy that is neglected in the Hartree-Fock approximation.

$$V_i[\rho(\vec{r})] = E_H[\rho(\vec{r})] + (V_i[\rho(\vec{r})] - E_H[\rho(\vec{r})]) = E_H[\rho(\vec{r})] + E_x[\rho(\vec{r})] \tag{II.53}$$

Where

$E_H[\rho(\vec{r})]$: Term of Hartree.

$E_x[\rho(\vec{r})]$: Exchange energy that is neglected by Hartree.

$$F[\rho(\vec{r})] = T_0[\rho(\vec{r})] + (E_c[\rho(\vec{r})] - E_H[\rho(\vec{r})] + E_x[\rho(\vec{r})]) \tag{II.54}$$

$$F[\rho(\vec{r})] = T_0[\rho(\vec{r})] + E_H[\rho(\vec{r})] + E_{xc} \tag{II.55}$$

Therefore, the functional energy of Hohenberg and Kohn can be expressed by the following equation

$$E[\rho(\vec{r})] = T_0[\rho(\vec{r})] + E_H[\rho(\vec{r})] + E_{xc}[\rho(\vec{r})] + \int \rho(\vec{r})\, V_{ext}(\vec{r}) d\vec{r} \tag{II.56}$$

With $E_x[\rho(\vec{r})]]$ Exchange-correlation energy is due to the difference between the noninteracting and the interacting kinetic energies as well as to the difference between real interaction energy and that of Hartree. The equations of Kohn and Sham that solve the problem is

$$\left[-\frac{h^2}{2m_e}\vec{\nabla}_i^2 + V_{eff}(\vec{r})\right]\varphi_i(\vec{r}) = \varepsilon_i\varphi_i(\vec{r}) \quad ,i = 1, \dots\dots\dots\dots N \tag{II.57}$$

The lowest eigenvalues are ε_i., where each of the N orbitals has one electron with $\varphi_i(\vec{r})$ The auxiliary system's density is made up of

$$\rho(\vec{r}) = \sum_{i=1}^{N}|\varphi_i(\vec{r})|^2 \tag{II.58}$$

The effective potential is of the form

$$V_{eff}(\vec{r}) = V_{ext}[\rho(\vec{r})] + V_H[\rho(\vec{r})] + V_{xc}[\rho(\vec{r})] \quad \text{(II.59)}$$

With

$V_H[\rho(\vec{r})] = \frac{1}{2}\int \frac{e^2}{4\pi\varepsilon_0}\frac{\rho(\vec{r}')}{|\vec{r}-\vec{r}'|}d^3\vec{r}'$: Hartree potential

$V_{xc}[\rho(\vec{r})] = \frac{\delta E_{xc}[\rho(\vec{r})]}{\delta\rho(\vec{r})}$: Exchange correlation potential

So far, Density Functional Theory (DFT) continues to be a precise method. Nevertheless, to make it feasible for practical use, it is essential to provide a representation of $[\rho(\vec{r})]$, which requires us to proceed with an approximation.

9-4- Solving kohn-sham equations

Through the utilization of the Kohn-Sham equations provide a way to determine the exact density and energy of the ground state of a condensed matter system using independent-particle methods. Because of the strong relationship between the electron density $\rho(\vec{r})$ and the effective KS potential $V_{eff}(\vec{r})$, the K_S equations must be solved consistently. Typically, this is accomplished numerically using a self-consistent iteration. Discovering an appropriate resolution can be achieved by adhering to these procedures

1. Start with an initial electron density for the first iteration.
2. Calculation of the effective KS.
3. Resolution of the Kohn-Sham equation with single particle eigenvalues and wavefunctions.
4. Calculation of the new electron density from the wavefunctions.
5. Examination of self-consistent condition(s) (by comparing the old and the new densities).
6. Calculation of the different physical quantities (Energy, forces, ...); End of calculation.

Self-consistency in calculations

The resolution of the Kohn-Sham equations for the high symmetry points in the first Brillouin zone allows for simplified calculations. The resolution of these equations is then done iteratively using a self-consistent iteration cycle illustrated by the flowchart. We start by injecting the density of initial charge to construct from a superposition of atomic densities

$$\rho_{in} = \rho_{cristal} = \sum_{at} \rho_{at}$$

Next, the orbitals are occupied and a new density is determined by

$$\rho_{out}(r) = \sum_{i=1}^{N} |\varphi_i(r)|^2$$

If the density or the energy has changed significantly (convergence criterion), we return to the first step, mixing the two charge densities as follows

$$\rho_{in}^{i+1} = (1-\alpha)\rho_{in}^{i} + \alpha\rho_{out}^{i}$$

i : represents the i-th iteration.

Alpha is a mixing parameter.

Thus, the iterative procedure can be continued until convergence is achieved. The eigenvalues and eigenfunctions are obtained by solving the Kohn-Sham equations.

i : represents the energy level of the system's state. The total energy of the system in its ground state is given by

$$E = \sum_{i=1}^{N} E_i - \frac{e^2}{8\pi\varepsilon_0} \iint \frac{\rho(r)\rho'(r)d^3r d^3r'}{|r-r'|} + E_{xc}[\rho(r)] - \int \rho(r) \frac{\partial E_{xc}}{\partial \rho(r)} d^3r$$

The wave functions known as Kohn-Sham orbitals can be written in any complete basis of wave functions. These bases can be atomic orbitals, plane waves, or Gaussian wave functions, etc.

So far, the only problem that remains to be solved is the formula for $E_{xc}[\rho(r)]$ so that DFT and the Kohn-Sham equations can be used in practice. For this, we will resort to approximations. the simplest and most widely used approximation is the LDA (Local Density Approximation).

The exchange-correlation energy

The exchange-correlation potential is the only term that remains unknown for DFT, this term compensates for the loss of information on the exchange and correlation properties of the electronic gas induced by the transition from a real multi-particle wave function to fictitious single-particle wave functions without interactions using the Kohn-Sham method. The different possible interactions between electrons can be grouped into three categories

The exchange effect, which is directly related to the Pauli principle and does not involve the electron's charge. This principle is the direct cause of the antisymmetry of the wave function. It corresponds to the fact that two electrons with the same spin S (have a zero probability of being in the same place. The Hartree-Fock approximation offers a solution to this problem (the Slater determinant represents the antisymmetry of the wave function).

The charge of the electron is responsible for The Coulomb correlation. It corresponds to the repulsion of electrons. It is independent of spin. This contribution is neglected by Hartree-Fock theory. it is essentially due to the correlation effects of core electrons.

The third effect arises from the fact that electronic wave functions are formulated in terms of independent particles, which must lead to a correct counting of the number of electron pairs.

The exchange-correlation functional must take into account, in addition to these three contributions, the difference in kinetic energy between the fictitious non-interactive system and the real system. Thus The calculation of energy and exchange-correlation potential relies on a number of approximations.

10- Methodology

within this section,Fundamental concepts related to the linearized augmented plane wave plus local orbitals (LAPW+lo) are presented, outlining different versions and their developmental stages concerning linearization, full potential, and local orbitals. We also explore the treatment of exchange-potential correlation through various approximations (LDA, GGA, and GGA+mBJ).

10-1- Augmented plane wave methods

Various methodologies have been devised to ascertain the electronic, optical, thermal, or mechanical properties of materials, categorized into three distinct groups based on the data employed.

- Empirical methods rely on empirical data and experiential knowledge to determine parameter values, resulting in unified confirmations derived from this empirical insight.
- Semi-empirical methods necessitate pre-calculated data along side experimental results to predict properties that haven't been experimentally determined. This approach accelerates calculations significantly, enabling the computation of even large molecules.
- Ab-initio methods demand only fundamental data for their calculations, by passing the need for additional empirical or pre-calculated information. In the recent years, researchers have developed ab-initio methods with no inclusion of experimental data, based on theoretical principles, known as "first principles methods" one of the most widely used method is : Full Potential Linearized Augmented Plane Wave (FP LAPW) developed by Andersen which is just an amelioration of another approximation called augmented plane wave method (APW).

10-2- APW method

The APW approach stands as one of the most favored methods for addressing electronic structure via Kohn-Sham (KS) equations. Slater introduced this technique in 1937, His proposition involved considering that, at a distance from the atomic nuclei, electrons tend to be relatively unrestrained, being delineated by plane waves. When closer to the nuclei, electrons exhibit behavior akin to those in free atoms and can be more effectively represented by atomic-like functions. Consequently, space is segregated into two zones as shown in figure II.1: a spherical area around each atom defined by a radius (referred to as S αor "muffin tin sphere" [9]. comprising the interstitial zone (I), which is the remaining area outside of these spheres, and the muffin tin region. In the expansion, an augmented plane wave (APW) was used. can be specified as

$$\phi(\vec{r}) = \begin{cases} \phi_i(\vec{r}) = \frac{1}{\Omega^{\frac{1}{2}}} \sum_G C_G e^{i(\vec{k}+\vec{G})} \vec{r}_r > R_\alpha \\ \phi_s(\vec{r}) = \sum_{lm} A_{lm} U_l^\alpha(r, E_l) Y_{lm}(\vec{r}) r < R_\alpha \end{cases} \qquad \text{(II.60)}$$

From (II.39) with ϕ representing the wave function and Ω the unit cell volume, CG and $Alm$are expansion coefficients , Yl,$m$are spherical harmonics ;$Ul\alpha$is the numerical solution to the radial Schrödinger equation which is given by

$$\left\{-\frac{d^2}{dr^2}+\frac{l(l+1)}{r^2}+V(r)-E_n\right\}rU_l(r)=0 \qquad \text{(II.61)}$$

1. Slater advocated employing these functions by emphasizing that 2. radial functions are solutions of Schrödinger's equation in a spherical potential, whereas plane waves are solutions of the equation in a consistent potential. In the dual representation defined in equation (II.39), a constraint must be applied to guarantee continuity at the sphere boundaries. By defining the U_l^α utilizing CG within the spherical harmonic expansion of the plane waves, the APW approach achieves this requirement.

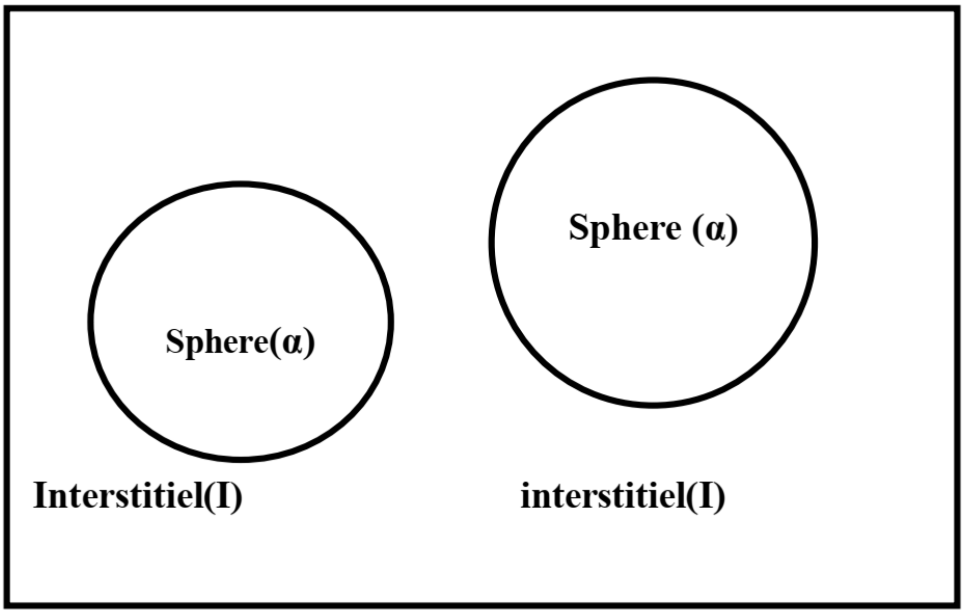

Figure II.1. The unit cell is divided into atomic spheres and interstitial areas in order to adapt the basis.

Within the APW method, continuous basis sets (functions) are utilized, encompassing the entire space within the sphere. Despite being a widely employed technique for computing properties like structural, electronic, optical, and magnetic aspects of solids, it does come with inherent limitations. One notable constraint is its inability to extend beyond the average spherical muffin-tin approximation. The fundamental functions in this method exhibit a discontinuity at the muffin-tin border, resulting in a kink, thus making their derivatives discontinuous at the boundary. Additionally, a drawback lies in the radial function (r, El), which relies on energy, thereby creating an eigenvalue problem that is nonlinear. Numerical problems may result if $Ul\alpha\alpha$ becomes extremely small at the empty sphere boundary. Consequently, various modifications have been introduced to the APW method to address these issues, notably proposed by Koellingand Andersen

10-2-1- The linearized augmented plane wave (LAPW) method

To circumvent the challenges associated with the APW method, arising from the discontinuity of the initial derivative of the basis functions at the muffin-tin boundary, which divides the interstitial area from the core, linearized methods emerged in the mid-1970s. Andersen and Koelling with Arbman pioneered these methods, inspired by an idea introduced by Marcus. Andersen introduced an added term within the basis within the MT sphere to address this issue. The radial wave function is linearized using a linear combination in the LAPW technique, specifically within the MT region. of $Ul(r, El)$and $\dot{U}l(r, El)$

The energy derivative's Blm coefficients are equivalent to the Alm. Within the spheres, the basic functions are linear combinations of radial functions. In addition to their energy derivatives, $(r)(\vec{r})$ These are the augmenting functions: $\dot{U}l(r)Ylm(r_l)$. The energy derivative, $\dot{U}(r)Ylm(\vec{r})$, fulfills the following equation, and the Ul are defined as in the APW method

$$\left\{-\frac{d^2}{dr^2}+\frac{l(l+1)}{r^2}+V(r)-E_n\right\}r\dot{U}_l(r)=0 \qquad \text{(II.62)}$$

In the augmented plane wave method, the interstitial regions exclusively utilize plane waves, akin to the APW method. However, in the Muffin-tin regions, more fitting functions than APW functions are employed. The radial basis-function is consequently substituted by the Taylor series to better suit this context

$$U_l(r,E)=U_l(r,E_l)+(E-E_0)\dot{U}_l(r-E_0)+O((E-E_l)^2)\left\{-\frac{d^2}{dr^2}+\frac{l(l+1)}{r^2}+V(r)-E_n\right\}r=0 \qquad \text{(II.63)}$$

While $\dot{U}_l(r,E_0)=\frac{\partial U_l(r)}{\partial E}$

Consequently, the wave functions incur A quadratic mistake in the difference between the energy parameter El and the eigenvalue E. This indicates that the eigenvalue error only reaches the fourth order. As a result, the LAPW approach ensures that the wave function at the MT sphere's surface is continuous.

10-2-2- (LAPW+FP) METHOD

The APW basis functions, much like LAPW, can undergo modifications by incorporating local orbitals. Sjosted et al [94]. enhanced APW by introducing local orbitals (lo), forming the APW+lo basis. Similar to the APW approach, the radial wave function is computed at a fixed energy, but this new technique integrates additional types of orbitals for increased flexibility, denoted as lo instead of LO in LAPW[95].The equation defining the function $\phi(\vec{r})$ consists of distinct expressions for regions inside and outside the MT sphere

$$\phi(\vec{r}) = \begin{cases} \qquad\qquad 0 \qquad\qquad r > R_\alpha \\ \left[A_{lm}U_l(r,E_l) + B_{lm}\dot{U}_l(r,E_l)\right]Y_{lm}(\vec{r}) \quad r < R_\alpha \end{cases} \tag{II.64}$$

The two coefficients in this equation are determined by the normalization requirement of the function $(r^{\rightarrow})$ at the MT radii. Ul is only included for specific l quantum numbers in this APW+lo approach and is not dependent on the plane waves. Instead of being included in every plane wave as in LAPW, the energy derivative term in the APW+lo approach is only included in a small number of lo's. Consequently, while the APW+lo method converges more swiftly than LAPW

and delivers comparable accuracy, uncertainties persist regarding the accuracy of energy linearization in APW+lo akin to LAPW.

11- Exchange-potential correlation

11-1- Local density approximation (LDA)

Kohn and Sham's Local Density Approximation (LDA) in 1965, a widely used method, assumes density as a uniform electron gas, implying exchange correlation energy is the same for homogeneous electron gases.

$$E_{xc}^{LDA}[\rho(\vec{r})] = \int \rho\,(\vec{r})\varepsilon_{xc}^{hom}[\rho(\vec{r})]d^3\vec{r} \tag{II.65}$$

Whereε xc hom$[\rho(\vec{r})]$ each particle's exchange-correlation energy. Next, we obtain the exchange correlation potential using

$$V_{xc}\big(\rho(\vec{r})\big) = \frac{\delta E_{xc}[\rho(\vec{r})]}{\delta\rho(\vec{r})} = \varepsilon_{xc}^{hom}[(\vec{r})] + \rho(\vec{r})\frac{\delta\varepsilon_{xc}[\rho(\vec{r})]}{\delta\rho(\vec{r})} \tag{II.66}$$

In order to apply the LDA in practical computations, the exchangecorrelation energy for a uniform electron gas with a specific density must be found. It is typical to divide $\varepsilon_{xc}(\rho(\vec{r}))$ into correlation and exchange potentials.

$$\varepsilon_{xc}(\rho(\vec{r})) = \varepsilon_{x}(\rho(\vec{r})) + \varepsilon_{c}(\rho(\vec{r})) \qquad \text{(II.67)}$$

The exchange term, commonly referred to Dirac's exchange [21] (symbolized by S, means that this expression was taken over by Slater)

$$\varepsilon_{x}^{s}(\rho(\vec{r})) = -\frac{3}{4}\left(\frac{3\rho(\vec{r})}{\pi}\right)^{1/3} \qquad \text{(II.68)}$$

the exactly Accurate values for $\varepsilon_{x}^{s}(\rho(\vec{r}))$ obtained by Quantum Monte Carlo (QMC) computations. Following that, these were interpolated to yield an analytical form for $\varepsilon_{c}(\rho(\vec{r}))$.

11-2- Generalized gradient approximations (GGA)

As previously noted, the Local Density Approximation (LDA) overlooks the inhomogeneity present in the actual charge density. This limitation spurred the development of various generalized-gradient approximations (GGAs) that incorporate

Corrections for density gradients $|\vec{\nabla}\rho(\vec{r})|$ and the electron density's higher spatial derivatives . $\rho(\vec{r})$ Consequently, the correlation energy can be formulated as

$$E_{xc}^{GGA}(\rho(\vec{r})) = \int f_{xc}[\rho(\vec{r}), \nabla\rho(\vec{r})]\, d^{2}\vec{r} \qquad \text{(II.69)}$$

Different generalized-gradient approximations (GGAs) distinguish themselves based on the choice of the functional f_{xc}. Among The GGAs put out by Becke [96] , Perdew et al [97]. and Perdew, Burke, and Enzerhof [98]. are the most commonly used. In general, GGAs perform better than LDA in predicting characteristics like bond length, molecular binding energy, and crystal lattice constants, particularly in systems with rapidly fluctuating charge. densities. However, in some scenarios, GGA tends to overcorrect LDA outcomes, particularly in ionic crystals where LDA calculations align well with experimental data regarding lattice constants, whereas GGA tends to overestimate them. Despite the advancements offered by GGAs, both LDA and GGA struggle with materials where electrons exhibit localization and strong correlation, Examples include complexes of rare-earth elements and transition metal oxides. This disadvantage has prompted the exploration of approximations beyond LDA and GGA to better capture the complexities inherent in such materials.

11-3- GGA+mBJ

To achieve better results in energy gap calculations, Tran and Blaha [98,99]. proposed the use of a modified version of the Becke and Johnson functional [100]. referred to as the

modified Becke-Johnson mBJ in DFT. The mBJ approximation widens the energy gap, thus closely aligning with experimental observations [79]. unlike the LDA and GGA approximations that yield narrow gaps. The gaps obtained using mBJ span a range of different systems, extending from semiconductors with small gaps to insulators with wider gaps.

Construction of radial functions

In the interstitial region, the basis functions of the FP-LAPW methods are plane waves. While inside the MT spheres, they are developed in the form of numerical radial functions. With the condition that the basis functions and their derivatives are continuous at the surface of the MT sphere. thus the construction of the basis functions of the FP-LAPW methods comes down to:

Determine the radial functions and their derivatives with respect to energy. The coefficients and must satisfy the boundary conditions.

The boundary condition allows for the determination of the cut-off of the angular momentum and the cut-off representation of the spheres in terms of the plane wave coefficient. One of the strategies to follow is to choose these cutoffs such that[101].

G_{max}: the cut-off in reciprocal space that limits the number of plane waves used in the development of the charge density and the potential in the interstitial region.

$R_a^{min}.\,k_{max}$represents the product between the smallest radius of the chosen MT sphere and the largest value of k that presents the cut-off of the wave functions, which limits the number of reciprocal lattice vectors that enter into the development of the Kohn-Sham wave functions on the LAPW basis functions.

l_{max}: limits the number of harmonics of the network used for the development of the charge density and the potential within the MT spheres

Code WIEN2k

The Vienna University of Technology's Institute of Materials Chemistry developed the WIEN2K simulation code, which was released in 1990 by Blaha P., Schwartz K., Sorintin P., and Trickey S. B. [102,103]. The WIEN2k code has been updated to use the FP-LAPW technique.

In the following years, this code was continuously revised and underwent several updates. Versions of the original WIEN code were developed (named according to the year of their release, WIEN93, WIEN95, WIEN97…). We used the WIEN2K version (year 2011).

The WIEN2K package is written in FORTRAN, it runs under the LINUX operating system. It consists of several independent programs that are linked by C-SHELL SCRIPT. These programs perform electronic structure calculations in solid bodies based on Density Functional Theory (DFT).

Initialisation

It involves constructing the spatial configuration (geometry), symmetry operations, initial density, the quantity of unique points required for integration in the Brillouin zone, which cannot be reduced, etc. A number of auxiliary programs are used to do all of these tasks, producing

NN a sub-program that checks the distances between nearest neighbors and equivalent positions (the non-overlapping of spheres) as well as determines the atomic radius of the sphere.

LSTART it allows generating atomic densities; it also determines how the different atomic orbitals are treated in the band structure calculation.

SYMMETRY it allows generating the symmetry operations of the space group and determining the point group of individual atomic sites.

KGEN it generates the number of k points in the Brillouin zone.

DSTART it creates a starting density for the auto-coherent cycle (the SCF cycle) by superimposing the atomic densities produced in LSTART.

Calcul auto-cohérent (ou self-consistant) :

In this step, the energies and the electronic density of the ground state are calculated according to a convergence criterion (energy, charge density, force). Les sous-programmes utilisés sont

LAPW0 it generates the potential for the density calculation.

LAPW1 it allows calculating the valence bands, the eigenvalues, and the eigenvectors.

LAPW2 il calcule les densités de valence pour les vecteurs propres.

LCORE il calcule les états et les densités de cœur.

MIXER it performs the mixing of density of input and output (initial, valence, and core).

12- Determination of properties

Once the self-consistent calculation is completed, it is possible to access the properties of the ground state (charge density, band structure, thermodynamic properties, thermoelectric properties, etc.). each of these properties is calculated separately with a "package" program that runs with consecutive steps[65]. These main calculation steps using the Wien2k code are illustrated in the flowchart .

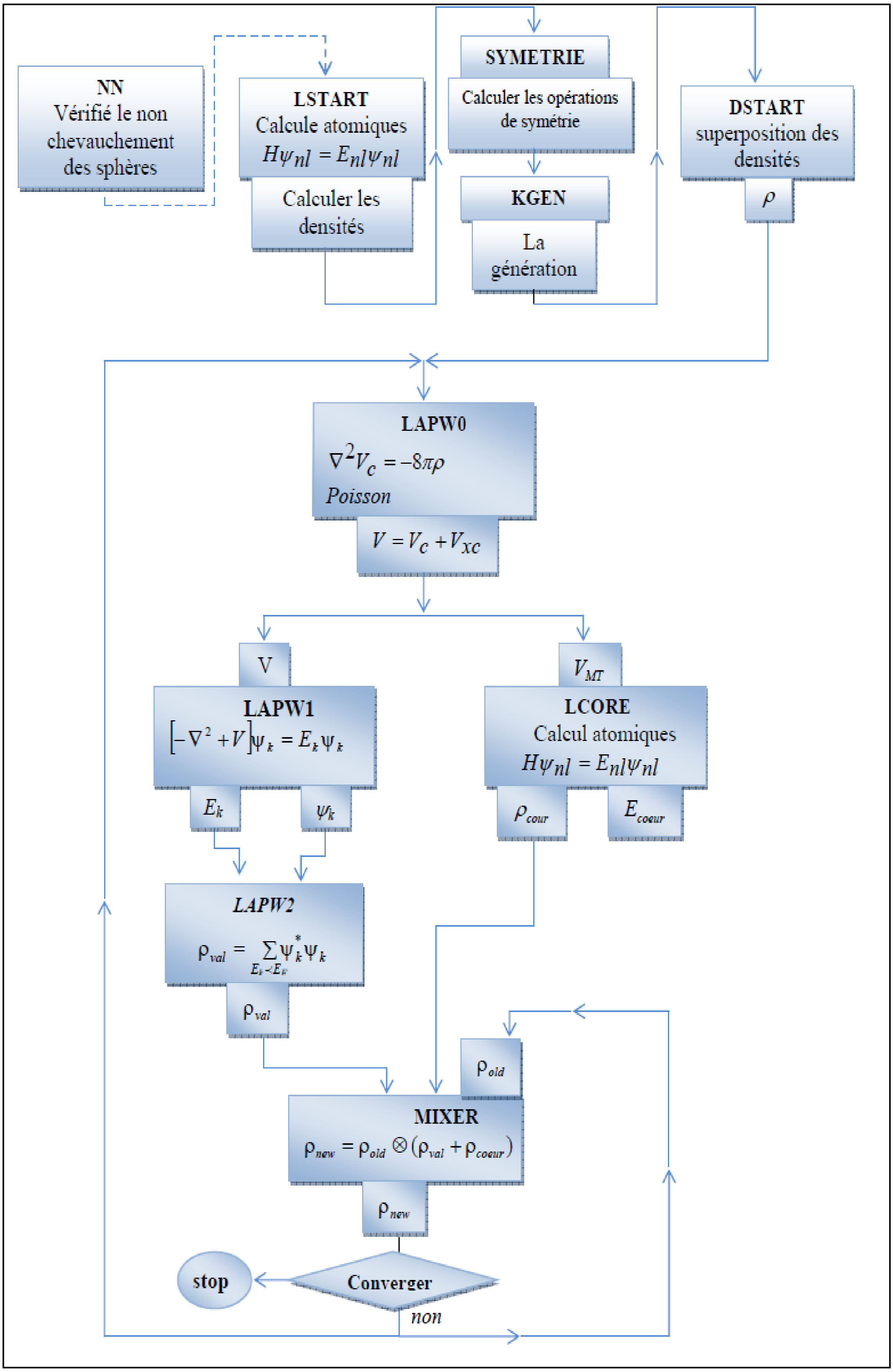

Figure II.2. Flowchart of the WIEN2K program modules

]

CHAPTER 3 :

RESULTS AND DISCUSSIONS

1- Introduction

Perovskite solar cells (PSCs) are becoming a major contender in photovoltaic technology, which is developing at an unprecedented rate. This is because of their remarkable power conversion efficiency (PCE) and affordability. The efficiency of solution-processed halide perovskite solar cells in single-junction topologies has surpassed 22% [104]. Both Ghaleb and Arrar combined two perovskite types—the inorganic halide $CsPbI_3$ and the organic halide $CH_3NH_3SnBr_3$—as well as heterojunction $MASnBr_3$/CZTGS in a single solar cell to achieve an efficiency of over 30% [2,3]. This outstanding performance is due to the remarkable optical and electrical properties of perovskites, especially those based on lead, including their low exciton binding energy, long carrier lifetime, high optical absorption coefficient, small bandgap, and efficient charge carrier transport. This implies that these special materials have additional benefits that have not yet been realized [4,5].

While the majority of the study was initially focused on basic perovskites (ABX_3), more notable complex structures, like double perovskites ($A_2BB'X_6$), brought additional inventiveness by combining two different new opportunities for enhancing solar cell performance through the use of rare earth and alkaline earth elements in conjunction with transition metals.[6,7].

Our investigation will examine the optical, structural, elastic, and thermodynamic features of the novel perovskite $A_2BB'X_6$ as well as the amount to which it contributes to the field of solar cells, particularly given that it is composed of the components Cs_2ZnPbX_6(X=Br,Cl). Its formula is $A_2BB'X_6$, where X6 represents Br/Cl, B for Zn, B' for Pb, and A for Cs. We will examine this compound based on earlier studies on especially [8,9], phase, in the cube phase with the space group (Fm-3m). [113]. Nevertheless, there is a dearth of experimental, stability, and theoretical information regarding these materials' structural characteristics.

The two novel double perovskite compounds, $Cs_2ZnPbCl_6$ and $Cs_2ZnPbBr_6$, that are presented in this paper have not been thoroughly investigated. Their optical and thermoelectric characteristics are examined, emphasizing their potential for energy efficiency and renewable energy applications.

The theoretical study's results show a strong correlation with the experimental findings of other double perovskites research[114]. We analyzed the data and theoretical models using a similar methodology, which improved the validity of our findings.

Figure III.1. illustrates the crystal structures of Cs_2ZnPbX_6 compounds, highlighting the materials' potential for use in upcoming energy applications. Further developments in solar energy technology are anticipated as a result of ongoing research and development in perovskite materials. No experimental or theoretical evidence exists about the structural qualities to compare with in the scientific literature.

2- Computational details

This section presents the results of calculations performed utilizing the WIEN2k algorithm, which is based on Density Functional Theory (DFT). The total potential linearized augmented plane wave notion is implemented by this code. (FP-LAPW) [13,15]. Perdew, Burk, and Ernzerhof describe the generalized gradient approximation (GGA) for the exchange and correlation energy [118].

To fully characterize the systems under study, the most crucial characteristics that require improvement are the muffin-tin spheres' (RMT) radii. of $Cs_2ZnPbCl_6$ and $Cs_2ZnPbBr_6$. For Cs, Zn, Pb, and Cl atoms in $Cs_2ZnPbCl_6$, the RMT values were set at 2.35, 2.35, 2.35, and 2.04 atomic units (a.u.), respectively. For Cs, Zn, Pb, and Br atoms, the RMT values for $Cs_2ZnPbBr_6$ were set at 2.5, 2.33, 2.5, and 2.22 a.u., respectively. CeS is [Xe] $6s^1$, zinc is [Ar] $3d^{10}$ $4s^2$, plomb is [Xe] $4f^{14}$ $5d^{10}$ $6s^2$ $6p^2$, and chlore [Ne] $3s^2$ $3p^5$ is its electronic configuration. but Brome's is [Ar] $3d^{10}$ $4s^2$ $4p^5$. When integrating the Brillouin zone, 1000 k-points are used.

The approach created by Charpin [119]. was applied in WIEN2K to calculate elastic constants. This idea states that only three elastic constants (C_{11}, C_{12}, and C_{44}) for a cubic structure Cij must be determined. When calculating these elastic constants, the total energy as a function of volume-conserving strains. The following relation should be met by the computed values for the cubic structure: $(C_{11}-C_{12})>0$, $C_{11}>0$, $C_{44}>0$, $(C_{11} + 2C_{12})>0$, and $C_{12}<B<C_{11}$ [120,121]. the values of the elastic constant that we correctly determined.

3- Results and discussions

3-1- Structural properties

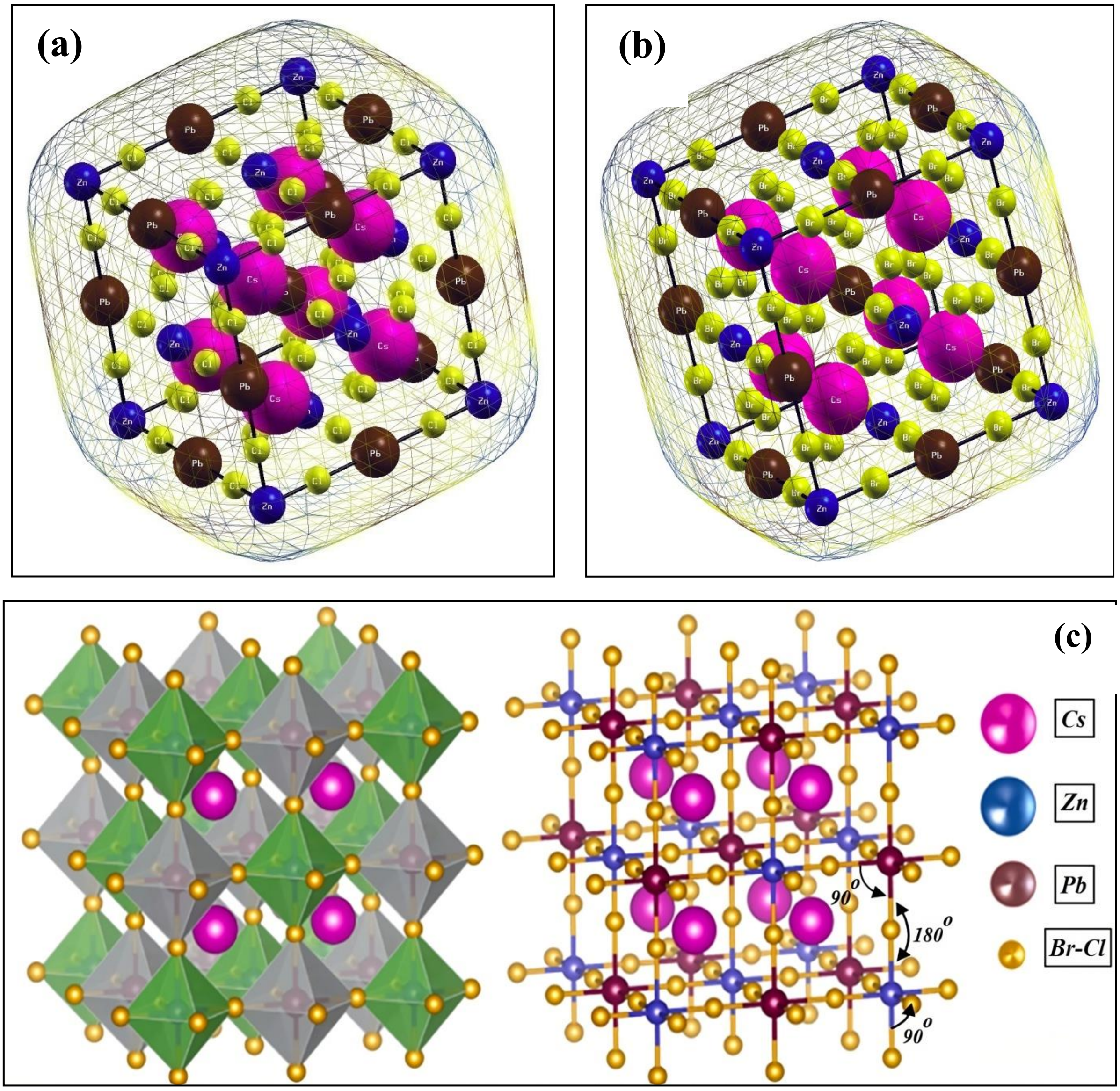

Figure III.1. Crystal structure double perovskite as prototype of Cs_2ZnPbX_6 (X=Br, Cl).

The general structural formula for cubic double perovskites is A_2BX_6 (space group: Fm3m(225)). Figure III.1. shows that the single-unit cells of the A, B, and X atoms have Wyckoff positions of 8c (0.25, 0.25, 0.25), 4a (0, 0, 0) at 4b (0.5, 0.5, 0.5), and 24e (0.25, 0, 0). Figure III.2. displays the double perovskites' optimized structural characteristics. The total energies of our compounds at various volumes were fitted using the Murnaghan state equation to determine their fundamental properties [122]. The following table presents information on a number of particular properties of our materials, specifically $Cs_2ZnPbCl_6$ and $Cs_2ZnPbBr_6$.Among these properties are the bulk modulus B, optimum volume V, lattice parameter a, and first-order derivative B'. $Cs_2ZnPbBr_6$ has a greater lattice constant than $Cs_2ZnPbCl_6$, This might result from Br having a greater than Cl in ionic radius.

It is demonstrated that the estimated bulk modulus varies inversely with the lattice constant since a bigger ionic radius raises the lattice constant and less stress may change the volume. Double perovskite's crystal stability can be evaluated empirically utilizing the Goldschmidt tolerance factor (t) and the octahedral factor (μ).

When halide perovskites develop, octahedral factors of 0.44 to 0.9 and Goldschmidt tolerance factors of 0.81 to 1.0 are commonly seen [21,22]. For our type of perovskite, equations (3) and (4) define t and μ. The symbols RCs, RZn, RPb, and RX(X=Br,Cl) represent the corresponding ionic radii of Cs, Zn, Pb, and (X=Br,Cl). $t \approx 0.8629$ and 0.86199, $\mu \approx 0.79$ and 0.73, since the molecule contains the anions Cl and Br, respectively, are the octahedral factors and tolerance. Both compounds have stable structures as a result. By assessing thermodynamic stability and calculating the formation energy, this result can be further confirmed. Ef (eV). Formulas (5) estimated Ef (eV), which has a negative sign, supports the stability of the compounds by showing energy is released during the process of compound formation.

Generally speaking, bromide-driven It is believed that double perovskites are more stable than chloride-based ones. ones because of the greater formation energy magnitude of $Cs_2ZnPbBr_6$ compared to $Cs_2ZnPbCl_6$.

We calculated the two different structural types' total energy vs volume.in order to determine our compound's ground-state structure. Following the total energy versus volume analysis, the data was fitted using the Birch-Murnaghan equation of state. was calculated in order to optimize the quaternary alloy's structure [125].

$$E(V) = E_0 + \frac{9V_0B_0}{16}\left\{\left[\left(\frac{V_0}{V}\right)^{2/3} - 1\right]^3 \grave{B}_0 + \left[\left(\frac{V_0}{V}\right)^{2/3} - 1\right]^2 \left[6 - 4\left(\frac{V_0}{V}\right)^{2/3}\right]\right\} \qquad \text{(III.1)}$$

$$B = V\frac{\partial^2 E}{\partial V^2} \qquad \text{(III.2)}$$

$$t = \frac{\mathrm{R_{Cs}} + \mathrm{R_X}}{\sqrt{2}\left(\frac{R_{Zn} + R_{Pb}}{2} + R_X\right)} \qquad \text{(III.3)}$$

$$\mu = (\mathrm{R_{Zn}} + \mathrm{R_{Pb}})/2R_X \qquad \text{(III.4)}$$

$$E_f = \mathrm{E_{total}}(\mathrm{Cs_2ZnPbX_6}(\mathrm{X = Br, Cl})) - 2\mathrm{E_{Cs}} - \mathrm{E_{Zn}} - \mathrm{E_{Pb}} - 6\mathrm{E_X} \qquad \text{(III.5)}$$

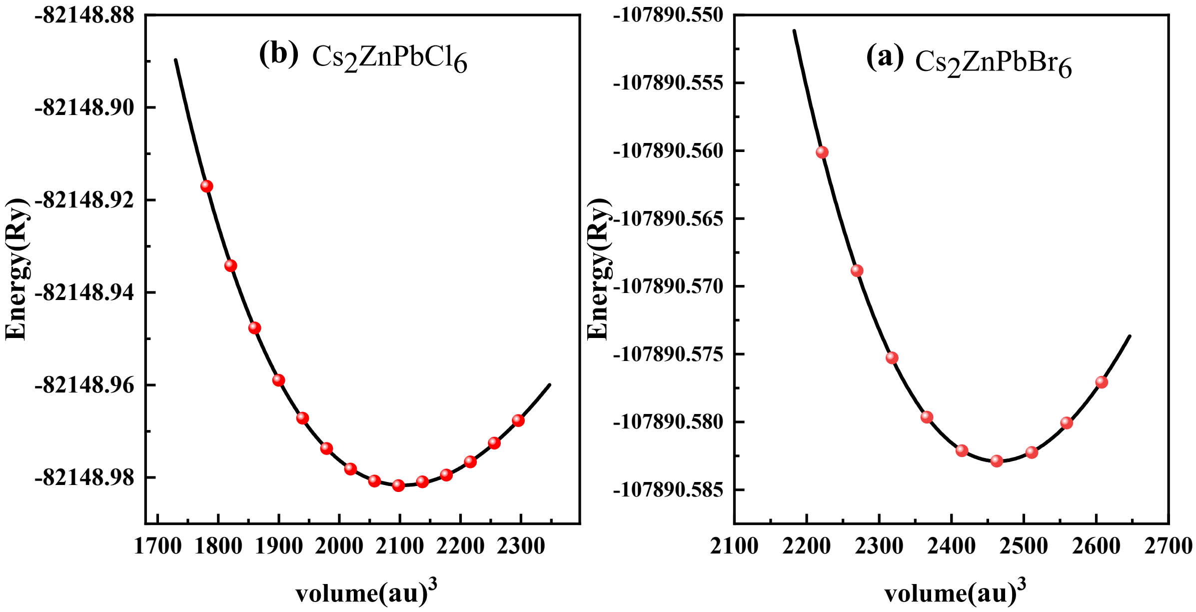

Figure III.2. Cs_2ZnPbX_6 (X=Br, Cl). A plot of energy against volume.

Table III.1. PBE-GGA's computation of the For $Cs_2ZnPbCl_6$ and $Cs_2ZnPbBr_6$ in cubic phase, the lattice constant a0 (Å), B0 (GPa), Ef (eV), Eg (eV), Etot (eV), (t), and (μ)

Properties	$Cs_2ZnPbBr_6$	$Cs_2ZnPbCl_6$
a (Å)	11.3451	10.7643
V_0	2463.5850	2104.2488
B(GPA)	22.9608	27.8476
B'(GPA)	4.8664	4.7126
Bandgap (eV)	1.727	2.472
E_{tot}	-107890.582888	-82148.981671
E_f (eV)	-1.24	-1.13
Tolerance factor (t)	0.86199	0.8629
Octahedral factor (μ)	0.73	0.79

The thermodynamic stability of $Cs_2ZnPbCl_6$ and $Cs_2ZnPbBr_6$ is demonstrated by their negative formation energies, Ef(eV), which were computed. $Cs_2ZnPbBr_6$'s greater negative formation energy indicates that it is more stable than $Cs_2ZnPbCl_6$, indicating stronger internal connections and a higher resistance to breakdown in the circumstances under study.

3-2- Chemical bonding

The electronic charge interpretation density provides a unique insight into the chemical stabilities of Cs_2ZnPbX_6 (X=Br, Cl).

With a more thorough examination in the ground state, the electron charge density shown in Figure III.3. offers a basic and intriguing characterization of the hybridization between various atomic orbitals. To illustrate the chemical bonding In this research, we used charge density diagrams in the (110) plane. Covalent and ionic bonds can be formed between atoms. The sharing of electrons or the increase in electron density between bonded atoms creates covalent bonds. There was also another similar association discovered. Thus, all of the research points to the presence of a well preserved In these semiconductor alloy systems, polar covalent bonds a combination of covalent and ionic bonds are present. Electron density distributions were created in order to comprehend them.

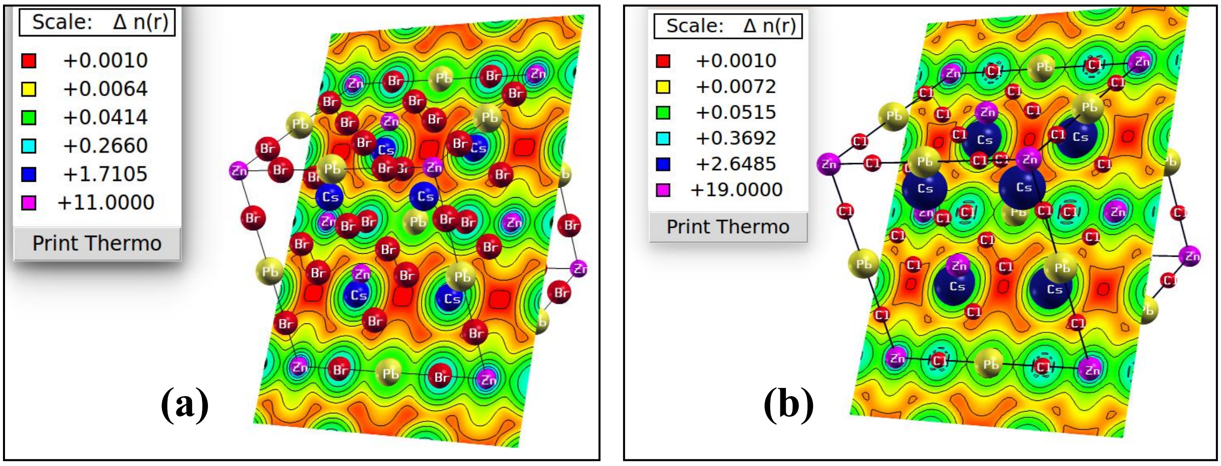

Figure III.3. Electron density distributions of Cs_2ZnPbX_6 (X=Br, Cl)

3-3- Electronic properties

Electron density is a tool for describing the electronic structure and bonding of materials in detail. Figure III.4.shows the total density of states of Cs_2ZnPbX_6(X=Br, Cl). compounds. It is aindirect projection of the electronic structure.

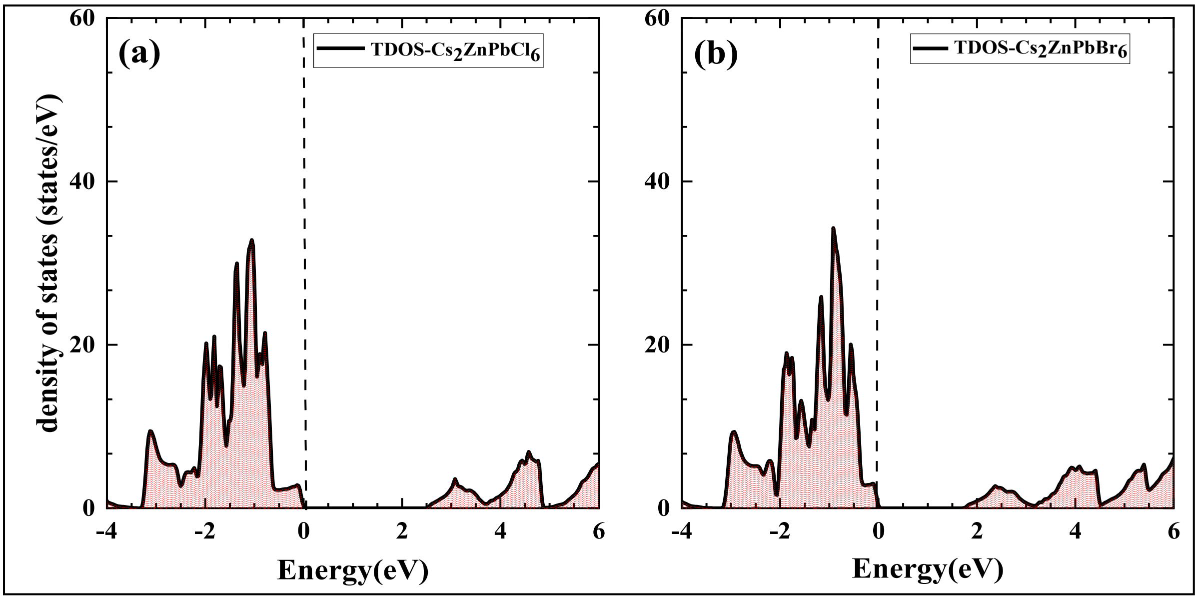

Figure III.4. The total density of states of Cs_2ZnPbX_6(X=Br, Cl).

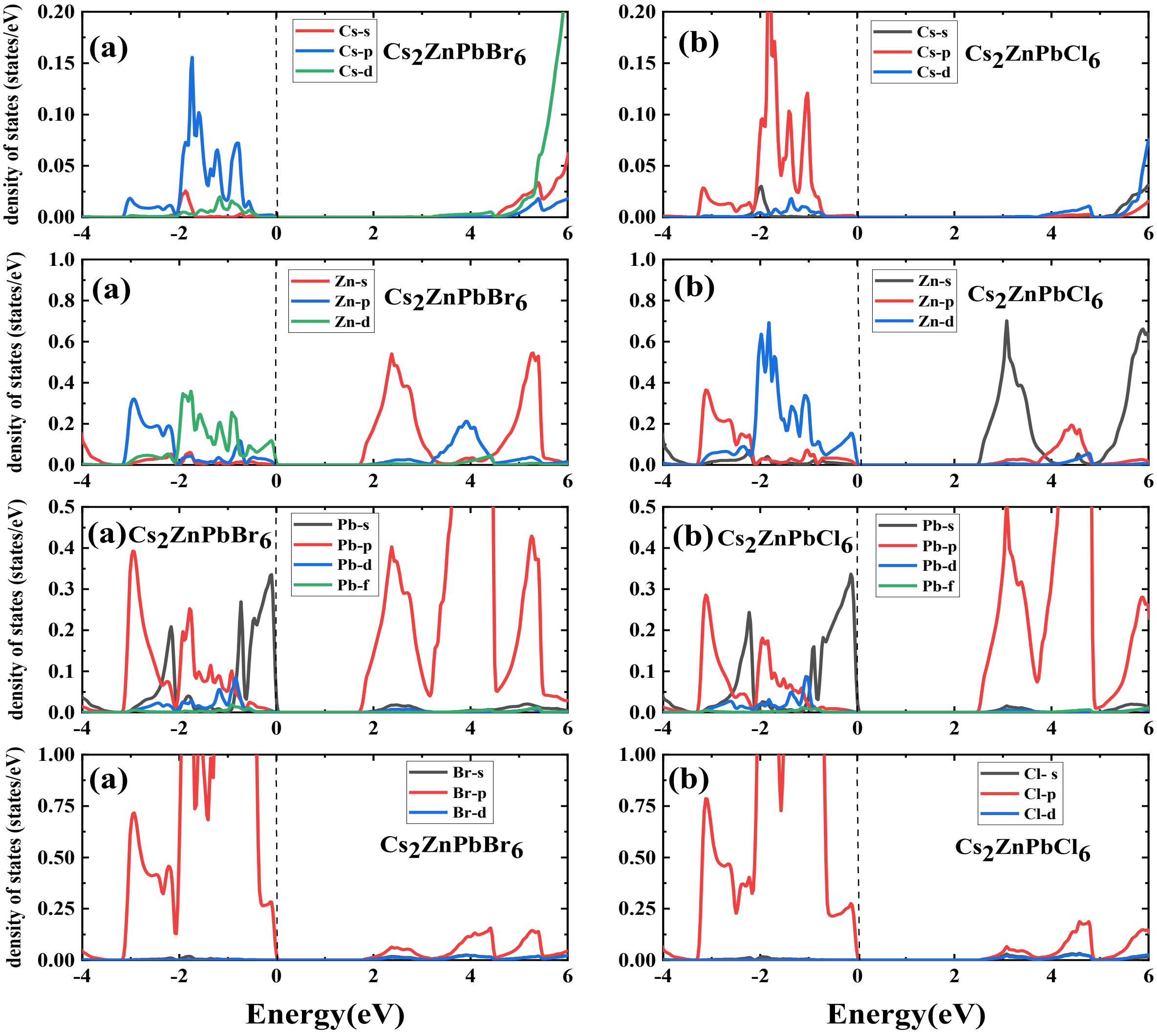

Figure III.5. An incomplete density of states for $Cs_2ZnPbBr_6$ and $Cs_2ZnPbCl_6$

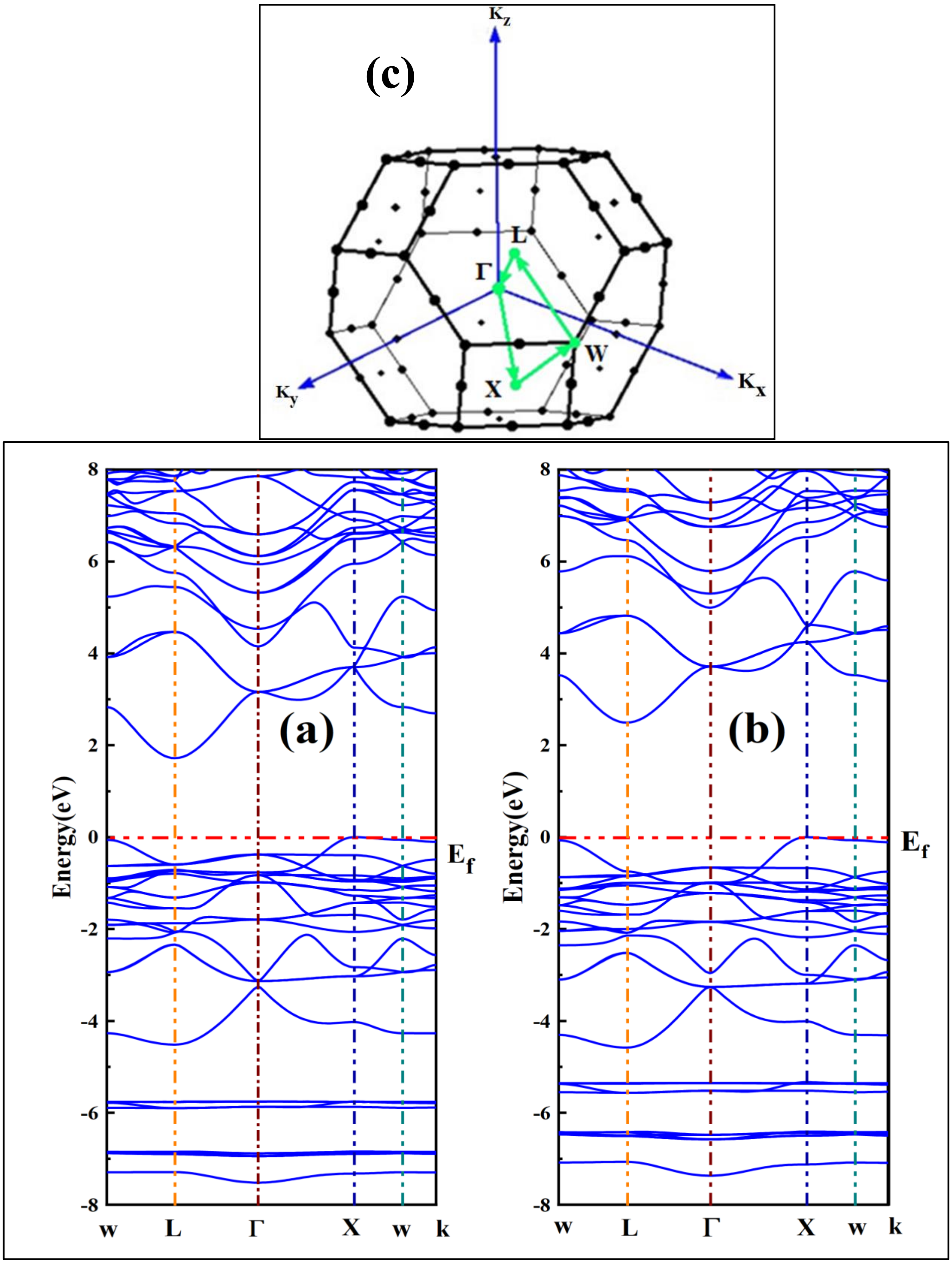

Figure III.6. (a) $Cs_2ZnPbBr_6$ and (b) $Cs_2ZnPbCl_6$ electronic band structures, and (c) the Brillouin zone of the Cs_2ZnPbX_6(X=Br, Cl) compounds.

The double perovskite's overall density of states is found to be between -4 and 0 volts. Below the Fermi level, the energy levels are what we currently occupy. However, the empty energy levels above the Fermi level are between 0 and 8 eV. Figure III.4. shows this, with the reference point at 0 eV serving as the Fermi level. as illustrated in Figure III.4. Because there is no overlap A band gap exists between the valence and conduction bands.

It is thought that determining possible areas for real-world applications requires a thorough examination of the density of states and band structures (BS) of the compounds. Figure III.5.(a.b) and Figure III.6.(a.b) show the first Brillouin zone's (BZ) calculated band structures, high symmetry directions, and density of states. respectively (Figure III.6.(c)). The indirect band gap values of $Cs_2ZnPbBr_6$ and $Cs_2ZnPbCl_6$ are 1.727 eV and 2.472 eV, respectively.

Right now Consequently, the conduction band minimum is converted into reduced energy when Br, a material with a larger ionic radius, takes the place of Cl, a substance with a smaller ionic radius. The $Cs_2ZnPbBr_6$ band gap is reduced by this substitution. The electrical states' net repulsion with one another must be changed in order to continuously modify the lattice.

This kind of band gap reduction has been connected to the quantum size effect. The computed Further clarification of the energy band arrangement in the computed band structures can be achieved by utilizing the overall density of states, as shown in Figure III.5.(b) and Figure III.5. (a.b), respectively. The Cs-p, Zn-p, Pb-p/s, and Cl/Br-p/ states predominate in the lower energy range (−2 eV to − 3.2 eV). The Cs/Zn-s states contribute slightly to the hybridization between −2 eV and −1.1 eV in the Cs-p, Zn-d, and Cl/Br-p states. Cl/Br-p, Zn-p/d, and Pb-s/d are hybridizing states.between -1.1 eV and -0.3 eV in energy. Fascinatingly, These three energy bands have no effect on the created electronic states. Pb-p/s, Cl/Br-p/d, Zn-s, and Cs-d hybridization all occur in the energy range 2.5 to 5 eV above the prohibited energy zone. The energy range between 5 and 6 eV is where the Cs-s/p/d, Zn-s, Pb-s/p, and Cl/Br-d hybridized states are most evident, and the energy range has little effect on these states. The energy band arrangement is nearly the same for both materials. Therefore, the states that constitute the valence band maximum and the conduction band minimum are the only ones that give birth to the physical attributes of both molecules.

3-4- Optical properties

A detailed analysis of the optical properties of the substances under investigation in order to employ them for optical applications. One can use the dielectric constant, ε(ω), to identify different optical properties and describe any material's optical behavior. This is the value of the complex dielectric constant:

$$\varepsilon_{(\omega)} = \varepsilon_{1(\omega)} + i\varepsilon_{2(\omega)} \qquad \text{(III.7)}$$

The dielectric constant's real part is represented by $\varepsilon_{1(\omega)}$ and its imaginary part by $\varepsilon_{2(\omega)}$ The actual part, $\varepsilon_{1(\omega)}$, shows the polarization and dispersion of the entering light, whereas the imaginary part, $\varepsilon_2(\omega)$, shows light absorption. Figure III.7.The calculated values of $\varepsilon_1(\omega)$ and $\varepsilon_2(\omega)$are shown against incident energy in (a.b.). At zero energy, the static dielectric constant $\varepsilon_1(\omega)$for $Cs_2ZnPbBr6$ is 4.4 eV, while for $Cs_2ZnPbCl_6$, it is 3.5 eV. It increases proportionately to the energy of the incident electromagnetic radiation. Both resonance peaks are located at 6.1 /3.4 eV and 7.4 /3.21 eV in the instance of Cs_2ZnPbX_6 (X=Br, Cl) indicate the precise light energy at which plane-polarization occurs. With ωp and ħ standing for the plank's constant and plasma resonance frequency, respectively, the bandgap energy and ε_1 (0) are computed from the band structures. are compatible with Penn's model. $\varepsilon_1(0) \approx 1 + \frac{\hbar\omega_p}{E_g}$ [126]. The inverse relationship between Table 1 makes the bandgap and $\varepsilon_1(0)$ clear. The Kramer-Kroning relation establishes a relationship between $\varepsilon_1(\omega)$ and $\varepsilon_2(\omega)$ [125].

$$\varepsilon_1(\omega) = 1 + \frac{2}{\pi} \mathrm{P} \int_0^{\infty} \frac{\omega' \varepsilon_2(\omega')}{\omega'^2 - \omega^2} d\omega' \qquad \text{(III.8)}$$

$$\varepsilon_2(\omega) = \frac{2e^2 h'}{\pi m^2 \omega^2} \sum_{v,c}' \int_{BZ}^{\infty} |M_{cv}(k)\ |^2 \delta[\omega_{cv}(k) - \omega] d^3k\, p \qquad \text{(III.9)}$$

This shows the wave vector (k) and the primary quantum number (P), respectively. The molar mass is denoted by M, h plank's constant, and ω angular frequency. The $\varepsilon_2(\omega)$ explains how impinging energy is absorbed as it passes through the molecule. If Br is used in place of Cl, the threshold absorption energy decreases to 1.91 eV for $Cs_2ZnPbCl_6$ and 1.06 eV for $Cs_2ZnPbBr_6$. The energy between the lowest and greatest of the bands of conduction and valence (X→Γ) is the threshold energy in the first Brillion zone. Inter-band transitions are responsible for the energy peaks at 2.93 eV/3.51 eV and 4.2 eV/5 eV in the computed $\varepsilon_2(\omega)$ spectra for Cs_2ZnPbX_6 (X=Br, Cl). The transitions [127]. from Zn/Pb-p/d to Cl/Br-p states are responsible for the second peak, whereas the Zn/Pb-d to Cl/Br-p states may be the origin of the initial peak. because the band gap narrows and the conduction band energy states decrease.

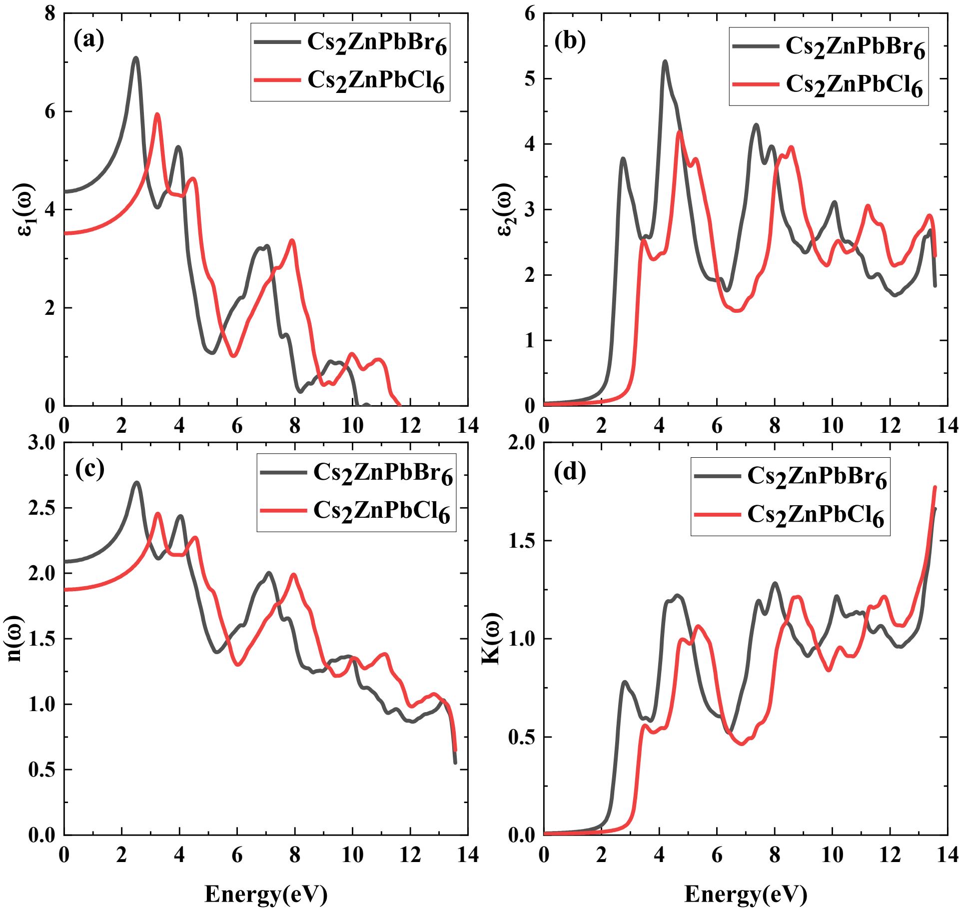

Figure III.7. (a) The dielectric constant's real portion, (b) its imaginary part, (c) the refractive index, and (d) the extinction coefficient of $Cs_2ZnPbBr_6$ and $Cs_2ZnPbCl_6$.

In Figure III.7.(c). Energy is displayed against the wavelength, group velocity, and material type all affect the refractive index, n(ω). The computed n(ω) for Cs_2ZnPbX_6 (X=Br, Cl) illustrates how energy is distributed across different wavelengths., with a maximum at 2.74 eV/2.4 eV and a minimum at 1,35 eV/.26 eV, respectively. The formula $n^2 - k^2 = \varepsilon_1(\omega)$. can be used to understand the connection between ε_1 (ω) and the refractive index n (ω).Thus, as Fig. 7 illustrates. (a.c.). At zero frequency, $n_0^2 = 0$ satisfied by the refractive index and the real dielectric constant, ε_1(0). Additionally, n (ω) in the energy range of 1–3 eV shows that these compounds have special optical properties for IR and UV light, which makes them important for optical applications. It suggests that these chemicals' unique infrared and ultraviolet optical characteristics

They are crucial for optical applications because of their wavelengths. Cs_2ZnPbX_6 (X=Br, Cl) has n(0) values of 2.125/1.62, which makes appropriate for solar cells that produce energy from visible light [125].

The material exhibits attenuation of light ($k > 0$), as indicated by the value of ε_2 (ω) is, k (ω).

Using the Kramer-Kroning connection, the spectra of k(ω) and ε_2(ω) are linked. connection [111]. making them similar (see Figure III.7.). (d.b)).

When considering expected absorption coefficients α(ω) for optical/solar cell applications, Figure III.8.(a) demonstrates that Cs_2ZnPbX_6 (Br, Cl) possesses the highest absorption peaks of 4.9/5.53eV.

The optical current produced by free carrier liberation due to incident energy is demonstrated by the electrical conductivity, σ(ω). Valence electrons become energized and move into the conduction band when photons with enough energy strike them. The graphs of the optical conductivity and absorption coefficients share the same features because of the increased electron concentration in the conduction band brought about by the decrease in input light. based on the data shown in Figure III.8. (b). Cs_2ZnPbX_6 (X=Br, Cl) has peak values of 4.1/4.9 eV. Materials can reflect, transmit, and absorb light all at once.

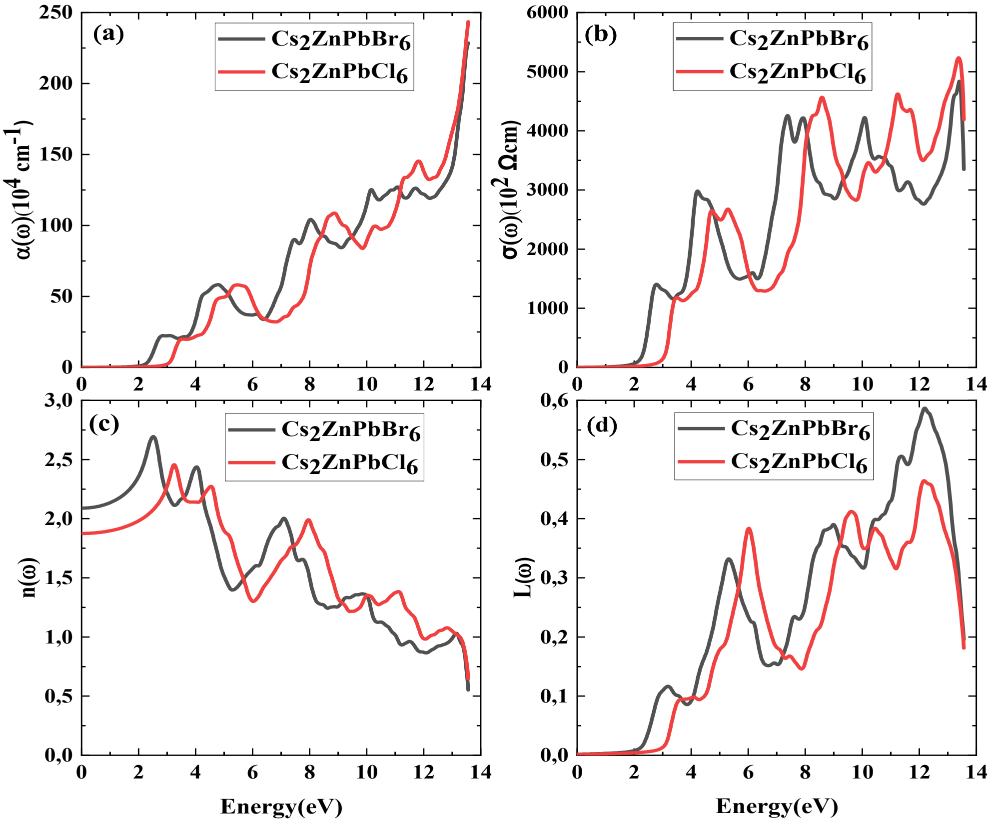

Figure III.8. (a) coefficient of absorption, optical loss factor, optical conductivity, and reflectivity of $Cs_2ZnPbBr_6$ and $Cs_2ZnPbCl_6$

Figure III.8. (c). determines and shows the reflectivity coefficient, or R (ω), in order to examine the light that is reflected from the surface. Up to 2 eV, the calculated R (ω) is relatively constant. Cs_2ZnPbX_6 (X=Br, Cl) reaches its greatest value at 2.5 eV for 0.30 and 3 eV for 1.9 energy levels.

The examination of the energy loss spectra shows that this parameter has no effect on The optical properties of the substances being studied. The projected L (ω) spectra, which have peaks at about 5.3/6.1 eV (see Figure III.8. (d)), make this clear. The range where the greatest absorption occurs is shown by these peaks. Because of their strong absorption in the visible spectrum, which lowers energy loss, reflection, and dispersion, the compounds under investigation are therefore appropriate for use in optical and solar cell applications.III.3.5 Elastic characteristics

We investigated the elastic properties of our material to verify its stability, as these qualities give us information on the material's stiffness, anisotropy, thermal expansion, and

Debye temperature. The linear elastic characteristics law known as Hooke's law serves as the foundation for most models that describe the elastic behavior of materials. Our alloy's elastic constants were recently calculated using Thomas Charpin's approach, which was used in the WIEN2k [128].

After taking certain symmetry considerations into account, the number of elastic moduli in a cubic crystal can be broken down into C_{11}, C_{12}, and C_{44}, three separate non-zero constants.To determine these constants, the three equations that must be solved which are produced by applying Three distinct kinds of deformation must be arranged on M. Mehl's method, which involves applying pressure-induced volume conservation to the sample, elastic constants are calculated from total energy [129].

We determine In conserved volume, the orthorhombic deformation tensor to determine the modulus (C_{11}-C_{12}). using the Mehl model [130].

$$\vec{\varepsilon} = \begin{bmatrix} \delta & 0 & 0 \\ 0 & -\delta & 0 \\ 0 & 0 & \dfrac{\delta^2}{1-\delta} \end{bmatrix} \tag{III.10}$$

where applied strain is represented by δ. The overall energy is affected when this constraint is applied:

$$E(\delta) = E(-\delta) = E(0) + (C_{11} - C_{12})V\delta^2 + o[\delta^4] \tag{III.11}$$

V is the elementary cell's conserved volume, and $E(0)$ is the system's energy in its single initial state (without constraints). We will get the following formula based on the curve:

$$E(\delta) = b\delta^2 + E(0) \tag{III.12}$$

Considering that b is the graph's slope coefficient $E(\delta) = f(\delta)$.

The following phrase is obtained by combining relations 3 and 4:

$$C_{11} - C_{12} = \frac{b}{V_0} \tag{III.13}$$

The compressibility modulus for an isotropic cubic frame provides a second equation. crystal, is required in order to determine the values of C_{11} and C_{12}.

$$B = \frac{1}{3}(C_{11} + 2C_{12}) \tag{III.14}$$

Lastly, we use the equation provides A deformation that is monoclinic and conserves volume. that follows, to find the third elastic constant, C_{44}

$$\vec{\varepsilon} = \begin{bmatrix} 0 & \frac{\delta}{2} & 0 \\ \frac{\delta}{2} & 0 & 0 \\ 0 & 0 & \frac{\delta^2}{4-\delta^2} \end{bmatrix} \text{after diagonalization } \vec{\varepsilon} = \begin{bmatrix} \frac{\delta}{2} & 0 & 0 \\ 0 & -\frac{\delta}{2} & 0 \\ 0 & 0 & \frac{\delta^2}{4-\delta^2} \end{bmatrix} \quad \text{(III.15)}$$

The total energy becomes

$$E(\delta) = E(-\delta) = E(0) + \frac{1}{2} C_{44} V \delta^2 + o[\delta^4] \quad \text{(III.16)}$$

Additionally, the equation for total energy looks like this

$$E(\delta) = b\delta^2 + E(0) \quad \text{(III.17)}$$

Equation 10 can be substituted into equation 11 to identify the elastic constant C_{44} using the following relationship

$$C_{44} = \frac{2b}{V_0} \quad \text{(III.18)}$$

The slope is indicated by b. These are the definitions of the stability criteria

$$C_{11} > 0, C_{44} > 0,\ C_{11} > C_{12}, (C_{11} + 2C_{12}) > 0 \text{ et } C_{12} < B < C_{11}$$

We can ascertain crucial elastic properties like these from elastic constants

If the anisotropy A is equal to 1, the crystal is said to be isotropic; if it is It is considered anisotropic if it is larger than or less than 1.

$$A = \frac{2C_{44}}{C_{11} - C_{12}} \quad \text{(III.19)}$$

The resistance to the planes' internal sliding motion when they are parallel to it is measured by the shear modules G. [131],

$$G = \frac{1}{5}(3C_{44} + C_{11} - C_{12}) \quad \text{(III.20)}$$

Young's modulus E, which gauges a solid's resistance to length variations.

$$E = \frac{9BG}{3B + G} \quad \text{(III.21)}$$

The solid's contraction v, using to characterize forces that are perpendicular to the direction of application.

$$\nu = \frac{1}{2}\left(1 - \frac{E}{3B}\right) \tag{III.22}$$

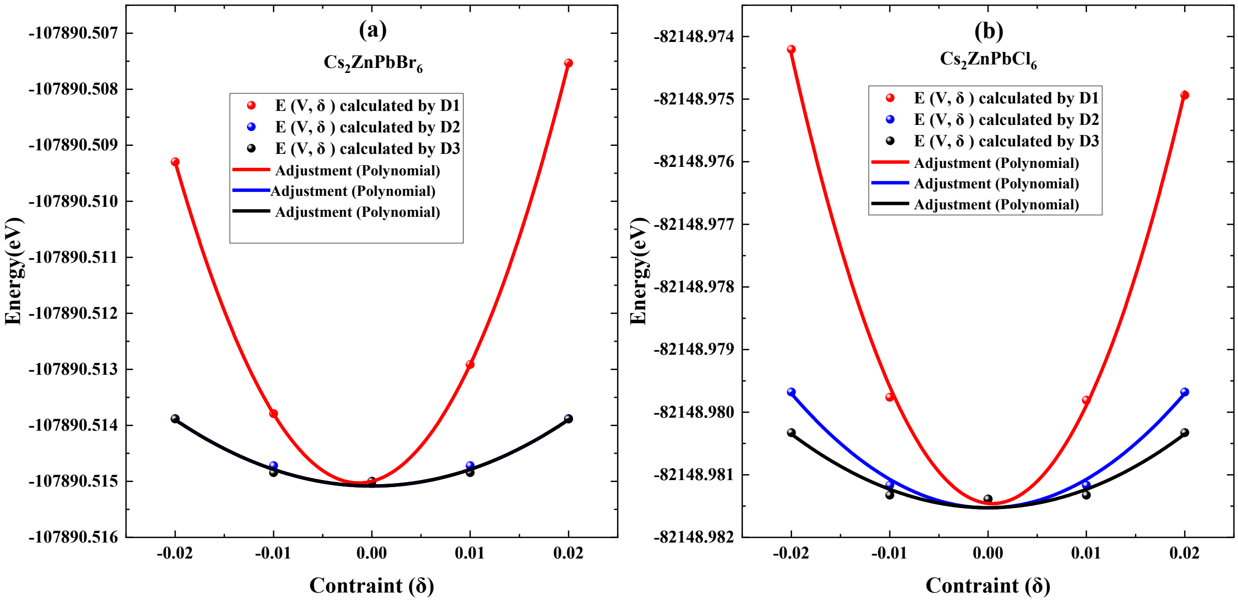

Figure III.9. E variation with the compound "Di" of Cs_2ZnPbX_6 (where X=Br, Cl)

The changes in total energy for the compounds $Cs_2ZnPbBr_6$ and $Cs_2ZnPbCl_6$ applying stresses EDi(δ) for three polynomially adjusted $\overrightarrow{D}_i$ at various orders are described in the caption for Figure III.9.Table III.2. provides a summary of all the values derived from the elastic constants. Since all of the elastic constant values satisfy Born's mechanical stability requirements, this evidence validates the mechanical stability of every compound under investigation. This result is supported by the given figure, which illustrates how the overall energy varies with stress and confirms our conclusions regarding The consistency of the materials.

Table III.2. shows E values determined at static equilibrium B_0 using the functional (GGA). These results demonstrate that the quantity mechanical values generated are very similar to the structural component's values. by altering the E=F(V) curved form. The strength of the used theoretical model and the correctness of our conclusions are strengthened by this fresh evidence.

Table III.2. Elastic constant C_{11}, C_{12}, and C_{44} (GPa), B/G ratio of Cs_2ZnPbX_6 (X=Br, Cl), and the B0 (GPa) modulus of elasticity at static equilibrium:

Materials	C_{11}	C_{12}	C_{44}	B_0	B/G
$Cs_2ZnPbBr_6$	32.973	16.273	8.833	21.840	2.5276
$Cs_2ZnPbCl_6$	47.968	16.054	10.281	26.692	2.1755

3-5- Elasticanisotropy

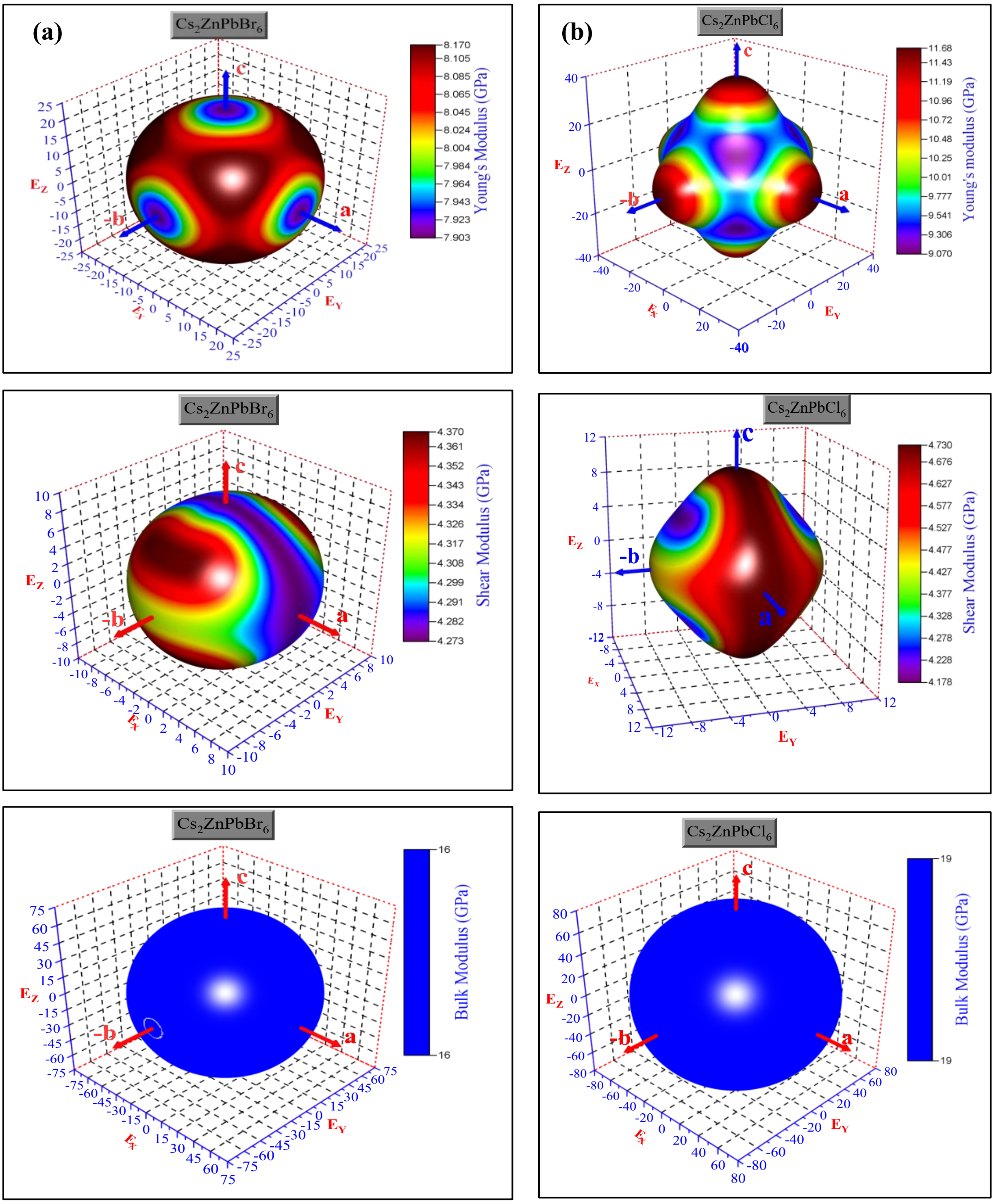

FigureIII.10. Young's modulus, bulk modulus, and shear modulus directional dependency surface for Cs_2ZnPbX_6 (X=Br, Cl) is shown in three dimensions.

Elastic properties' stability in three spatial orientations is shown by elastic variation, which makes it a crucial elastic feature. The two substances' elastic anisotropy/Zener contrast factor Az [130]. and the total contrast index Au [131]. of was examined in this study It was computed with the following formulas:

$$A^{Z} = \frac{2C_{44}}{C_{11} - C_{12}} \quad \text{(III.23)}$$

$$A^{U} = \frac{5G_{V}}{\mathrm{G_R}} + \frac{\mathrm{B_V}}{\mathrm{B_R}} - 6 \quad \text{(III.24)}$$

These calculations If the AU is near zero, the material is elastically anisotropic; if the Zener contrast factor value is near unity, the opposite is true. Otherwise, elastically anisotropic. Furthermore, the further the outcome departs from these preset parameters, the more contrast. Table III.3. values are close to this threshold. The low value of the two compounds under investigation is once again demonstrated by the flexible contrast.

According to the (100), (101), and (001) directions, The (AU), G(GPa), E(GPa), and υ surface forms in (FigureIII.10.(a) for $Cs_2ZnPbBr_6$) are almost spherical with slight distortions, indicating that these orientations are caused by this mild elastic anisotropy. But we also see this in other contexts, especially when it comes to respect. The substance has a practically isotropy along these axes because there is comparatively little deformation in them (111).

The material's divergence from bulk modulus, shear modulus, and Young's modulus all of which are significant in FigureIII.10. confirms its elastic variation. for $Cs_2ZnPbCl_6$ (b). The surface is found to be less (anisotropically) distorted along the (110) and (111) directions and more (anisotropically) deformed along the (100), (010) and (001) directions with respect to this shape.Therefore, any divergence from a spherical shape in the three-dimensional representation indicates the extent to which the elastic moduli imply anisotropy. The surface's topological critical values (average, minimum, and maximum) are also displayed in three dimensions in Table III.3., which accommodates variations between the greatest and lowest values.

Table III.3. Antisotropy factor by Zener AZ, Reuss, Voigt, and Hill's universal anisotropy index (AU), G(GPa), E(GPa), and υ for the following compounds were determined: (X=Br, Cl) Cs_2ZnPbX_6

	$Cs_2ZnPbBr_6$	$Cs_2ZnPbCl_6$
G_V	8.640	12.551
G_R	8.633	11.986
G_H	8.637	12.269
E_V	22.900	32.552
E_R	22.884	32.552
E_H	22.892	31.917
υ_V	0.3252	0.2967
υ_R	0.3254	0.3047
υ_H	0.3253	0.3007
A^U	0.0038	0.2357
A^Z	1.0578	0.6443

3-6- Transport properties

The following formulas were utilized to determine the compounds' thermoelectric properties under investigation, including (σ (κe), and (S).

$$\sigma_{\alpha\beta}(\alpha, \mu) = \frac{1}{\Omega}\int \sigma_{\alpha\beta}(\varepsilon)\left[\frac{\partial f_0(T, \varepsilon, \mu)}{\partial_\varepsilon}\right]d\varepsilon \tag{25}$$

$$k_e = \frac{1}{e^2T}\int (\varepsilon - \mu)^2\sigma(\varepsilon)\left[\frac{\partial f(\varepsilon)}{\partial_\varepsilon}\right]d\varepsilon \tag{26}$$

$$S_{\alpha\beta}(T, \mu) = \frac{1}{eT\Omega\alpha_\beta(T, \mu)}\int \sigma_{\alpha\beta}(\varepsilon)\,(\varepsilon - \mu)\left[\frac{\partial f_0(T, \varepsilon, \mu)}{\partial_\varepsilon}\right]d\varepsilon \tag{27}$$

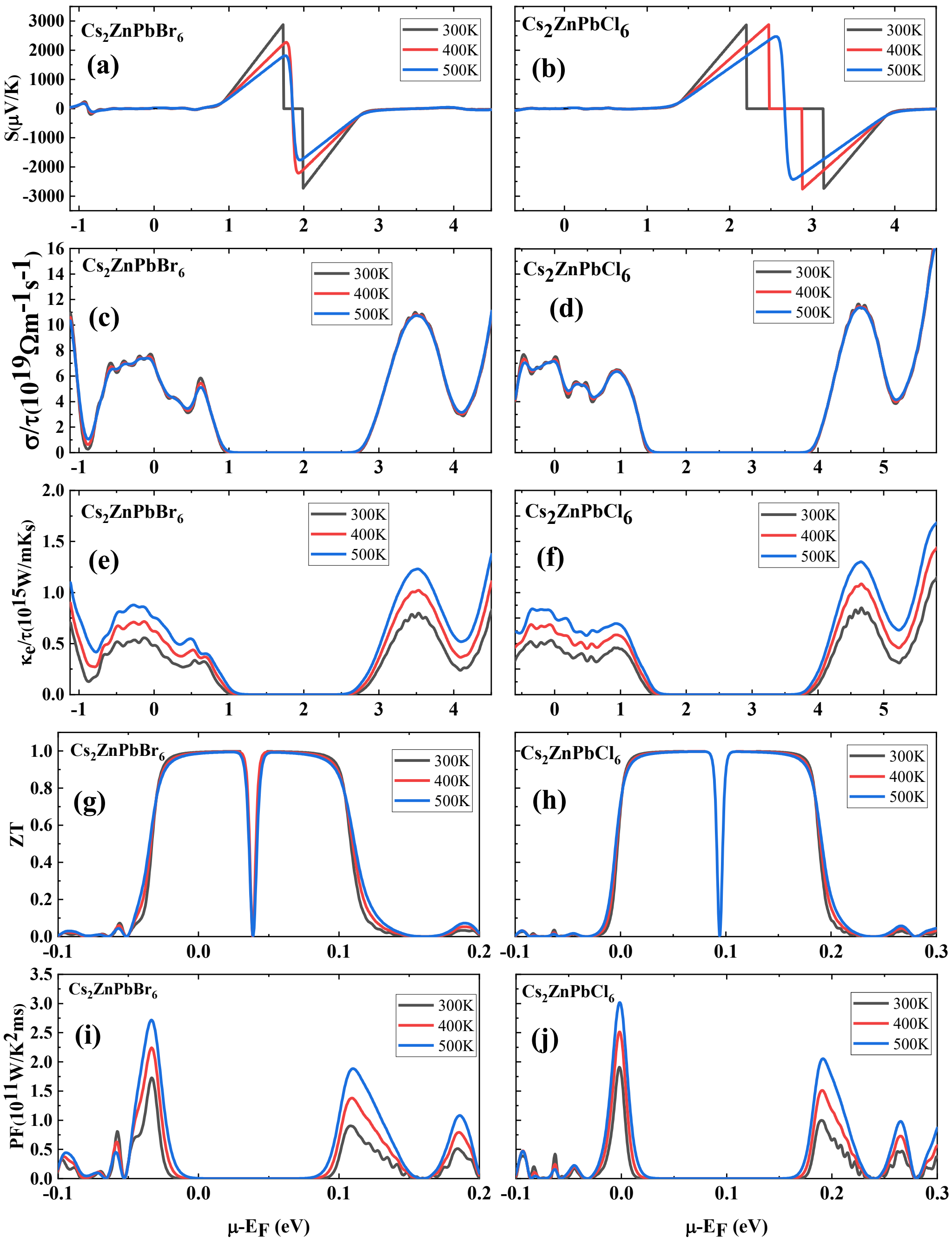

Figure III.11. variant of temperatures, R,σ,k_e,S relation to chemical potential.

Figure III.11.(**a.b)** displays The Seebeck modulus (S) is a measure of a material's thermal properties based on its chemical potential (μ-EF). The maximum value of S is reached at 300 K, with the highest values for $Cs_2ZnPbBr_6$ and $Cs_2ZnPbCl_6$ being 2880 μV/K and 2870 μV/K, respectively. The relationship between the chemical potential and thermal properties is quantitative, with P-type materials having a negative chemical potential [132]. and n-type materials having a positive one. The electrical conductivity (σ/τ) of the compounds is based on the amount of carrier movement and the functionality of the thermoelectric sensors. The one that σ/τ values for $Cs_2ZnPbCl_6$ and $Cs_2ZnPbBr_6$ peak at 11,66 and 10,98, respectively, on the p-type side at 300 K.

In this work, the thermoelectric characteristics of Cs_2ZnPbX_6 (X=Br, Cl) double perovskites are examined utilizing the BoltzTrap program's implementation of the semi-classical Boltzmann transport phenomenon [133].The merit (ZT) value has been calculated using equation (28). This equation incorporates balance between relaxation time and electrical conductivity(σ/τ), temperature (T), power factor (PF), and σ, and absolute S to the two relaxation time ratio (κ/τ). We have used the formulas from references [134]. to determine the parameters. Additionally, the Cs_2ZnPbX_6 (X = Cl, Br) Double Perovskite's figure of merit (ZT) Figure III.11. **(g.h).** is consistent with the rise near the Fermi level.

In the area of (μ-μ0 = 0.025 eV), the highest values are approximately equal to unity (higher than 0.98). eV is present in Cs_2ZnPbX_6 (X=Br, Cl). Furthermore, the PF of Cs_2ZnPbX_6 (X=Br, Cl) is shown against temperature and chemical potential in the following graphs:

The pair substances shown in Figure III.11. (i.j). The ability of a substance to generate energy is usually assessed using this thermoelectric property. According to Figure III.11. (i.j), Within the p-type charge area, PF values for both substances being investigated are more important. than those for n type charges. As the temperature increases, the PF value increases. does. exhibit remarkable thermoelectric material efficiency, offering guidance for the development of future innovative thermoelectric devices. The highest values for $Cs_2ZnPbBr_6$ and $Cs_2ZnPbCl_6$ are approximately (μ-μ0 = − 0.03 eV and (μ-μ0 = 0.01 eV) correspondingly). The corresponding maximum for $Cs_2ZnPbBr_6$ and $Cs_2ZnPbCl_6$ are roughly $(PF = 1{,}70 \times 1011\, W.K^{-1}.m^{-1}.s^{-1})$ and $(PF = 1{,}82 \times 1011 W.K^{-1}.m^{-1}.s^{-1}$) respectively.By verifying that both substances are highly effective thermoelectric materials at normal temperature , our studies suggest how to develop new thermoelectric devices in the future.

$$ZT = \frac{S^2\sigma T}{\kappa} \qquad (28)$$

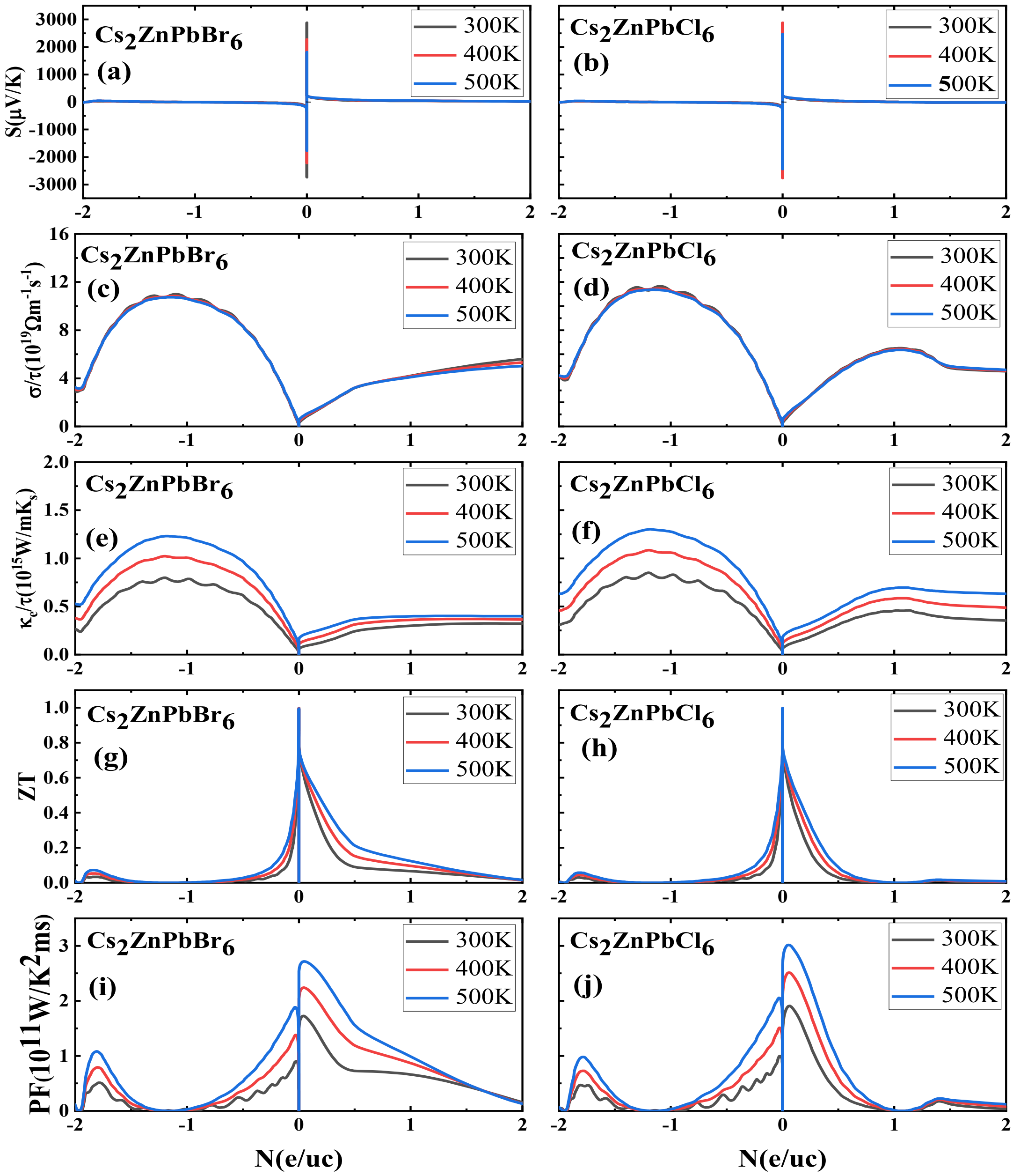

Figure III.12. shows the power factor, figure of marit, S; σ; K_e calculated against carrier concentration at various temperatures.

Finally, as seen in Figure III.12, we examine thermal characteristics based on the concentration of carriers, spanning $[-2n;\ 2n]$. (a.f.) Figure III.12.(a.b) displays the σ/τ value at various T, respectively. Cs_2ZnPbX_6 (X = Cl, Br) has σ/τ values of 11.63 on the p-type side.and 10.98 at 300 K, respectively, showing no appreciable temperature change. As the As Both good and negative effects of rising temperatures, Figure III.12 (c.d) shows an increase in thermal conductivity. As shown in Figure III.12 (e.f.), the Seebeck coefficient values for $Cs_2ZnPbBr_6$ and $Cs_2ZnPbCl_6$ are identical. illustrates. On both the +ve and -ve sides, the

Seebeck coefficient increases linearly as n's value rises. Overall, we concluded that the Cs_2ZnPbX_6(X = Cl, Br) molecule's positive or negative side did not alter as the temperature increased.

As the temperature rises, the power factor and marit figure in Figure III.12 (g.h) and Figure III.12 (i.j) respectively demonstrate an increase at 0. Because they are used in thermoelectric devices, their value rises as the temperature does.

3-7- Thermodynamic properties

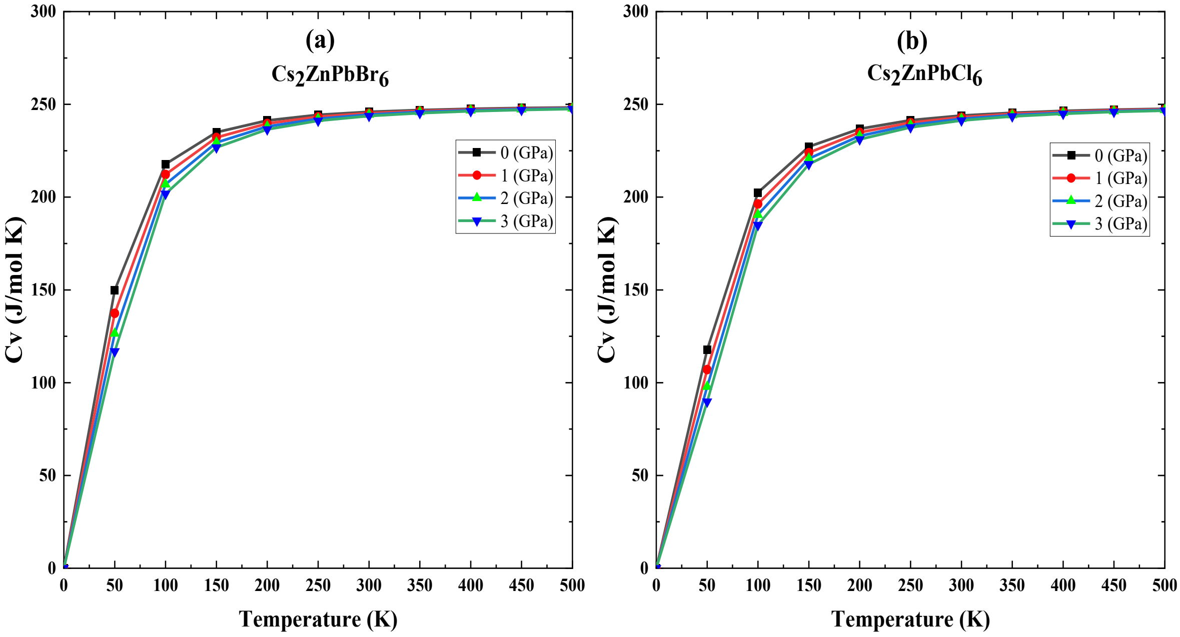

Figure III.13. A plot that demonstrates the heat capacity under continuous pressure. according to temperature.

Using the Gibbs program, the thermodynamic characteristics of Cs_2ZnPbX_6 (X = Br, Cl) double perovskites are examined [135]. These Properties were computed in the range of 0 to 500 K for temperature and 0 to 3 GPa for pressure. To understand the vibrational properties of materials, one of the most important factors is (CV). Figure III.13. illustrates how T and P affect the heat capacity (CV) of $Cs_2ZnPbBr_6$ and $Cs_2ZnPbCl_6$. In the lower temperature range, T3 is proportional to these curves. and follow the Debye lows [136]. The Dulong-Petit limit [136]. which is roughly $247.7\,J\,mol^{-1}\,K^{-1}$, is approached by the specific heat (CV) as the temperature increases and approaches the Debye model. This suggests a simulation that includes all phonon modes in this range as well as thermal energy. Additionally, we can note that as pressure (P) decreases, these compounds' heat capacity rises.

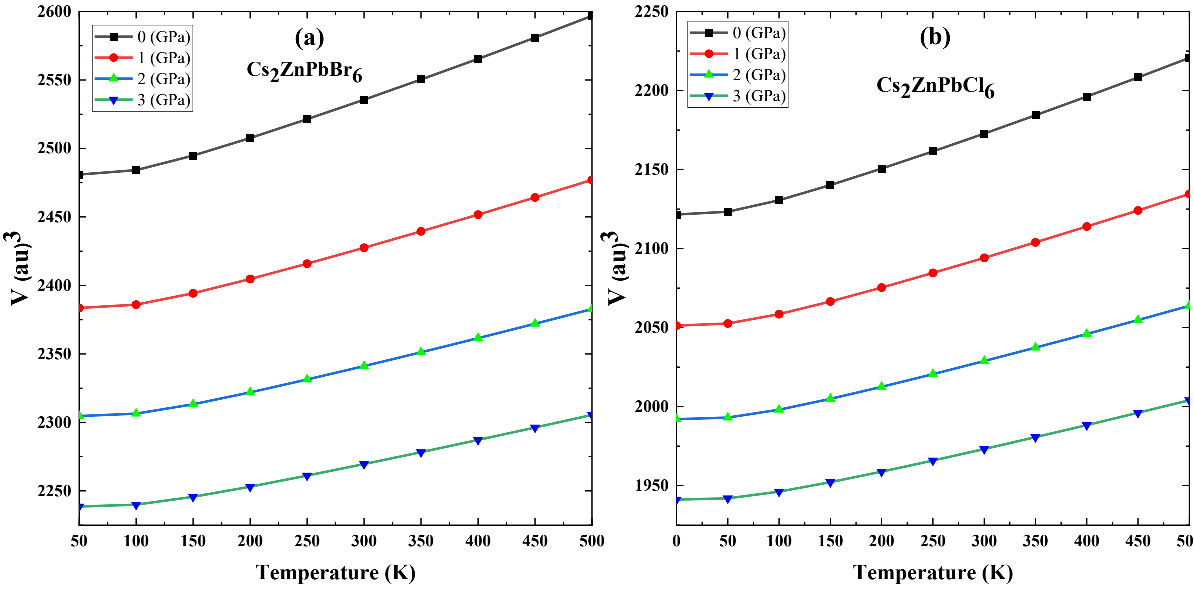

Figure III.14. A plot showing variation of V with T under constant pressure.

Furthermore, Figure III.14. shows how (T) and (P) affect the amount of Cs_2ZnPbX_6 (X = Br, Cl) crystals. These charts clearly show that the volume rises with decreasing pressure values and expands with increasing temperature.

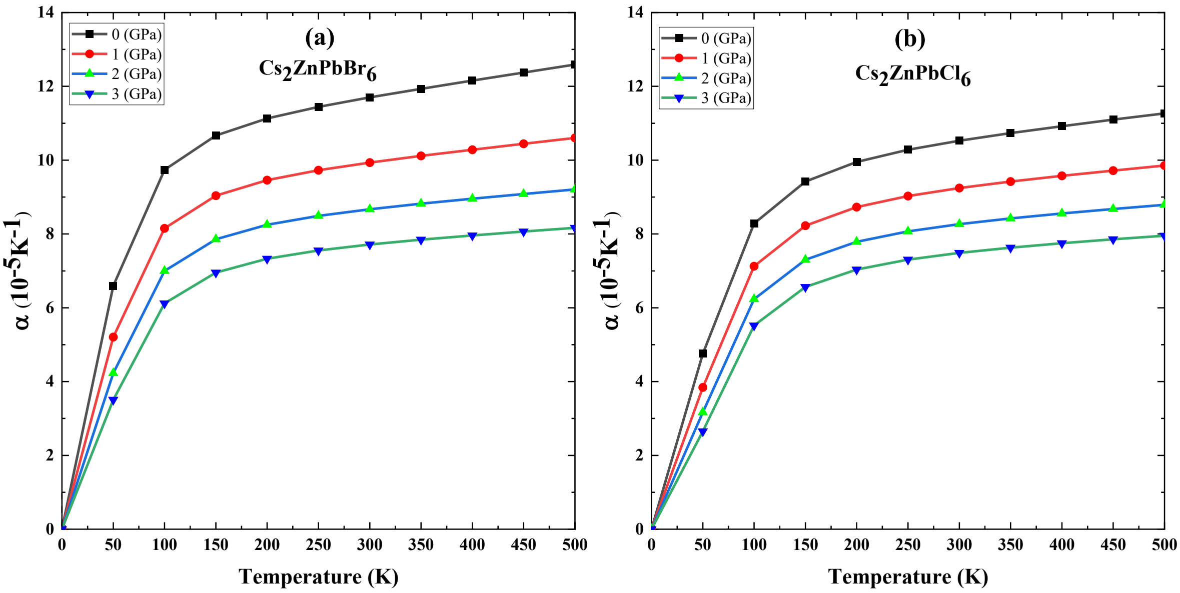

Figure III.15. shows a plot of the coefficient of thermal expansion at constant pressure as a function of temperature.

Moreover, Figure III.15.shows how temperature (T) and pressure (P) affect the thermal expansion coefficient (α) of $Cs_2ZnPbBr_6$ and $Cs_2ZnPbCl_6$. Among these spectra is that (α) reaches a significant nonlinear growth in the $T < 200K$ range at low temperatures. As the temperature rises, $T > 200K$ begins to take on a linear shape and progressively increases.

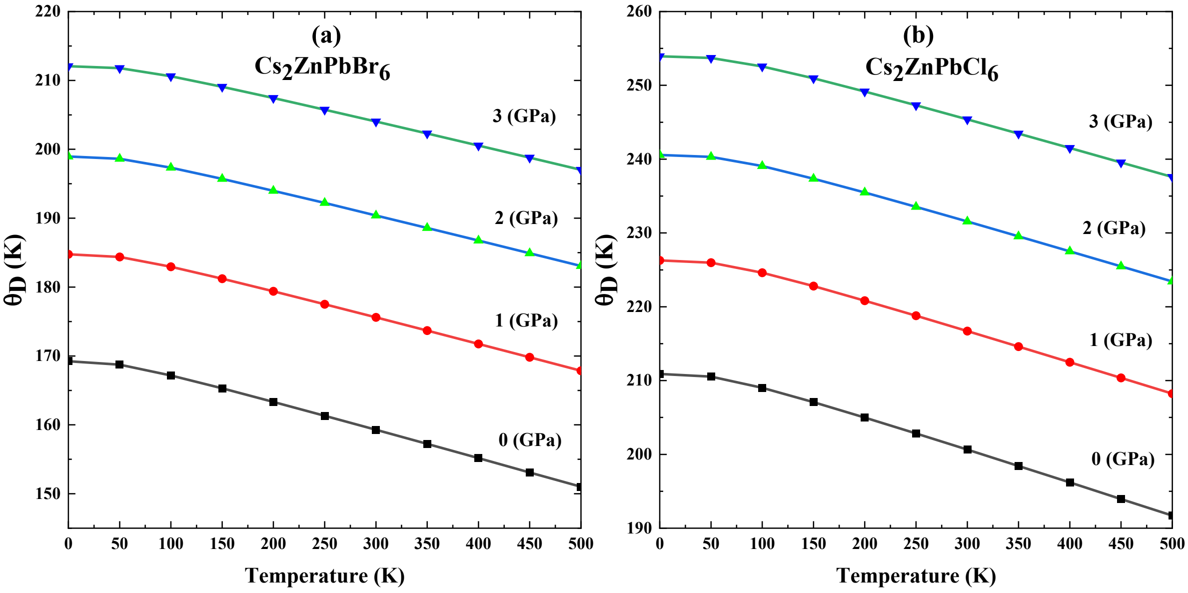

Figure III.16. Debye temperature plot at constant pressure as a function of temperature.

Furthermore, as illustrated in Figure III.16., We investigate the changes in the Debye temperature (θ_D) as the temperature (T) varies from 0 K to 500 K. These charts demonstrate that (θ_D) exhibits a linear drop as the temperature rises and the pressure increases. As the ionic atom X moves from Cl to Br, the values for the two compounds (θ_D) decrease. The temperature of Debye of $Cs_2ZnPbBr_6$ is roughly 159.28 K at ambient temperature and zero pressure, while that of $Cs_2ZnPbCl_6$ is about 200.64 K.

GENERAL CONCLUSION

General conclusion

Finally, the transportation and structural, elastic, and optoelectical characteristics of the perovskite cubic halide $Cs_2ZnPbX6$ (X = Br, Cl) were investigated. using a thorough DFT search with the WIEN2k code.

For these materials, the best lattice constants were discovered at zero Kelvin, a temperature for which there aren't any experimental support. The most probable cubic structure in the number 225 for the space group corresponds to the ground state. (Fm-3m). of Cs_2ZnPbX_6 (X=Br, Cl). Structural strength is addressed by octahedral and tolerance factors. By figuring out the elastic constants, we were able to show that all composites were mechanically stable. In this computation, PBE-GGA was utilized. These perovskites exhibit characteristics of semiconductors.

For Cs_2ZnPbX_6 (X = Br, Cl), the band structure and DOS of these compounds were confirmed They possessed a small indirect band gap of 1.727 eV for Chemical link covalent ionic mixing and an indirect band gap of 2.472 eV for the (L-X) direction. semiconductor properties of substance.

These substances is applicable to optoelectical devices and provide strong visible optical absorption. devices.

We've examined these materials' mechanical, optical, and transport properties for the first time, as far as we are aware. Additionally, because of their extraordinarily low kL values, these materials might be used in thermoelectric generators. Keep in mind, nevertheless, that this substance is still being studied and needs more thorough and in-depth dynamic investigations.

We strongly advise that more research be done on this molecule in order to completely comprehend its possible uses and characteristics, both theoretically and experimentally.

Diagram illustrating the work completed

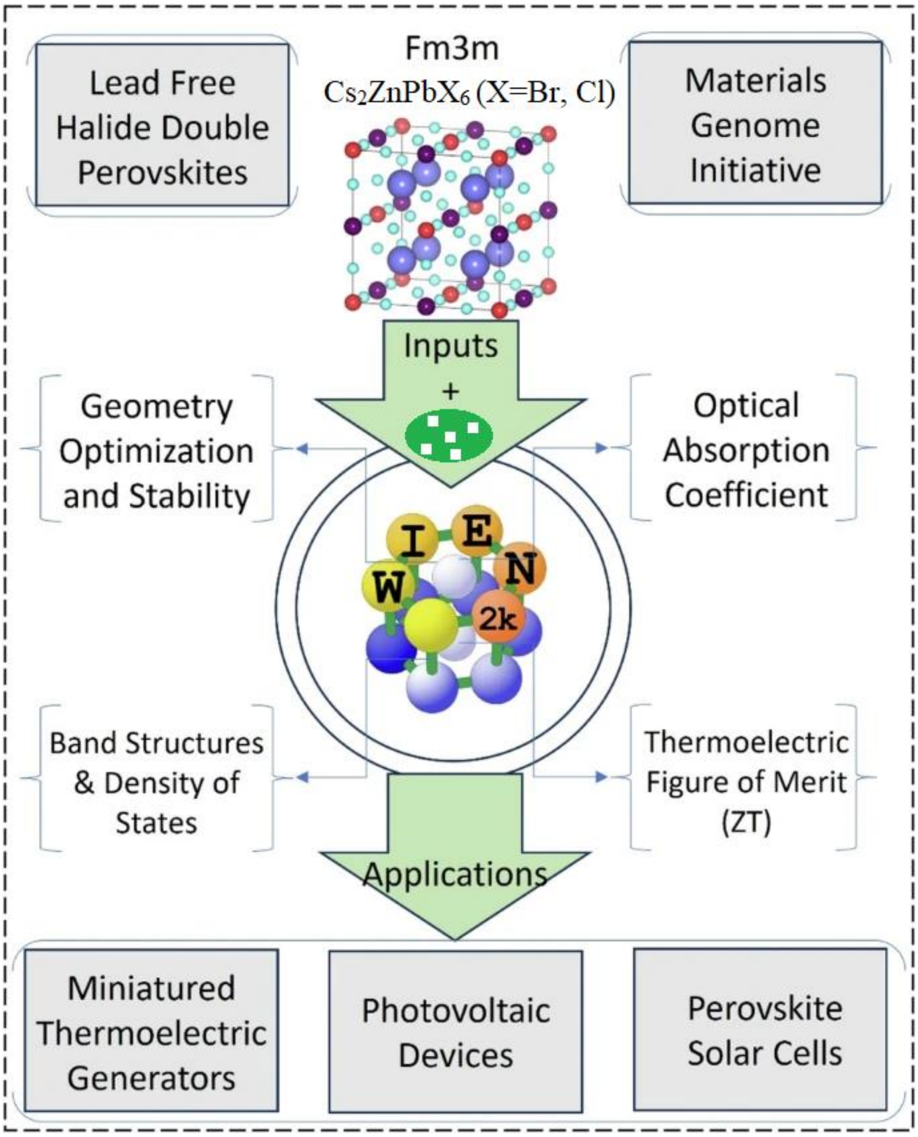

Figure IV.1 : Conceptual framework for the investigation of lead-based halide double perovskites

This figure presents a systematic and integrated overview of the theoretical methodology adopted for investigating lead-free halide double perovskites, specifically compounds with the chemical formula Cs_2ZnPbX_6 (X = Br, Cl) crystallizing in the cubic $Fm\bar{3}m$ space group. The diagram illustrates the logical progression from material selection and structural modeling to the evaluation of fundamental physical properties and their relevance to practical applications, at the top of the framework, the focus is placed on lead-free halide double perovskites, which are considered promising alternatives to conventional lead-based perovskites due to their reduced toxicity, improved chemical stability, and tunable physical properties. These materials belong to the $A_2BB'X_6$ double perovskite family, where two different cations (Zn and Pb) occupy the B-sites, leading to enhanced structural robustness, the central part of the figure shows the crystal structure of Cs_2ZnPbX_6, characterized by a highly symmetric cubic arrangement. In this structure, ZnX_6 and PbX_6 octahedra are alternately distributed and connected through corner-sharing, forming a three-dimensional framework, the high crystallographic symmetry ($Fm\overline{3}m$) plays a crucial role in determining the electronic band dispersion, optical transitions, and thermal transport properties of the material.

The Materials Genome Initiative (MGI) concept highlighted in the diagram reflects the use of a computationally driven materials discovery approach, by integrating structural data with theoretical modeling, this approach enables an efficient and predictive evaluation of material properties, thereby accelerating the identification of compounds with optimized performance, the green arrow labeled “Inputs” represents the essential structural and computational inputs, including optimized lattice parameters, atomic positions, and symmetry information, these inputs serve as the foundation for subsequent theoretical analyses,the circular workflow surrounding the central structure emphasizes the interconnection between different physical properties, on the left side of the framework, geometry optimization and stability analysis are conducted to confirm the structural feasibility and energetic stability of the compounds, this step ensures that the proposed structures correspond to physically realizable configurations, subsequently, the electronic band structure and density of states are calculated to investigate the nature of the band gap, charge carrier dispersion, and orbital contributions near the Fermi level, on the right side, the optical absorption coefficient is evaluated to assess the interaction of the material with electromagnetic radiation, which is essential for optoelectronic and photovoltaic applications, additionally, the thermoelectric figure of merit (ZT) is analyzed to quantify the efficiency of the material in converting thermal gradients into electrical energy, finally, the bottom part of the figure links the investigated physical properties to potential applications, including miniaturized thermoelectric generators, photovoltaic devices, and perovskite-based solar cells.

This highlights the multifunctional nature of Pb-containing double perovskites and their potential for next-generation energy conversion technologies.

REFERENCES

References

[2] S. Nazir, N. A. Noor, A. Gassoumi, K. Abid, M. S. Mumtaz, et H.-E. M. Saad, « Investigation of Opto-Electronic and Thermoelectric Characteristics of Halide Perovskite CdLiCl3 for Energy Conversion Applications at Different Pressure », *J Inorg Organomet Polym*, vol. 35, nº 1, p. 493-502, janv. 2025, doi: 10.1007/s10904-024-03284-0.

[3] L. Ortega-San-Martin, « Introduction to Perovskites: A Historical Perspective », in *Revolution of Perovskite*, N. S. Arul et V. D. Nithya, Éd., in Materials Horizons: From Nature to Nanomaterials. , Singapore: Springer Singapore, 2020, p. 1-41. doi: 10.1007/978-981-15-1267-4_1.

[4] N.-G. Park, « Crystal growth engineering for high efficiency perovskite solar cells », *CrystEngComm*, vol. 18, nº 32, p. 5977-5985, 2016, doi: 10.1039/C6CE00813E.

[5] A. DI VERA, « Alternative halide perovskite structures for light-based applications », 2025.

[6] J. S. Manser, J. A. Christians, et P. V. Kamat, « Intriguing Optoelectronic Properties of Metal Halide Perovskites », *Chem. Rev.*, vol. 116, nº 21, p. 12956-13008, nov. 2016, doi: 10.1021/acs.chemrev.6b00136.

[7] H. Dong, C. Ran, W. Gao, M. Li, Y. Xia, et W. Huang, « Metal Halide Perovskite for next-generation optoelectronics: progresses and prospects », *eLight*, vol. 3, nº 1, p. 3, janv. 2023, doi: 10.1186/s43593-022-00033-z.

[8] Y. Dong, Y. Zou, J. Song, X. Song, et H. Zeng, « Recent progress of metal halide perovskite photodetectors », *Journal of Materials Chemistry C*, vol. 5, nº 44, p. 11369-11394, 2017.

[9] S. Liu, V. P. Biju, Y. Qi, W. Chen, et Z. Liu, « Recent progress in the development of high-efficiency inverted perovskite solar cells », *NPG Asia Mater*, vol. 15, nº 1, p. 27, mai 2023, doi: 10.1038/s41427-023-00474-z.

[10] J. Jeng *et al.*, « CH_3 NH_3 PbI_3 Perovskite/Fullerene Planar-Heterojunction Hybrid Solar Cells », *Advanced Materials*, vol. 25, nº 27, p. 3727-3732, juill. 2013, doi: 10.1002/adma.201301327.

[11] P. Baraneedharan *et al.*, « Recent Advances and Remaining Challenges in Perovskite Solar Cell Components for Innovative Photovoltaics », *Nanomaterials*, vol. 14, nº 23, p. 1867, nov. 2024, doi: 10.3390/nano14231867.

[12] M. Ren, X. Qian, Y. Chen, T. Wang, et Y. Zhao, « Potential lead toxicity and leakage issues on lead halide perovskite photovoltaics », *Journal of Hazardous Materials*, vol. 426, p. 127848, mars 2022, doi: 10.1016/j.jhazmat.2021.127848.

[13] Y. Liu, A. Nag, L. Manna, et Z. Xia, « Lead-Free Double Perovskite Cs_2 $AgInCl_6$ », *Angewandte Chemie*, vol. 133, nº 21, p. 11696-11707, mai 2021, doi: 10.1002/ange.202011833.

[14] V. Kumar, A. Kathiravan, et M. A. Jhonsi, « Beyond lead halide perovskites: Crystal structure, bandgaps, photovoltaic properties and future stance of lead-free halide double perovskites », *Nano Energy*, vol. 125, p. 109523, juin 2024, doi: 10.1016/j.nanoen.2024.109523.

[15] A. EL KENZ *et al.*, « A DFT study of structural, electronic, optical and transport properties of Lead-free simple, inverse and double perovskite compounds for photovoltaic, photocatalytic and thermoelectric applications ».

[16] Z. Ashraf, D. Rafique, T. Mehmood, et D. Akbar, « Ab-Initio Study of Electronic and Structural Properties for BaSnO3 Compound Using DFT Calculations and FP-LAPW Technique in Wein2k Software », 24 mars 2021, *In Review*. doi: 10.21203/rs.3.rs-325590/v1.

[17] Q. Dong *et al.*, « Electron-hole diffusion lengths > 175 μm in solution-grown CH_3 NH_3 PbI_3 single crystals », *Science*, vol. 347, nº 6225, p. 967-970, févr. 2015, doi: 10.1126/science.aaa5760.

[18] E. A. Katz, « Perovskite: Name Puzzle and German-Russian Odyssey of Discovery », *Helvetica Chimica Acta*, vol. 103, nº 6, p. e2000061, juin 2020, doi: 10.1002/hlca.202000061.

[19] P. M. Woodward, *Structural distortions, phase transitions, and cation ordering in the perovskite and tungsten trioxide structures*. Oregon State University, 1997.

[20] R. M. Hazen, « Perovskites », *Scientific American*, vol. 258, nº 6, p. 74-81, 1988.

[21] M. A. Green et A. Ho-Baillie, « Perovskite Solar Cells: The Birth of a New Era in Photovoltaics », *ACS Energy Lett.*, vol. 2, nº 4, p. 822-830, avr. 2017, doi: 10.1021/acsenergylett.7b00137.

[22] N. Tsuda, K. Nasu, A. Fujimori, et K. Siratori, *Electronic Conduction in Oxides*, vol. 94. in Springer Series in Solid-State Sciences, vol. 94. Berlin, Heidelberg: Springer Berlin Heidelberg, 2000. doi: 10.1007/978-3-662-04011-9.

[23] I. El Harrad, « Contribution à l'étude structurale et spectroscopique de céramiques pérovskites PLZT [...] et PZTN [...] et de leurs transitions de phases », 1994.

[24] F. Ünlü *et al.*, « Understanding the interplay of stability and efficiency in A-site engineered lead halide perovskites », *APL Materials*, vol. 8, n° 7, p. 070901, juill. 2020, doi: 10.1063/5.0011851.

[25] D. Ji *et al.*, « Regulatory tolerance and octahedral factors by using vacancy in APbI3 perovskites », *Vacuum*, vol. 164, p. 186-193, juin 2019, doi: 10.1016/j.vacuum.2019.03.018.

[26] Q. A. Akkerman et L. Manna, « What Defines a Halide Perovskite? », *ACS Energy Lett.*, vol. 5, n° 2, p. 604-610, févr. 2020, doi: 10.1021/acsenergylett.0c00039.

[27] S. Burger, M. G. Ehrenreich, et G. Kieslich, « Tolerance factors of hybrid organic–inorganic perovskites: recent improvements and current state of research », *J. Mater. Chem. A*, vol. 6, n° 44, p. 21785-21793, 2018, doi: 10.1039/C8TA05794J.

[28] T. Sato, S. Takagi, S. Deledda, B. C. Hauback, et S. Orimo, « Extending the applicability of the Goldschmidt tolerance factor to arbitrary ionic compounds », *Sci Rep*, vol. 6, n° 1, p. 23592, avr. 2016, doi: 10.1038/srep23592.

[29] C. M. Guvenc *et al.*, « Breaking the Boundaries of the Goldschmidt Tolerance Factor with Ethylammonium Lead Iodide Perovskite Nanocrystals », *ACS Nano*, vol. 19, n° 1, p. 1557-1565, janv. 2025, doi: 10.1021/acsnano.4c14536.

[30] C. J. Bartel *et al.*, « New tolerance factor to predict the stability of perovskite oxides and halides », *Sci. Adv.*, vol. 5, n° 2, p. eaav0693, févr. 2019, doi: 10.1126/sciadv.aav0693.

[31] M. R. Filip et F. Giustino, « The geometric blueprint of perovskites », *Proc. Natl. Acad. Sci. U.S.A.*, vol. 115, n° 21, p. 5397-5402, mai 2018, doi: 10.1073/pnas.1719179115.

[32] W. Travis, E. N. K. Glover, H. Bronstein, D. O. Scanlon, et R. G. Palgrave, « On the application of the tolerance factor to inorganic and hybrid halide perovskites: a revised system », *Chem. Sci.*, vol. 7, n° 7, p. 4548-4556, 2016, doi: 10.1039/C5SC04845A.

[33] S. Wang *et al.*, « Temperature-Dependent Band Gap in Two-Dimensional Perovskites: Thermal Expansion Interaction and Electron–Phonon Interaction », *J. Phys. Chem. Lett.*, vol. 10, n° 10, p. 2546-2553, mai 2019, doi: 10.1021/acs.jpclett.9b01011.

[34] T. Işık, « Solar Cells review », 2015, *Unpublished*. doi: 10.13140/RG.2.1.4298.6404.

[35] Md. S. Hossain *et al.*, « Pressure induced semiconductor to metal phase transition in cubic CsSnBr3 perovskite », *AIP Advances*, vol. 11, nº 5, p. 055024, mai 2021, doi: 10.1063/5.0048979.

[36] G. Volonakis *et al.*, « Cs_2 $InAgCl_6$: A New Lead-Free Halide Double Perovskite with Direct Band Gap », *J. Phys. Chem. Lett.*, vol. 8, nº 4, p. 772-778, févr. 2017, doi: 10.1021/acs.jpclett.6b02682.

[37] A. Capitaine et B. Sciacca, « Monocrystalline Methylammonium Lead Halide Perovskite Materials for Photovoltaics », *Advanced Materials*, vol. 33, nº 52, p. 2102588, déc. 2021, doi: 10.1002/adma.202102588.

[38] H. J. Snaith, « Perovskites: The Emergence of a New Era for Low-Cost, High-Efficiency Solar Cells », *J. Phys. Chem. Lett.*, vol. 4, nº 21, p. 3623-3630, nov. 2013, doi: 10.1021/jz4020162.

[39] S. D. Stranks *et al.*, « Electron-Hole Diffusion Lengths Exceeding 1 Micrometer in an Organometal Trihalide Perovskite Absorber », *Science*, vol. 342, nº 6156, p. 341-344, oct. 2013, doi: 10.1126/science.1243982.

[40] W. Xiang, S. (Frank) Liu, et W. Tress, « A review on the stability of inorganic metal halide perovskites: challenges and opportunities for stable solar cells », *Energy Environ. Sci.*, vol. 14, nº 4, p. 2090-2113, 2021, doi: 10.1039/D1EE00157D.

[41] M. Kaltenbrunner *et al.*, « Flexible high power-per-weight perovskite solar cells with chromium oxide–metal contacts for improved stability in air », *Nature Mater*, vol. 14, nº 10, p. 1032-1039, oct. 2015, doi: 10.1038/nmat4388.

[42] M. E. Lines et A. M. Glass, *Principles and applications of ferroelectrics and related materials*. Oxford university press, 2001.

[43] D. B. Mitzi, « ChemInform Abstract: Synthesis, Structure, and Properties of Organic—Inorganic Perovskites and Related Materials », *ChemInform*, vol. 30, nº 31, p. chin.199931300, août 1999, doi: 10.1002/chin.199931300.

[44] G. Kieslich, S. Sun, et A. K. Cheetham, « Solid-state principles applied to organic–inorganic perovskites: new tricks for an old dog », *Chem. Sci.*, vol. 5, nº 12, p. 4712-4715, 2014, doi: 10.1039/C4SC02211D.

[45] B. Lee *et al.*, « Air-Stable Molecular Semiconducting Iodosalts for Solar Cell Applications: Cs_2 SnI_6 as a Hole Conductor », *J. Am. Chem. Soc.*, vol. 136, nº 43, p. 15379-15385, oct. 2014, doi: 10.1021/ja508464w.

[46] D. H. Cao, C. C. Stoumpos, O. K. Farha, J. T. Hupp, et M. G. Kanatzidis, « 2D Homologous Perovskites as Light-Absorbing Materials for Solar Cell Applications », *J. Am. Chem. Soc.*, vol. 137, nº 24, p. 7843-7850, juin 2015, doi: 10.1021/jacs.5b03796.

[47] M. D. Smith, B. A. Connor, et H. I. Karunadasa, « Tuning the Luminescence of Layered Halide Perovskites », *Chem. Rev.*, vol. 119, nº 5, p. 3104-3139, mars 2019, doi: 10.1021/acs.chemrev.8b00477.

[48] M. Saliba *et al.*, « Cesium-containing triple cation perovskite solar cells: improved stability, reproducibility and high efficiency », *Energy Environ. Sci.*, vol. 9, nº 6, p. 1989-1997, 2016, doi: 10.1039/C5EE03874J.

[49] G. Volonakis et F. Giustino, « Surface properties of lead-free halide double perovskites: Possible visible-light photo-catalysts for water splitting », *Applied Physics Letters*, vol. 112, nº 24, p. 243901, juin 2018, doi: 10.1063/1.5035274.

[50] D. Hao, Z. Yang, J. Huang, et F. Shan, « Recent Developments of Optoelectronic Synaptic Devices Based on Metal Halide Perovskites », *Adv Funct Materials*, vol. 33, nº 8, p. 2211467, févr. 2023, doi: 10.1002/adfm.202211467.

[51] G. Volonakis *et al.*, « Lead-Free Halide Double Perovskites via Heterovalent Substitution of Noble Metals », *J. Phys. Chem. Lett.*, vol. 7, nº 7, p. 1254-1259, avr. 2016, doi: 10.1021/acs.jpclett.6b00376.

[52] A. Walsh et A. Zunger, « Instilling defect tolerance in new compounds », *Nature Mater*, vol. 16, nº 10, p. 964-967, oct. 2017, doi: 10.1038/nmat4973.

[53] C. J. Howard et H. T. Stokes, « Group-Theoretical Analysis of Octahedral Tilting in Perovskites. Erratum », *Acta Crystallogr B Struct Sci*, vol. 58, nº 3, p. 565-565, juin 2002, doi: 10.1107/S010876810200890X.

[54] S. Vasala et M. Karppinen, « A2B′B″O6 perovskites: A review », *Progress in Solid State Chemistry*, vol. 43, nº 1-2, p. 1-36, mai 2015, doi: 10.1016/j.progsolidstchem.2014.08.001.

[55] S. Sun, D. Yuan, Y. Xu, A. Wang, and Z. Deng, "Ligand-mediated synthesis of shape-controlled cesium lead halide perovskite nanocrystals," *ACS Nano*, vol. 10, no. 3, pp. 3648–3657, 2016.
DOI: 10.1021/acsnano.5b08193

[56] T. M. Brenner et al., “Hybrid organic–inorganic perovskites: low-cost semiconductors with intriguing charge-transport properties,” *Nature Reviews Materials*, vol. 1, 2016. DOI: 10.1038/natrevmats.2016.7

[57] A. M. Glazer, « The classification of tilted octahedra in perovskites », *Acta Crystallogr B Struct Crystallogr Cryst Chem*, vol. 28, nº 11, p. 3384-3392, nov. 1972, doi: 10.1107/S0567740872007976.

[58] A. Togo et I. Tanaka, « First principles phonon calculations in materials science », *Scripta Materialia*, vol. 108, p. 1-5, nov. 2015, doi: 10.1016/j.scriptamat.2015.07.021.

[59] A. H. Slavney, T. Hu, A. M. Lindenberg, et H. I. Karunadasa, « A Bismuth-Halide Double Perovskite with Long Carrier Recombination Lifetime for Photovoltaic Applications », *J. Am. Chem. Soc.*, vol. 138, nº 7, p. 2138-2141, févr. 2016, doi: 10.1021/jacs.5b13294.

[60] Y. Su *et al.*, « Origin of low lattice thermal conductivity and mobility of lead-free halide double perovskites », *Journal of Alloys and Compounds*, vol. 962, p. 170988, nov. 2023, doi: 10.1016/j.jallcom.2023.170988.

[61] L. H. Thomas, « The calculation of atomic fields », *Math. Proc. Camb. Phil. Soc.*, vol. 23, nº 5, p. 542-548, janv. 1927, doi: 10.1017/S0305004100011683.

[62] E. Fermi, « Statistical method to determine some properties of atoms », *Rend. Accad. Naz. Lincei*, vol. 6, nº 602-607, p. 5, 1927.

[63] D. R. Hartree, « The wave mechanics of an atom with a non-Coulomb central field. Part I. Theory and methods », présenté à Mathematical Proceedings of the Cambridge Philosophical Society, Cambridge university press, 1928, p. 89-110.

[64] P. A. M. Dirac, « Quantum mechanics of many-electron systems », *Proceedings of the Royal Society of London. Series A, Containing Papers of a Mathematical and Physical Character*, vol. 123, nº 792, p. 714-733, 1929.

[65] V. Fock, « Näherungsmethode zur Lösung des quantenmechanischen Mehrkörperproblems », *Zeitschrift für Physik*, vol. 61, p. 126-148, 1930.

[66] E. Schrödinger, « SCHRÖDINGER 1926C », *Annalen der Physik*, vol. 79, p. 734, 1926.

[67] J. Mehra, « Erwin Schrödinger and the rise of wave mechanics. II. The creation of wave mechanics », *Found Phys*, vol. 17, nº 12, p. 1141-1188, déc. 1987, doi: 10.1007/BF01889592.

[68] M. Born et R. Oppenheimer, « Zur quantentheorie der molekeln annalen der physik, v. 84 », 1927.

[69] J. C. Slater, « The theory of complex spectra », *Physical review*, vol. 34, n° 10, p. 1293, 1929.

[70] C. C. J. Roothaan, « New developments in molecular orbital theory », *Reviews of modern physics*, vol. 23, n° 2, p. 69, 1951.

[71] A. R. Leach, *Molecular modelling: principles and applications*. Pearson education, 2001.

[72] P. W. Atkins et M. J. De Paula, *Chimie physique*. De Boeck Supérieur, 2013.

[73] O. K. Andersen, « Linear methods in band theory », *Phys. Rev. B*, vol. 12, n° 8, p. 3060-3083, oct. 1975, doi: 10.1103/PhysRevB.12.3060.

[74] Walter Kohn and Lu Jeu Sham, "Self-Consistent Equations Including Exchange and Correlation Effects," *Physical Review*, vol. 140, no. 4A, pp. A1133–A1138, 1965. https://doi.org/10.1103/PhysRev.140.A1133

[75] K. B. Lipkowitz et D. B. Boyd, Éd., *Reviews in Computational Chemistry*, 1re éd., vol. 8. in Reviews in Computational Chemistry, vol. 8. Wiley, 1996. doi: 10.1002/9780470125854.

[76] J. A. Pople, D. P. Santry, et G. A. Segal, « Approximate Self-Consistent Molecular Orbital Theory. I. Invariant Procedures », *The Journal of Chemical Physics*, vol. 43, n° 10, p. S129-S135, nov. 1965, doi: 10.1063/1.1701475.

[77] P. Hohenberg and W. Kohn, "Inhomogeneous electron gas," *Physical Review*, vol. 136, pp. B864–B871, 1964. DOI: 10.1103/PhysRev.136.B864

[78] L. Hedin, "New method for calculating the one-particle Green's function with application to the electron-gas problem," *Physical Review*, vol. 139, 1965.

[79]R. M. Martin, *Electronic Structure: Basic Theory and Practical Methods*, Cambridg University Press

[80] E. Schrödinger, « An Undulatory Theory of the Mechanics of Atoms and Molecules », *Phys. Rev.*, vol. 28, n° 6, p. 1049-1070, déc. 1926, doi: 10.1103/PhysRev.28.1049.

[81] P. Kiréev, « La physique des semiconducteurs. 2e édition, édition Mir », 1975.

[82] F. Fuster et P. Chaquin, « Analysis of carbon-carbon bonding in small hydrocarbons and dicarbon using dynamic orbital forces: Bond energies and sigma/pi partition.

Comparison with sila compounds », *Int J of Quantum Chemistry*, vol. 119, nº 20, p. e25996, oct. 2019, doi: 10.1002/qua.25996.

[83] R. E. Christoffersen, « Beyond Hartree-Fock Theory », in *Basic Principles and Techniques of Molecular Quantum Mechanics*, in Springer Advanced Texts in Chemistry. , New York, NY: Springer US, 1989, p. 576-656. doi: 10.1007/978-1-4684-6360-6_12.

[84] Chr. Møller et M. S. Plesset, « Note on an Approximation Treatment for Many-Electron Systems », *Phys. Rev.*, vol. 46, nº 7, p. 618-622, oct. 1934, doi: 10.1103/PhysRev.46.618.

[85] M. Born et W. Heisenberg, « Zur Quantentheorie der Molekeln », in *Original Scientific Papers Wissenschaftliche Originalarbeiten*, W. Blum, H. Rechenberg, et H.-P. Dürr, Éd., Berlin, Heidelberg: Springer Berlin Heidelberg, 1985, p. 216-246. doi: 10.1007/978-3-642-61659-4_16.

[86] B. Philippe et F. Delatte, « Périodiques », *Revue belge de Philologie et d'Histoire*, vol. 12, nº 4, p. 1299-1364, 1933.

[87] J. A. Pople, R. Seeger, et R. Krishnan, « Variational configuration interaction methods and comparison with perturbation theory », *Int. J. Quantum Chem.*, vol. 12, nº S11, p. 149-163, juin 2009, doi: 10.1002/qua.560120820.

[88] W. Kohn et L. J. Sham, « Self-consistent equations including exchange and correlation effects », *Physical review*, vol. 140, nº 4A, p. A1133, 1965.

[89] F. Giustino, *Materials modelling using density functional theory: properties and predictions*. Oxford University Press, 2014.

[90] F. Igbari, Z. Wang, et L. Liao, « Progress of Lead-Free Halide Double Perovskites », *Advanced Energy Materials*, vol. 9, nº 12, p. 1803150, mars 2019, doi: 10.1002/aenm.201803150.

[91] M. A. Green, Y. Hishikawa, E. D. Dunlop, D. H. Levi, J. Hohl-Ebinger, et A. W. Y. Ho-Baillie, « Solar cell efficiency tables (version 52) », *Progress in Photovoltaics*, vol. 26, nº 7, p. 427-436, juill. 2018, doi: 10.1002/pip.3040.

[92] M. Kulbak, D. Cahen, et G. Hodes, « How Important Is the Organic Part of Lead Halide Perovskite Photovoltaic Cells? Efficient $CsPbBr_3$ Cells », *J. Phys. Chem. Lett.*, vol. 6, nº 13, p. 2452-2456, juill. 2015, doi: 10.1021/acs.jpclett.5b00968.

[93] C. C. Stoumpos *et al.*, « Crystal Growth of the Perovskite Semiconductor $CsPbBr_3$: A New Material for High-Energy Radiation Detection », *Crystal Growth & Design*, vol. 13, nº 7, p. 2722-2727, juill. 2013, doi: 10.1021/cg400645t.

[94] J. P. Perdew *et al.*, « Atoms, molecules, solids, and surfaces: Applications of the generalized gradient approximation for exchange and correlation », *Phys. Rev. B*, vol. 46, n° 11, p. 6671-6687, sept. 1992, doi: 10.1103/PhysRevB.46.6671.

[95] J. P. Perdew, K. Burke, et M. Ernzerhof, « Perdew, Burke, and Ernzerhof Reply »:, *Phys. Rev. Lett.*, vol. 80, n° 4, p. 891-891, janv. 1998, doi: 10.1103/PhysRevLett.80.891.

[96] D. J. Singh and L. Nordström, *Planewaves, Pseudopotentials and the LAPW Method*,

[97] F. Bloch, « Quantum mechanics of electrons in crystal lattices », *Z. Phys*, vol. 52, p. 555-600, 1928.

[98] J. C. Slater, « Energy Band Calculations by the Augmented Plane Wave Method », in *Advances in Quantum Chemistry*, vol. 1, Elsevier, 1964, p. 35-58. doi: 10.1016/S0065-3276(08)60374-3.

[99] C. Herring, « A New Method for Calculating Wave Functions in Crystals », *Phys. Rev.*, vol. 57, n° 12, p. 1169-1177, juin 1940, doi: 10.1103/PhysRev.57.1169.

[100] A. D. McLaren, « Optimal numerical integration on a sphere », *Math. Comp.*, vol. 17, n° 84, p. 361-383, 1963, doi: 10.1090/S0025-5718-1963-0159418-2.

[101] A. D. Becke, "Density-functional exchange-energy approximation with correct asymptotic behavior," *Physical Review A*, 1988.

[102] F. Tran, « WIEN2k: an augmented plane wave plus local orbitals program for calculating crystal properties ».

[103] S. BENDAIF, « Etude des propriétés structurales, électroniques, thermodynamiques et thermiques des alliages quaternaires », 2015.

[104] H. Tang, S. He, et C. Peng, « A Short Progress Report on High-Efficiency Perovskite Solar Cells », *Nanoscale Res Lett*, vol. 12, n° 1, p. 410, déc. 2017, doi: 10.1186/s11671-017-2187-5.

[105] M. Ghaleb, A. Arrar, et Z. Touaa, « Optimization and Performance Analysis of a TiO_2 /i-$CH_3NH_3SnBr_3$ /$CsPbI_3$ /Al(BSF) Heterojunction Perovskite Solar Cell for Enhanced Efficiency », *ACS Omega*, vol. 8, n° 40, p. 37011-37022, oct. 2023, doi: 10.1021/acsomega.3c03891.

[106] M. Ghaleb, A. Arrar, A. Hadji Chikh, H. Bendjilali, et O. Zerrouki, « I-$MASnBr_3$ /CZTGS Heterojunction Solar Cell Layer Optimization Investigated Using Scaps-1D

Software Exhibited Excellent Performance at 50 % », *Annals of West University of Timisoara - Physics*, vol. 0, nº 0, juin 2024, doi: 10.2478/awutp-2024-0012.

[107] Z. Xiao, Z. Song, et Y. Yan, « From Lead Halide Perovskites to Lead-Free Metal Halide Perovskites and Perovskite Derivatives », *Advanced Materials*, vol. 31, nº 47, p. 1803792, nov. 2019, doi: 10.1002/adma.201803792.

[108] W. S. Yang *et al.*, « Iodide management in formamidinium-lead-halide–based perovskite layers for efficient solar cells », *Science*, vol. 356, nº 6345, p. 1376-1379, juin 2017, doi: 10.1126/science.aan2301.

[109] L. Schade *et al.*, « Structural and Optical Properties of Cs $_2$ AgBiBr $_6$ Double Perovskite », *ACS Energy Lett.*, vol. 4, nº 1, p. 299-305, janv. 2019, doi: 10.1021/acsenergylett.8b02090.

[110] G. King et P. M. Woodward, « Cation ordering in perovskites », *J. Mater. Chem.*, vol. 20, nº 28, p. 5785, 2010, doi: 10.1039/b926757c.

[111] F. Elfatouaki *et al.*, « Optoelectronic and thermoelectric properties of double halide perovskite Cs 2 AgBiI 6 for renewable energy devices », *Solar Energy*, vol. 260, p. 1-10, août 2023, doi: 10.1016/j.solener.2023.05.032.

[112] S. Murugan et E.-C. Lee, « Recent Advances in the Synthesis and Application of Vacancy-Ordered Halide Double Perovskite Materials for Solar Cells: A Promising Alternative to Lead-Based Perovskites », *Materials*, vol. 16, nº 15, p. 5275, juill. 2023, doi: 10.3390/ma16155275.

[113] S. Al-Qaisi *et al.*, « First-principles investigation of structural, elastic, thermodynamic, electronic and optical properties of lead-free double perovskites halides: Cs2LiYX6 (X = Br, I) », *Materials Chemistry and Physics*, vol. 258, p. 123945, janv. 2021, doi: 10.1016/j.matchemphys.2020.123945.

[114] M. R. Filip, S. Hillman, A. A. Haghighirad, H. J. Snaith, et F. Giustino, « Band Gaps of the Lead-Free Halide Double Perovskites Cs $_2$ BiAgCl $_6$ and Cs $_2$ BiAgBr $_6$ from Theory and Experiment », *J. Phys. Chem. Lett.*, vol. 7, nº 13, p. 2579-2585, juill. 2016, doi: 10.1021/acs.jpclett.6b01041.

[115] S. Berri, D. Maouche, M. Ibrir, et F. Zerarga, « A first-principle study of half-metallic ferrimagnetism in the CoFeTiSb quaternary Heusler compound », *Journal of magnetism and magnetic materials*, vol. 354, p. 65-69, 2014.

[116] P. Blaha, « Improved and updated Unix version of the original copyrighted WIEN-code, which was published by P. Blaha, K. Schwarz, P. Sorantin, and SB Trickey », *Comput. Phys. Commun*, vol. 59, p. 339, 1990.

[117] P. Blaha, K. Schwarz, G. K. Madsen, D. Kvasnicka, et J. Luitz, « wien2k », *An augmented plane wave+ local orbitals program for calculating crystal properties*, vol. 60, n° 1, 2001.

[118] *C. Lee, W. Yang, and R. Parr, "Development of th*e Colle-Salvetti correlation-energy formula into a functional of the electron density," *Physical Review B*, 1988.

[119] T. Charpin, « Laboratory of geometrix F-75252 Paris », *France A package for Calculating elastic tensors of cubic phase using WIEN*, 2001.

[120] D. Heciri *et al.*, « First-principles elastic constants and electronic structure of beryllium chalcogenides BeS, BeSe and BeTe », *Computational Materials Science*, vol. 38, n° 4, p. 609-617, févr. 2007, doi: 10.1016/j.commatsci.2006.04.003.

[121] A. Bouhemadou, R. Khenata, M. Kharoubi, T. Seddik, A. H. Reshak, et Y. Al-Douri, « FP-APW+lo calculations of the elastic properties in zinc-blende III-P compounds under pressure effects », *Computational Materials Science*, vol. 45, n° 2, p. 474-479, avr. 2009, doi: 10.1016/j.commatsci.2008.11.013.

[122] F. Birch, « Finite Elastic Strain of Cubic Crystals », *Phys. Rev.*, vol. 71, n° 11, p. 809-824, juin 1947, doi: 10.1103/PhysRev.71.809.

[123] M. A. Kinani, A. Lekdadri, Y. Mir, et M. Zazoui, « First-principles study of double perovskites Cs2Sn(Br1−I)6 for the design of high-efficiency thin-film photovoltaics », *Computational Condensed Matter*, vol. 30, p. e00634, mars 2022, doi: 10.1016/j.cocom.2021.e00634.

[124] K. Momma and F. Izumi, "VESTA 3 for three-dimensional visualization of crystal, volumetric and morphology data," *Journal of Applied Crystallography*, 2011.

[125] H. Jiang, « Band gaps from the Tran-Blaha modified Becke-Johnson approach: A systematic investigation », *The Journal of Chemical Physics*, vol. 138, n° 13, p. 134115, avr. 2013, doi: 10.1063/1.4798706.

[126] D. R. Penn, « Wave-Number-Dependent Dielectric Function of Semiconductors », *Phys. Rev.*, vol. 128, n° 5, p. 2093-2097, déc. 1962, doi: 10.1103/PhysRev.128.2093.

[127] N. A. Noor, Q. Mahmood, M. Rashid, B. Ul Haq, et A. Laref, « The pressure-induced mechanical and optoelectronic behavior of cubic perovskite PbSnO3 via ab-initio investigations », *Ceramics International*, vol. 44, n° 12, p. 13750-13756, août 2018, doi: 10.1016/j.ceramint.2018.04.217.

[128] R. Khenata *et al.*, « Full-potential calculations of structural, elastic and electronic properties of MgAl2O4 and ZnAl2O4 compounds », *Physics Letters A*, vol. 344, nº 2-4, p. 271-279, sept. 2005, doi: 10.1016/j.physleta.2005.06.043.

[129] J. F. Nye, *Physical properties of crystals: their representation by tensors and matrices*. Oxford university press, 1985.

[130] H. M. Ledbetter et E. R. Naimon, « Elastic Properties of Metals and Alloys. II. Copper », *Journal of Physical and Chemical Reference Data*, vol. 3, nº 4, p. 897-935, oct. 1974, doi: 10.1063/1.3253150.

[131] S. I. Ranganathan et M. Ostoja-Starzewski, « Universal Elastic Anisotropy Index », *Phys. Rev. Lett.*, vol. 101, nº 5, p. 055504, août 2008, doi: 10.1103/PhysRevLett.101.055504.

[132] H. A. Rahnamaye Aliabad, M. Ghazanfari, I. Ahmad, et M. A. Saeed, « Ab initio calculations of structural, optical and thermoelectric properties for CoSb3 and ACo4Sb12 (A=La, Tl and Y) compounds », *Computational Materials Science*, vol. 65, p. 509-519, déc. 2012, doi: 10.1016/j.commatsci.2012.08.013.

[133] C. Hurd, *The Hall effect in metals and alloys*. Springer Science & Business Media, 2012.

[134] S. Al-Qaisi *et al.*, « Study of mechanical, optical, and thermoelectric characteristics of Ba2XMoO6 (X= Zn, Cd) double perovskite for energy harvesting », *Journal of Computational Chemistry*, vol. 44, nº 32, p. 2442-2452, 2023.

[135] M. A. Blanco, E. Francisco, et V. Luaña, « GIBBS: isothermal-isobaric thermodynamics of solids from energy curves using a quasi-harmonic Debye model », *Computer Physics Communications*, vol. 158, nº 1, p. 57-72, mars 2004, doi: 10.1016/j.comphy.2003.12.001.

[136] « On the relation of Debye theory and the lattice theory of specific heats », *Proc. R. Soc. Lond. A*, vol. 181, nº 984, p. 58-67, sept. 1942, doi: 10.1098/rspa.1942.0058.

Annexes

Materials Science and Engineering B 310 (2024) 117707

Contents lists available at ScienceDirect

Materials Science & Engineering B

journal homepage: www.elsevier.com/locate/mseb

Ab initio study of the optoelectronic and thermoelectric properties of the new double perovskite Cs_2ZnPbX_6(X=Br, Cl)

Chikh Ali Hadji [a,b,*], Amina Arrar [a,b,*], Mohamed Ghaleb [a,b], Hadjer Bendjilali [c], Otmane Zerrouki [a]

[a] *Faculty of sciences and Technology, University of RELIZANE, BOURMADIA, BP 48000 W. Relizane, Algeria*
[b] *Laboratory of Physics Thin Layer & Advanced Technologies, University of RELIZANE, Bourmadia, BP 48000 W. Relizane, Algeria*
[c] *Condensed Matter and Sustainable Development Laboratory (LMCDD), University of Sidi Bel-Abbes, Sidi Bel-Abbes 22000, Algeria*

ARTICLE INFO

Keywords:
Double-perovskite
Structural
Optoelectric
Thermoelectric
Elastic
DFT

ABSTRACT

This study investigates the structural, optoelectronic, thermodynamic, and thermoelectric properties of the new double perovskite compounds $Cs_2ZnPbCl_6$ and $Cs_2ZnPbBr_6$ utilizing advanced computational methods. We analyze the stability and electronic characteristics of these materials in their cubic phase (space group Fm-3 m). Our findings reveal that both compounds exhibit promising thermoelectric performance, with peak Seebeck coefficients of 2880 μV/K for $Cs_2ZnPbBr_6$ and 2870 μV/K for $Cs_2ZnPbCl_6$ at 300 K. The electrical conductivity (σ/τ) values reach 11.66 and 10.98, respectively, indicating strong carrier mobility. Additionally, we observe significant changes in the Seebeck coefficient as a function of carrier concentration, attributed to the formation of electron-hole pairs and shifts in the Fermi level. Finally, the thermodynamic and thermoelectric attributes suggest that the double perovskite materials investigated hold promise for implementation in thermoelectric technology, showcasing a favorable figure of merit at ambient temperature.

1. Introduction

Photovoltaic technology is advancing at an unprecedented pace, with perovskite solar cells (PSCs) emerging as a leading contender due to their cost-effectiveness and exceptional power conversion efficiency (PCE).Solution-processed halide perovskite solar cells have reached record efficiencies of over 22 % in single-junction configurations[1]. Both Ghaleb and Arrar recorded an efficiency exceeding 30 % by combining two types of perovskite, the organic halide $CH_3NH_3SnBr_3$ and the inorganic halide $CsPbI_3$, a heterojunction in a single solar cell, and also heterojunction $MASnBr_3$/CZTGS [2,3]. The exceptional optical and electrical characteristics of perovskites particularly those based on lead, such as their small bandgap, high optical absorption coefficient, prolonged carrier lifetime, effective charge carrier transport, and low exciton binding energy are responsible for this outstanding performance. this suggests that there are still more advantages about these unique materials not yet exploited [4,5].

In the beginning, most of the research was based on simple perovskites (ABX_3), but as the research progressed more prominent complex structures, such as double perovskites ($A_2BB'X_6$), introduced further innovation by incorporating two distinct transition metals and a combination of rare earth and alkaline earth elements, offering new avenues for enhancing solar cell performance [6,7].

This compound, with the formula $A_2BB'X_6$ where A represents Cs, B is Zn, B' is Pb, and X_6 refers to Br/Cl. We will study it in the cubic phase with the space group (Fm-3 m) based on previous research that studied the double perovskites in the cubic phase [8,9], especially after calculating the factor tolerance, which exhibits near stability in its cubic phase (space group: Fm-3 m)[10]. However, both experimental and its stability and theoretical data on the structural properties of these materials are scarce.

The study examines how different iodide contents affect $Cs_2Sn(Br_{1-x}Ix)_6$ double perovskite materials. It finds that when iodide concentration increases, lattice constant and energy bandgap are improved [11]. Density functional theory is used in this work to investigate the thermodynamic stability and anion ordering of perovskite oxynitrides (PONs), discovering compounds that are stable and metastable and offering insights for potential applications in materials science and catalysis in the future [12].

Double perovskite compounds have become a focal point in recent

---

* Corresponding authors.
E-mail addresses: chikhali.hadji@univ-relizane.dz (C. Ali Hadji), Amina.arrar@univ-relizane.dz (A. Arrar).

https://doi.org/10.1016/j.mseb.2024.117707
Received 11 July 2024; Received in revised form 7 September 2024; Accepted 9 September 2024

Eur. Phys. J. B (2025)98:100
https://doi.org/10.1140/epjb/s10051-025-00949-8

THE EUROPEAN
PHYSICAL JOURNAL B

Regular Article - Computational Methods

Structural, elastic, optoelectronic, thermodynamic and thermoelectric properties of the new halide double perovskite Cs_2CaGeI_6: first-principles study

Chikh Ali Hadji[1,2,a], Amina Arrar[1,2,b], Mohamed Ghaleb[1,2], Otmane Zerrouki[3], and Hadjer Bendjilali[4]

[1] Laboratory of Physics Thin Layer and Advanced Technologies, University of Relizane, BP 48000, Bourmadia, W. Relizane, Algeria
[2] Department of Physics, Faculty of Science and Technology, University of Relizane, BP 48000, Bourmadia, W. Relizane, Algeria
[3] Department of Mechanics, Faculty of Science and Technology, University of Relizane, BP 48000, Bourmadia, W. Relizane, Algeria
[4] Physics Faculty, University of Sciences and Technology (USTHB), BP 32 El-Alia, Bab-Ezzouar, Algiers, Algeria

Received 21 February 2025 / Accepted 7 May 2025

Abstract. The structural, elastic, optical, thermodynamic, and thermoelectric properties of Cs_2CaGeI_6 double perovskite were investigated using density functional theory simulations. The calculations show that the material is elastically stable and isotropic. Furthermore, with an endurance factor of $t = 0.89$ and an energy of formation of $Ef = -0.97$ Ev. Our calculations demonstrate the high structural stability of perovskite materials. GGA-PBE and TB-mBJ are used to approximate the electrical properties while introducing spin–orbit coupling. The compound's high absorption and indirect bandgap semiconductor capabilities make it a prospective rival for solar cells. The thermal characteristics for temperatures between 50 and 1000 K were investigated using the BoltzTraP algorithm. Furthermore, we used the Gibbs software to compute the thermodynamic characteristics of Cs_2CaGeI_6 double halide perovskite. Additionally, the studied Cs_2CaGeI_6 combination has a good figure of merit at room temperature, suggesting that its thermodynamic and thermoelectric properties offer potential for use in thermoelectric technology.

1 Introduction

Halide perovskite-based compounds have recently gained widespread use as optical functional materials in a range of devices, including solar cell absorbers, quantum dot (QD) light-emitting diodes (LEDs), and photodetectors, due to their remarkable optoelectronic properties [1, 2].The first report of halide perovskite material in the field of optoelectronics was a halide perovskite sensitized solar cell developed by Miyaska in 2009 [3, 4].Recent advancements in perovskite halide (PSC) solar cells, particularly when the power conversion efficiency (PCE) of halide double perovskite solar cells has increased from 3.8 to more of 26% [5, 6] Consequently, the challenge facing materials science researchers across multiple disciplines is to develop novel materials and techniques that combine high efficacy and cheap cost [7, 8].

The halide double perovskite has a general formula $A_2BB'X_6$, where A is a monovalent cation, typically a large ion; B and B′ are divalent and trivalent cations, respectively. In some cases, two different divalent cations can be used. X: a halide anion, such as iodine (I), bromine (Br), or chlorine (Cl). They typically belong to the space group 225 (space group $Fm3m$) and have a cubic symmetry.

The halide double perovskite follows the general formula $A_2BB'X_6$, where A represents a monovalent cation, typically a large ion, while B and B′ are divalent and trivalent cations, respectively [9]. In some cases, two different divalent cations can be used. The X site is occupied by a halide anion such as iodine (I), bromine (Br), or chlorine (Cl) [10]. These compounds typically crystallize in the cubic symmetry of space group Fm-3 m (225) [11].

The investigation of Cs_2CaGeI_6 perovskites is of significant importance due to their promising properties as a lead-free alternative in photovoltaic applications, which addresses the environmental concerns associated with traditional lead-based perovskites. Additionally, their unique structural characteristics and high absorption coefficients make them suitable candidates for

---

[a] e-mail: chikhali.hadji@univ-relizane.dz (corresponding author)
[b] e-mail: amina.arrar@univ-relizane.dz (corresponding author)

Journal of Inorganic and Organometallic Polymers and Materials (2025) 35:4616–4630
https://doi.org/10.1007/s10904-024-03545-y

RESEARCH

The Structural, Electronic, Elastic, and Optical Properties of New Double Perovskite Cs_2CdPbI_6 were Investigated Using a DFT and SCAPS-1D Simulation

Mohamed Ghaleb[1,2] · **Amina Arrar**[1,2] · **Chikh Ali Hadji**[1,2] · **Hadjer Bendjilali**[3] · **Otmane Zerrouki**[2]

Received: 14 October 2024 / Accepted: 7 December 2024 / Published online: 9 March 2025

Abstract

The structural, electronic, optical and elastic properties of the cubic double perovskite Cs_2CdPbI_6 were calculated using a density functional theory DFT. The calculated values were reported to evaluate the photovoltaic (PV) performance of new device structures using the SCAPS-1D solar cell simulation software. The simulation findings demonstrate that the FTO/ETL/Cs_2CdPbI_6/HTL exhibited an efficiency of 32.06%, Voc = 1.4 V, Jsc = 27.99 mA/cm^2 and FF = 81.69% at 300 K temperature. The effect of the absorber and ETL thickness, capacitance–voltage, current density–voltage, quantum efficiency characteristics, series resistance, and shunt resistance were also evaluated for the devices. The results of these simulations provide valuable insight that will be useful in the development of efficient double perovskites solar cells based on Cs_2CdPbI_6.

Keywords Double perovskite · DFT · SCAPS-1D · Cs_2CdPbI_6 · Photovoltaic

1 Introduction

Perovskite materials have rapidly gained attention due to their abundance on Earth and ease of manufacturing, prompting significant interest among researchers. Their versatile properties have made them a focal point in various fields, with particular significance in solar cells and renewable energy technologies. Notably, their remarkable efficiency, surpassing 31% [1, 2], in solar cell applications has positioned them as an up-and-coming candidate for advancing sustainable energy solutions.

Halide perovskites with the chemical formula ABX_3 have emerged as breakthrough materials for photovoltaic solar cells. Among these, double perovskites have become a particularly active area of research. This structure allows the incorporation of a fourth element, significantly enhancing material stability and improving structural attributes that contribute to the stabilization of optical, electronic, and mechanical properties. Recent studies, such as those in [3, 4], have demonstrated promising improvements in stability and optoelectronic performance through such compositional adjustments. Moreover, several investigations have achieved optimized electronic properties in double perovskites by fine-tuning the bandgap to fall within an ideal range for efficient light absorption. This bandgap tuning is especially beneficial for applications in photovoltaics, where strong absorption in the visible spectrum is crucial [5, 6]. These advancements suggest that double perovskites hold strong promise for next-generation optoelectronic applications.

The search for environmentally friendly alternatives to lead-based perovskites has driven significant advancements in lead-free double perovskites. These materials,

✉ Mohamed Ghaleb
mohamed.ghaleb@univ-relizane.dz

✉ Amina Arrar
amina.arrar@univ-relizane.dz

[1] Laboratory of Physics Thin Layer & Advanced Technologies, University of RELIZANE, Bourmadia, BP 48000, W. Relizane, Algeria

[2] Faculty of Technology, University of RELIZANE, BOURMADIA, BP 48000, W. Relizane, Algeria

[3] Condensed Matter and Sustainable Development Laboratory (LMCDD), University of Sidi Bel-Abbes, 22000 Sidi Bel-Abbes, Algeria

ANNALS OF WEST UNIVERSITY OF
TIMISOARA PHYSICS

Vol. LXVI, 2024

DOI: 10.2478/awutp-2024-0012

I-MASnBr₃ /CZTGS HETEROJUNCTION SOLAR CELL LAYER OPTIMIZATION INVESTIGATED USING SCAPS-1D SOFTWARE EXHIBITED EXCELLENT PERFORMANCE AT 50 %

M. Ghaleb[1,2,*], A. Arrar[1,2,*], A. Hadji Chikh [1,2], H. Bendjilali[3], O. Zerrouki[1]

[1] *Faculty of Technology, University of Relizane, Bourmadia, BP 48000, W. Relizane, Algeria.*
[2] *Laboratory of Physics Thin Layer & Advanced Technologies*, ***,*** *University of Relizane, Bourmadia, BP 48000, W. Relizane, Algeria*
[3] *Condensed Matter and Sustainable Development Laboratory (LMCDD), University of Sidi Bel-Abbes, Sidi Bel-Abbes 22000, Algeria*
* *Corresponding authors* amina.arrar@univ-relizane.dz *and* mohamed.ghaleb@univ-relizane.dz
Tel. +213799035690

Article Info

Received: 05.03.2024
Accepted: 04.06.2024

Keywords:
heterojunction perovskite, SCAPS-1D, CZTGS, i-$CH_3NH_3SnBr_3$.

Abstract

This paper reports a novel prototype of heterojunction solar cells based on semiconductor/perovskite structure using the solar cell capacitance one-dimensional simulator (SCAPS 1D). The device schematic consists of Glass/ITO/ETL/$MASnBr_3$ /CZTGS/HTL layers with perovskite i-$MASnBr_3$ as the permeable layer. The thickness of the absorber layer, carrier charge concentration, and the effect of temperature and series resistances are optimized. The research examines several critical parameters essential for solar cell performance, including a power conversion efficiency PCE of 50%, an open-circuit voltage V_{oc} of 1.62 V, a fill factor FF of 91.5%, and a short-circuit current density J_{sc} of -34.06 mA/ cm^2. The temperature and series resistance effects, as well as quantum efficiency QE, and J-V curve simulations with varying acceptor density, are investigated.

1. Introduction

Improved solar technology has advanced significantly in recent years, exhibiting a variety of groundbreaking photovoltaic (PV) cell developments. These next-generation panels have various designs and improvements intended to improve overall dependability, minimize degradation, and increase efficiency. Nowadays, the most popular PV solar cell has given rise to several approaches, including PERC (Passivated Emitter Rear Cells) and HJT

Ministry of Higher Education and Scientific Research
RELIZANE University
Faculty of Sciences and Technology/ physics department
Laboratory of Thin Film Physics & Advanced Technologies

THE SECOND NATIONAL CONFERENCE OF MATERIALS SCIENCES AND RENEWABLE ENERGY
NOVEMBER, 09-10TH ,2024/ RELIZANE, ALGERIA

CERTIFICATE

OF APPRECIATION

proudly presented to

Mr. HADJI Chikh Ali

We would like to sincerely thank you for your invaluable contribution as a member of the organizing committee for The Second National Conference of Materials Sciences and Renewable Energy (CMSRE24), organized by the Physics Department on November 09-10 th, 2024, in Relizane, Algeria.

Dean of faculty

د . جيلالي بغدادي
عميد كلية العلوم والتكنولوجيا

President of conference

CMSRE24
30-31
October
2024

د. أمينة عرعار
رئيسة
المؤتمر

https://univ-relizane.dz/fst/ / tel :044-72-40-64/ Bourmadia, RELIZANE

People's Democratic Republic of Algeria
Ministry of Higher Education and Scientific Research
Ahmed Zabana Relizane University
Science and Technology Faculty
Chemistry Department
Environment and Sustainable Development Laboratory (ESDL)

CERTIFICATE OF PARTICIPATION

This certificate is awarded to:

CHIKH ALI HADJI

In recognition to their participation to the Second Edition of the Webinaire national Seminar entitled:
Matériaux pour l'Environnement et le Développement Durable.
held on 17-18 December 2024 in Relizane (Algeria) with oral communication entitled:
Recent developments of lead-free halide double perovskites: a new superstar in the optoelectronic field

MEDD-24-RL https://medd24.sciencesconf.org

MEDD 2024
2ème Séminaire National
Matériaux pour l'Environnement
et Développement Durable

https://medd24.sciencesconf.org/599112/document

Co-auteurs: Amina Arrar, Mohamed Abed Ghaleb

2ème Webinaire National MEDD'2024 17-18 Décembre 2024

Dr BOUCHERDOUD Ahmed
Président du séminaire

د . جيلالي بغدادي
عميد كلية العلوم والتكنولوجيا

secretariat.medd@univ-relizane.dz

University of Sciences and Technology of Oran- Mohamed Boudiaf
Faculty of Physics
The International Conference on Materials Physics and Fluids
ICMPF-2024
USTO-MB Oran, Algeria, 27 - 29 November 2024

CERTIFICATE OF PARTICIPATION

The organizing committee of the **ICMPF-2024** certifies that

Dr.HADJI CHIKH ALI

From University of Relizane, Algeria
has presented the paper referenced bellow as **Poster** presentation in the ICMPF-2024

Title: Ab-initio study of opto-electronic and thermoelectric properties of direct bandgap double Perovskite

Co-author (s) : Amina. ARRAR, Messadi Larbi and Mohamed GHALEB

ICMPF
2024

DATE: November 29, 2024

***Chairmen of the Conference* ICMPF-2024**

Prof. Mohamed Esseghir FERHAT ***Prof. Hocine ALLA***

ICMPF - 2024
NOV 27-29 ORAN
ALGERIA
CHAIRMEN
Pr.M.FERHAT
Pr.H.ALLA

University of Relizane
Faculty of Science and Technology
Civil Engineering Department

Certificate of Participation

in technical presentation, recognition and appreciation of research contributions to
***International Seminar on Materials and Engineering Structures* (ISMES'2024)**
to be
Held in RELIZANE, ALGERIA, during October, 26-27, 2024.
Hadji Chikh Ali

CO-AUTHOR: Arrar Amina; Mohamed Ghaleb
WITH THE PAPER ENTITLED:
A comprehensive examination of physical characteristic of Double perovskites towards optoelectronic and photovoltaic applications

SIGNATURE CHAIRMAN DEAN OF THE FACULTY
Dr. SALHI MOHAMED

د . جيلالي بعدادي
عميد كلية العلوم والتكنولوجيا

جامعة الجيلالي اليابس بسيدي بلعباس
Djillali Liabès University , Sidi Bel-Abbès
Faculty of Exact Sciences
Physics Department
Physico-Chemistry Laboratory Of Advanced Materials (LPCMA)

The 3rd edition of the international conference on materials science and engineering and their impact on the environment ICMSE'2024

Sidi bel abbés May 29-30, 2024

CERTIFICATE OF PARTICIPATION

The scientific committee certified that:

Mr. Chikh Ali. Hadji

Has presented online Communication, entitled:

« *ab initio study of the structural and electronic and Optical properties of The New Double Perovskite* ».

CO-AUTORS : Amina. ARRAR , Mohamed.GHALEB , zaza TOUAA

General Chair:

THE INTERNATIONAL CONFERENCE ON MATERIALS SCIENCE AND ENGINEERING AND THEIR IMPACT ON THE ENVIRONMENT
ICMSE 2024 - MAY 29 - 30

CHAIRMAN
Prof Mohammed AMERI

Physico-Chemistry Laboratory Of Advanced Materials (LPCMA), Djillali Liabès University , Sidi Bel-Abbès
Tél. : 048 79 90 02/048 74 56 19, Email: lttnsameri@yahoo.fr , https://www.univ-sba.dz/lpcma/

الجمهورية الجزائرية الديمقراطية الشعبية
وزارة التعليم العالي والبحث العلمي
المدرسة العليا للأساتذة بشار
مخبر رعاية الابتكار والمؤسسة الناشئة لخريجي التعليم العالي
في اتجاهات التنمية المستدامة والتعامل مع الظروف الطارئة والتنموية في الجزائر

شهادة مشاركة

يتشرف السيد مدير المدرسة العليا للأساتذة ببشار د.مسكين توفيق و رئيسة الملتقى د. عيسي جهيدة بتقديم هذه الشهادة الى السيد (ة): **Chikh Ali Hadji**

Arrar Amina, Touaa Zaza Ghaleb Mohamed

نظيرا لمشاركته (ها) في الملتقى الوطني الأول حول الكيمياء والحياة المنعقد يومي 23 و 24 أفريل2024

بمداخلة موسومة بـ:

Propriétés optoélectroniques et thermoélectriques de la pérovskite à double halogénure Cs2BaSrI6 pour les dispositifs à énergie renouvelable

مدير المدرسة
د. مسكين توفيق
مسكين توفيق
مكلف بتسيير شؤون إدارة مديرية
المدرسة العليا للأساتذة بشار

رئيس الملتقى
د. عيسي جهيدة
المدرسة العليا للأساتذة بشار
قسم العلوم الفيزيائية العلوم الدقيقة
الدكتورة عيسي جهيدة
رئيس الملتقى الوطني "الكيمياء و الحياة"

Ministry of Higher Education and Scientific Research
RELIZANE University
Faculty of Sciences and Technology/ physics department
Laboratory of Thin Film Physics & Advanced Technologies

THE SECOND NATIONAL CONFERENCE OF MATERIALS SCIENCES AND RENEWABLE ENERGY
NOVEMBER, 09-10 TH ,2024/ RELIZANE, ALGERIA

CERTIFICATE

OF PARTICIPATION

THE PRESIDENT OF THE SECOND NATIONAL CONFERENCE OF MATERIALS SCIENCES AND RENEWABLE ENERGY (CMSRE24) CERTIFIES THAT:

Chikh Ali HADJI

has delivered ***poster*** *communication entitled:*

ab initio study of the optoelectronic and thermoelectric properties of direct bandgap Double Perovskite

co-auteur(s): Amina ARRAR , Mohamed GHALEB

Dean of faculty

د . جيلالي بغدادي
عميد كلية العلوم والتكنولوجيا

President of conference

CMSRE24
09-10
2024

د. أمينة عرعار
رئيسة المؤتمر

https://univ-relizane.dz/fst/ / tel :044-72-40-64/ Bourmadia, RELIZANE

Ministry of Higher Education and Scientific Research
RELIZANE University
Faculty of Sciences and Technology/ physics department
Laboratory of Thin Film Physics & Advanced Technologies

THE THIRD NATIONAL CONFERENCE OF MATERIALS SCIENCES AND RENEWABLE ENERGY
DECEMBER, 13-14TH,2025/ RELIZANE, ALGERIA

CERTIFICATE OF APPRECIATION

THE PRESIDENT OF THE THIRD NATIONAL CONFERENCE OF MATERIALS SCIENCES AND RENEWABLE ENERGY (CMSRE25) CERTIFIES THAT:

Hadji Chikh Ali

has delivered ***an Oral*** *communication entitled:*

A DFT investigation of mechanical, optical and thermoelectric properties of double perovskites Cs2BaSrI6 halides

Co-author: *Amina. ARRAR*

Dean of faculty

كلية العلوم والتكنولوجيا
جامعة غليزان

President of conference

3rd National Conference Of Materials
Sciences And Renewable Energy
(CMSRE25)
Chair women. Dr.ARRAR Amina

Ministry of Higher Education and Scientific Research
RELIZANE University
Faculty of Sciences and Technology/ physics department
Laboratory of Thin Film Physics & Advanced Technologies

THE THIRD NATIONAL CONFERENCE OF MATERIALS SCIENCES AND RENEWABLE ENERGY
DECEMBER, 13-14TH,2025| RELIZANE, ALGERIA

CERTIFICATE OF APPRECIATION

This Certificate Is Presented To

Dr. HADJI Chikh Ali

We would like to sincerely thank you for your invaluable contribution as a member of the organizing committee for The Third National Conference of Materials Sciences and Renewable Energy (CMSRE25), organized by the Physics Department on December 13-14 th, 2025, in Relizane, Algeria.

Dean of faculty

عميد كلية العلوم والتكنولوجيا
جامعة غليزان
أ.د معمر جيلالي بيضة

President of conference

3rd National Conference Of Materials Sciences And Renewable Energy
(CMSRE25)
Chair women: Dr.ARRAR Amina

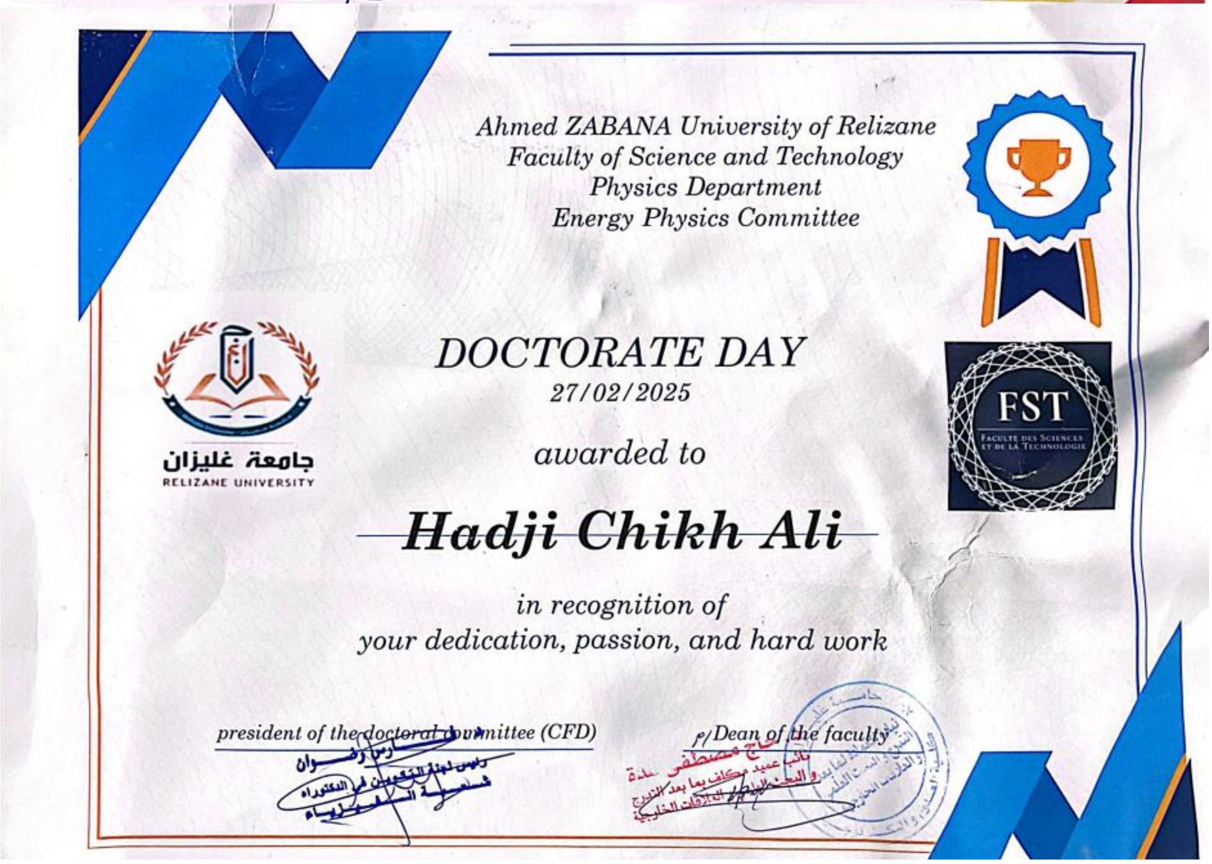

Ahmed ZABANA University of Relizane
Faculty of Science and Technology
Physics Department
Energy Physics Committee

DOCTORATE DAY
27/02/2025

awarded to

Hadji Chikh Ali

in recognition of
your dedication, passion, and hard work

president of the doctoral committee (CFD)

فارس رضوان
رئيس لجنة التكوين في الدكتوراه

م/Dean of the faculty

حاج مصطفى
نائب عميد مكلف بما بعد التدرج
والبحث العلمي والعلاقات الخارجية

ICMEMRE 2024

المؤتمر الـدولي الأول للهندسة
الـميكانيكية والمواد والطاقة المتجددة

1st International Conference on Mechanical Engineering, Materials and Renewable Energy

CERTIFICATE OF PARTICIPATION

This certifies that the paper entitled

Ab Initio Study of the Optoelectronic and Thermoelectric Properties of the New Double Perovskite Cs2BaSrI6

Authers:

Chikh Ali.Hadji, Amina Arrar, Mohamed Ghaleb, Zaza Touaa

Has been accepted and presented at the **1st International Conference on Mechanical Engineering, Materials and Renewable Energy** (***ICMEMRE 2024***) held in College of Mechanical Engineering Technology, Benghazi – Libya on September 14, 2024

رئيس المؤتمر

Conference Chair
Dr. Naser Alagouri

ICMEMRE 2025

المؤتمر الدولي الثاني للهندسة
الميكانيكية والمواد والطاقة المتجددة

2nd International Conference on Mechanical Engineering, Materials and Renewable Energy

CERTIFICATE OF PARTICIPATION

This certifies that the paper entitled

Thermoelectric Performance of Double Perovskites: A DFT-Based Approach

Authors:

Hadji Chikh Ali, Arrar Amina

has been accepted and presented at the **2nd International Conference on Mechanical Engineering, Materials and Renewable Energy** (***ICMEMRE 2025***) held at the Faculty of Engineering - University of Benghazi.

Benghazi - Libya, 13th and 14th/ December / 2025

Chairman of the Scientific Committee
Prof. Ayad A Abdalla

رئيس المؤتمر

Conference Chair
Prof. Gamal Hashem

جامعة غليزان
RELIZANE UNIVERSITY

University Ahmed Zabana Relizane
Faculty of Science & Technology
Department of Physics

FST

The First International Workshop on
Physics: Theory & Applications
Relizane, 23-24 February 2025

الورشة الدولية الأولى حول الفيزياء:
النظرية والتطبيقات
غليزان 23 - 24 فيفري 2025

Certificate Of Participation

This is to certify that

Chikh Ali Hadji

attended the First International Workshop on Physics; Theory & Applications (PTA2025), held 23-24 February 2025 at Relizane University, and presented a poster (in-person) entitled:

First principle study of the structural and optoelectronic properties of new double perovskite Cs2BaSrI6.

Co-authors: Amina ARRAR, Mohamed.GHALEB.

Dr. K. Khelifa-Kerfa
Chair, PTA2025

PTA2025
23-24 FEB
2025

https://sites.google.com/view/pta2025
UAZR: https://univ-relizane.dz, Tel: 044724064
Burmadiya district, Relizane province

LPCMTA

BENTHAM SCIENCE
Publishers of Quality Research

BENTHAM'S
APPROVED
REVIEWER
★★★★★

CERTIFICATE
of Recognition

In Recognition of Eminent Contributions

This is to certify that

Dr. Hadji C.Ali

Has completed the following eBook Proposal review
"Revolutionizing Communication Through Opto-VLSI and AI-Driven Remote Sensing"
On Mar 1, 2025 For publication in
Bentham Books | Bentham Science Publishers

Mahmood Alam
Director, Bentham Science

People's Democratic Republic of Algeria
Ministry of Higher Education and Scientific Research
University AHMED ZABANA of Relizane
Faculty of Science and Technology
Civil Engineering and Publics Works Department
Innovative Materials Laboratory and Renewable Energies

CERTIFICATE OF PARTICIPATION

THIS CERTIFICATE IS PROUDLY PRESENTED TO:

Chikh Ali hadji

In technical presentation, recognition and appreciation of contributions to the
Second Edition of the International Seminar on Materials and Engineering Structures ***(ISMES"25)***
Held in **Relizane, Algeria**, during February 07-08, 2026, with the paper entitled:

Tailoring Phonon and Electronic Properties of Double Perovskites via Ab-Initio Strain Engineering

Co-authors: Arrar amina

Seminar Chairwoman

Chair Women
LAQUFI Imene

ISMES 2025
07 - 08 February

Vice Dean of the faculty

د. حاج مصطفى عدة
نائب عميد مكلف بما بعد التدرج
و البحث العلمي و العلاقات الخارجية

Sponsors :